Bioisosteric replacement based on 1,2,4-oxadiazoles in the discovery of 1*H*-indazole-bearing neuroprotective MAO B inhibitors

Mariagrazia Rullo,[a] Gabriella La Spada,[a,#] Daniela Valeria Miniero,[b,#] Andrea Gottinger,[c] Marco Catto,[a] Pietro Delre,[d] Margherita Mastromarino,[a] Tiziana Latronico,[b] Sara Marchese,[c] Giuseppe Felice Mangiatordi,[d] Claudia Binda,[c] Anna Linusson,[e] Grazia Maria Liuzzi,[b] Leonardo Pisani[a,*]

[a] *Dept. of Pharmacy-Pharmaceutical Sciences, University of Bari Aldo Moro, via E. Orabona 4, 70125 Bari, Italy*

[b] *Dept. of Biosciences, Biotechnologies and Environment, University of Bari Aldo Moro, Via E. Orabona 4, 70125, Bari, Italy*

[c] *Dept. of Biology and Biotechnology, University of Pavia, via Ferrata 9, 27100 Pavia, Italy*

[d] *CNR, Institute of Crystallography, 70126 Bari, Italy*

[e] *Department of Chemistry, Umeå University, 90187, Umeå, Sweden*

[#] *these authors contributed equally*

[*]Corresponding author: Prof. Leonardo Pisani; tel: +390805442803; fax: +390805442230; email: leonardo.pisani@uniba.it

Highlights

- Twentyfive 1*H*-indazoles were designed and tested as *h*MAO inhibitors
- Bioisosteric amide replacement via 1,2,4-oxadiazoles was investigated
- Compound **20** was the most potent and selective MAO B inhibitor (IC_{50}=52 nM, SI>192)
- **20** protected both SH-SY5Y and astrocytes from H_2O_2 insult
- **20** displayed tight-binder's features toward *h*MAO B (T_m shift=+2.9 °C)

Abstract

Following a hybridization strategy, a series of 5-substituted-1*H*-indazoles were designed and evaluated *in vitro* as inhibitors of human monoamine oxidase (*h*MAO) A and B. Among structural modifications, the bioisostere-based introduction of 1,2,4-oxadiazole ring returned the most potent and selective human MAO B inhibitor (compound **20**, IC_{50} = 52 nM, SI > 192). The most promising inhibitors were studied in cell-based neuroprotection models of SH-SY5Y and astrocytes line against H_2O_2. Moreover, preliminary drug-like features (aqueous solubility at pH 7.4; hydrolytic stability at acidic and neutral pH) were assessed for selected 1,2,4-oxadiazoles and compared to

amide analogues through RP-HPLC methods. Molecular docking simulations highlighted the crucial role of molecular flexibility in providing a better shape complementarity for compound **20** within MAO B enzymatic cleft than rigid analogue **18**. Enzymatic kinetics analysis along with thermal stability curves (T_m shift = +2.9 °C) provided clues of a tight-binding mechanism for *h*MAO B inhibition by **20**.

Keywords

1H-indazole; monoamine oxidases; tight-binder; bioisostere; 1,2,4-oxadiazole; neuroprotection

1. Introduction

Monoamine oxidases (MAOs, EC 1.4.3.4) are FAD-dependent mammalian 60-kDa enzymes that catalyse the oxidative deamination of both endogenous (e.g., serotonin and dopamine) and exogenous arylalkyl amines (e.g., food tyramine) [1]. Two isoforms (termed MAO A and B) are encoded on X chromosome and have been well-characterized in terms of three-dimensional structures [2,3], tissue distribution, selectivity for substrates and inhibitors [4,5]. X-ray crystallography deciphered the main differences in the two active sites [2], even though the isoenzymes share more than 70% sequence identity. Both active sites show hydrophobic character, MAO B cavity being larger (700 $Å^3$ vs. 550 $Å^3$), longer, and narrower. Moreover, the enzymatic cleft within MAO B displays a bipartition between the entrance and the substrate cavity lined by gating residues responsible for ligand selectivity profiles (I199-Y326 in MAO B, F208-I335 in MAO A) [6,7].

These flavoenzymes exert a crucial role in detoxifying xenobiotics and terminating monoaminergic nerve impulse transmission, thus receiving great attention over the years from the medicinal chemistry community [8,9]. Starting from the seminal [10] and serendipitous discovery of mood-controlling effects of the anti-tubercular iproniazid, several drugs inhibiting MAOs have entered clinical practice. As safer replacement for hepatotoxic hydrazine-bearing compounds (*e.g.*, phenelzine), mechanism-based inactivators (clorgyline, selegiline, rasagiline) were initially developed by exploiting the suicide propargylamine moiety, able to covalently bind FAD cofactor. The issue of A/B selectivity was raised by the correlation of hypertensive crises, frequently observed after non-selective irreversible MAO inhibitors consumption, with peripheral MAO A inhibition. This side-effect was termed cheese-reaction owing to the abundancy of sympathomimetic tyramine in some foodstuffs (*i.e.*, cheese) [11]. Thereafter, selective reversible inhibitors were developed for treating depressive disturbs (MAO A selective; *e.g.*, moclobemide,

toloxatone) or marketed as levodopa add-on therapy of Parkinson's disease (PD, MAO B selective; *e.g.*, safinamide) by regulating neuroactive monoamine levels.

Since the catalytic cycle produces an aldehyde and H_2O_2 as the by-products, MAO activity is considered an endogenous source of reactive oxygen species (ROS) [12]. This pro-oxidant activity is harmful to cells whenever pathological conditions unbalance redox detoxifying systems. On this basis, a renewed interest toward MAOs is ongoing and the quest for selective and reversible MAO inhibitors gained consensus for treating several pathologies associated with oxidative stress conditions [13–15].

Apart from the well-established role in PD, increasing lines of evidence supported a key role for MAOs in cardiac senescence [16,17], substance abuse disorders [18], and cancer [19,20]. Moreover, radiolabelled MAO inhibitors [21] have been proposed as diagnostic tools to detect the increase of enzymatic expression and activity (mainly MAO B) as a marker of astrogliosis in neuroinflammatory disorders such as Alzheimer's disease (AD) [22]. In AD brains, MAO B co-localizes with amyloid plaques [23] and its neuronal staining is associated with $A\beta_{42}$ production [24]. Moreover, MAO B silencing enables $A\beta_{42}$ depletion. To this scope, sembragiline, initially developed for smoking-cessation, entered Phase I and II clinical trials for AD therapy. Unfortunately, this propargylamine was retired from the pipeline because of falling short of primary endpoints. More recently, researchers have provided sound explanations sustaining aberrant production of γ-aminobutyric acid (GABA) during long-term treatment based on irreversible MAO agents (e.g., selegiline) [25]. They proved that compensatory gene expression could explain the inefficacy of propargylamines, leaving the hope for selective and reversible compounds for treating AD.

In the last two decades, some of us have devoted great research endeavour to the identification of novel and selective MAO B inhibitors [26–29] through the chemical decoration of a coumarin core. With a scaffold-hopping strategy in mind, we took inspiration from nitrogen-containing scaffolds (pyrroles [30], 1*H*-indazoles [31], 1*H*-indoles [32], 9-deazaxanthines [33], pyridines, among others) already known from the literature or available in our molecular collection as MAO inhibitors (figure 1A). In many cases, the molecular framework is represented by *N*-heterocycles connected to a lipophilic moiety through a flexible or a rigid bridge. Thus, we envisaged the design of hybrid compounds (figure 1B) by merging the 1*H*-indazole nucleus installed on ***N*-Het5**, recently published by Müller's group [34], with a lipophilic motif from ***N*-Het3** (*e.g.*, biphenyl fragment), picked from an in-house library of anilides screened toward MAOs (unpublished data). Linker properties were studied by bridging the two main fragments in different ways: i) an amide bond

(and the reverse amide) to investigate hydrogen bonding features; ii) an oxymethylene bridge to study the impact of flexibility; iii) a sulphonamide linker to probe pK_a modulation; iv) regioisomeric 1,2,4-oxadiazoles as heteroaromatic bioisosteres for amides. After biological evaluation toward human MAOs, the cytotoxicity of the most potent inhibitors was studied in human neuroblastoma line. Then, non-toxic compounds were advanced to a deeper evaluation as neuroprotective agents in SH-SY5Y line insulted by hydrogen peroxide. The neuroprotective profile was assessed by measuring the effect over cell viability through 3-(4,5-dimethylthiazol-2-yl)-2.5-diphenyltetrazolium bromide (MTT) assay [35,36] and ROS production by means of 2',7'-dichlorofluorescein diacetate (DCFH-DA) test [37]. As a further proof, two inhibitors were also assayed as neuroprotectants in astrocytes against H_2O_2. Moreover, the most promising amides and 1,2,4-oxadiazoles congeners underwent a preliminary drug-likeness investigation by measuring kinetic aqueous solubility at physiological pH (7.4) and chemical stability in different test conditions (hydrolytic stability at physiological and acidic pH). Enzyme kinetics, biophysical techniques as well as docking simulations were performed to shed light on the pharmacodynamics features of the most potent hit compound.

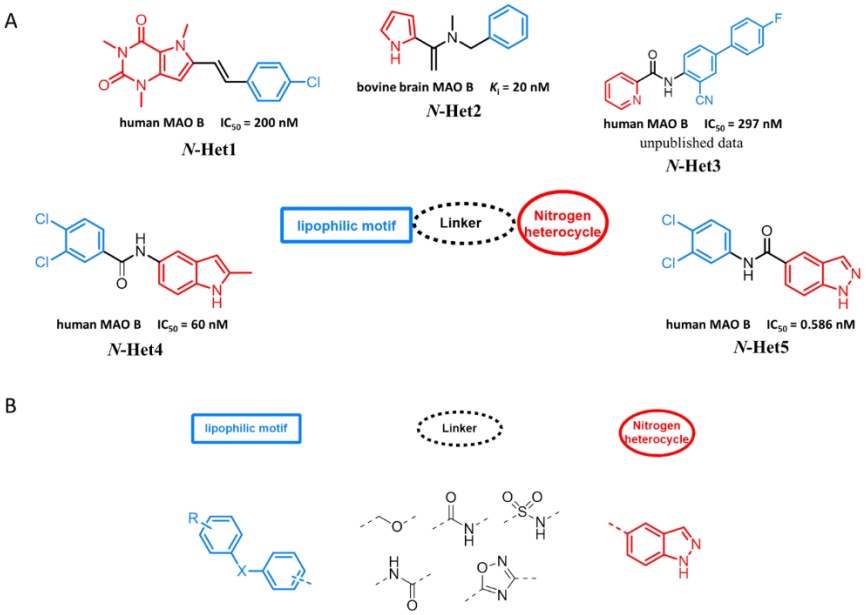

Figure 1. Design of hybrid molecules.

2. Chemistry

The synthetic protocols leading to final compounds tested as MAO inhibitors are illustrated in schemes 1-5. The preparation of indazoles **2-10**, **14-17** started from the reaction of 5-substituted-1*H*-indazole building block **i-iii** with the appropriate partner **iv-xii** (scheme 1). Sulphonamide **1a**

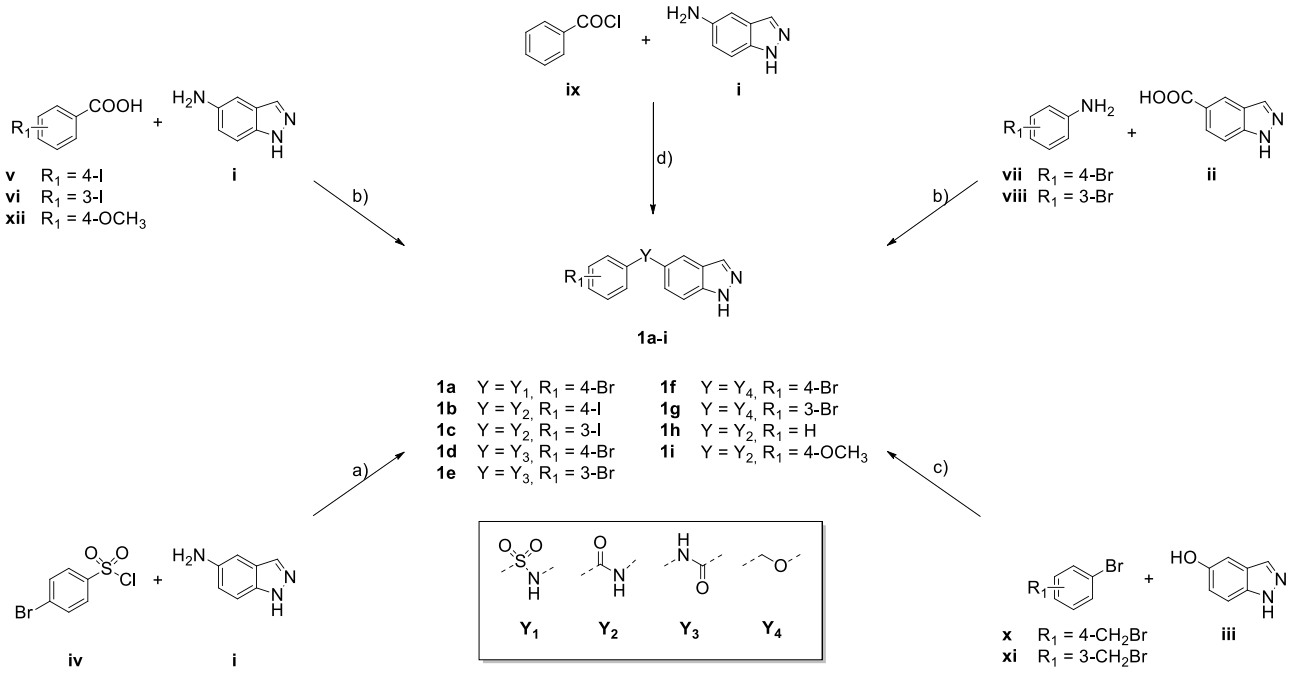

Scheme 1. Synthesis of intermediates **1a-i**. Reagents and conditions: a) for **1a**: DIPEA, THF, room temperature, 4 h; b) from **i**: **v** (for **1b**) or **vi** (for **1c**) or **xii** (for **1i**), EDC·HCl, HOBt, anhydrous DMF, room temperature, overnight; from **ii**: **vii** (for **1d**) or **viii** (for **1e**), EDC·HCl, HOBt, anhydrous DMF, room temperature, overnight; c) **x** (for **1f**) or **xi** (for **1g**), KI (cat.), K_2CO_3, absolute ethanol (Δ, 16 h, for **1f**) or anhydrous DMF (90 °C, 48 h, for **1g**); d) for **1h**: DIEA, THF, room temperature, 24 h.

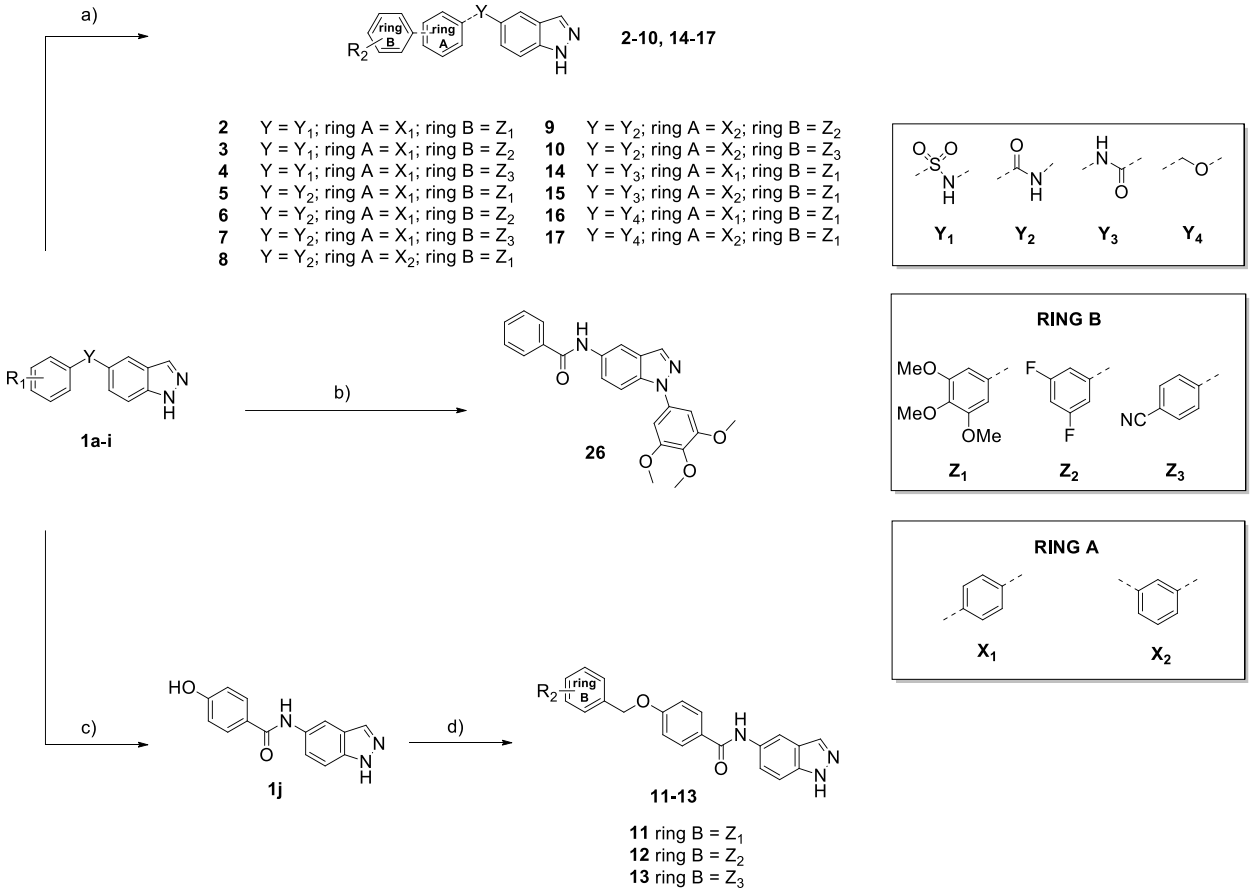

Scheme 2. Synthesis of final compounds **2**-**17**. Reagents and conditions: a) suitable phenylboronic acid, $Pd(PPh_3)_4$ (cat.), K_2CO_3, dioxane/water (4/1, v/v), 150 °C, 30 min, MW; b) from **1h**: 5-bromo-1,2,3-trimethoxybenzene, CuI (cat.), trans-*N*,*N*′-dimethylcyclohexane-1,2-diamine (ligand), K_2CO_3, dioxane/DMF (3:1 v/v), 150 °C, 1 h, MW; c) from **1i**: $AlCl_3$, *o*-xylene, Δ, 9 h; d) for **11**: 3,4,5-trimethoxybenzyl methanol, diisopropyl azodicarboxylate (DIAD), PPh_3, anhydrous THF, room temperature, 24 h; for **12**: 3,5-difluorobenzyl bromide, KI (cat.), K_2CO_3, acetonitrile, Δ, 7 h; for **13**: 4-cyanobenzyl bromide, KI (cat.), K_2CO_3, acetonitrile, Δ, 7 h.

was obtained from 1*H*-indazole-5-amine **i** and sulphonyl chloride **iv** in THF at room temperature. Amide coupling between appropriate (hetero)aromatic amine (**i**, **vii**-**viii**) and carboxylic acid (**ii**, **v**, **vi**, **xii**) mediated by EDC-HOBt system in anhydrous DMF yielded amides and reversed amides **1b**-**e**, **1i**. Nucleophilic substitution reaction between **iii** and benzyl bromides **x**-**xi** provided 5-benzyloxy-1*H*-indazoles **1f**-**g**. Finally, compounds **2**-**10**, **14**-**17** were furnished by microwave-assisted Suzuki-coupling reaction between aryl halide intermediate **1a**-**g** and differently substituted boronic acids in the presence of $Pd(PPh_3)_4$ and K_2CO_3, as base, in a dioxane/water mixture (scheme 2). The preparation of **26** started from the acylation of **i** with benzoyl chloride giving intermediate **1h**, that underwent a Ullmann-type copper-promoted direct *N*1-arylation with 5-bromo-1,2,3-

trimethoxybenzene in the presence of trans-*N*,*N*'-dimethylcyclohexane-1,2-diamine as ligand under microwave irradiation at 150 °C (scheme 2). *O*-demethylation of **1i** through $AlCl_3$ as Lewis acid afforded phenol intermediate **1j** that was subsequently alkylated through a Mitsunobu etherification (yielding **11**) or benzylated in the presence of appropriate bromides (yielding **12**-**13**) as shown in scheme 2.

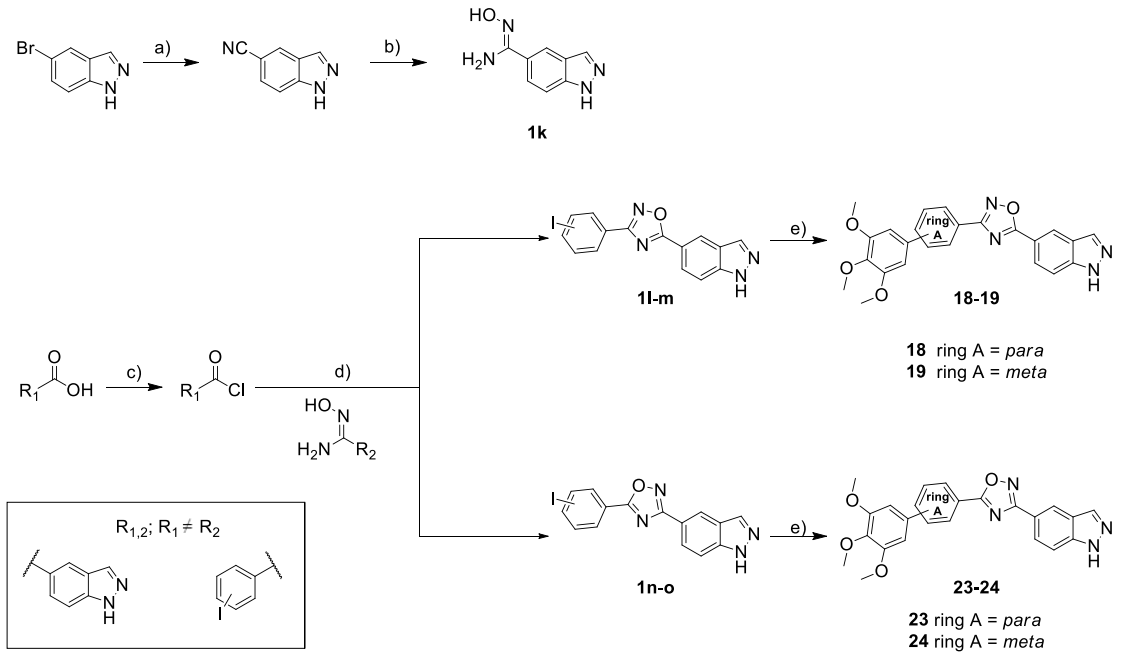

Scheme 3. Synthesis of final compounds **18-19**, **23-24**. Reagents and conditions: a) $Zn(CN)_2$, $Pd_2(dba)_3$ (cat.), XPhos, DMF/water (99/1, v/v), 160 °C, 30 min, MW; b) NH_2OH 50% wt. in H_2O, absolute ethanol, room temperature, 72 h; c) $SOCl_2$, anhydrous dichloromethane, Δ, 2 h; d) anhydrous pyridine, Δ, 5-20 h; e) 3,4,5-trimethoxyphenylboronic acid, $Pd(PPh_3)_4$ (cat.), K_2CO_3, dioxane/water (4/1, v/v), 150 °C, 30 min, MW.

The synthesis of rigid biphenyl-substituted 1,2,4-oxadiazoles **18-19**, **23-24** is illustrated by scheme 3. The preparation of intermediate amidoximes was achieved by reacting commercially available benzonitriles with hydroxylamine in ethanol. 1*H*-indazole-5-carbonitrile was obtained through a Pd-assisted Br-CN exchange in the presence of $Zn(CN)_2$ and XPhos. Pyridine promoted the cyclization of amidoximes with the suitable carboxylic acid, activated in situ as acyl chloride, to the desired regioisomeric 1,2,4-oxadiazoles **1l-o** under reflux conditions. Suzuki-coupling between 3,4,5-trimethoxyphenylboronic acid and aryl-halides **1l-o** furnished the desired final compounds **18-19**, **23-24** (scheme 3). As displayed in scheme 4, the synthetic pathway yielding flexible compounds **20-22** started from the preparation of desired nitriles **1q-s** that were transformed into the corresponding amidoximes **1t-w** by reacting with hydroxylamine. Pyridine-assisted cyclization of

1w with 1*H*-indazole-5-carbonyl chloride furnished derivative **20**. The 1,2,4-oxadiazole core of **21**-**22** was built through the direct cyclization between amidoximes **1t-u** and 1*H*-indazole-5-carboxylic acid in the presence of EDC-HOBt coupling system. Scheme 5 depicted the synthesis of compound **25** starting from the Mitsunobu alkylation of methyl *p*-hydroxybenzoate with 3,4,5-trimethoxybenzyl alcohol. LiOH·H_2O was employed to perform ester saponification to **1y** that was finally cyclized as previously described, thus furnishing final **25**.

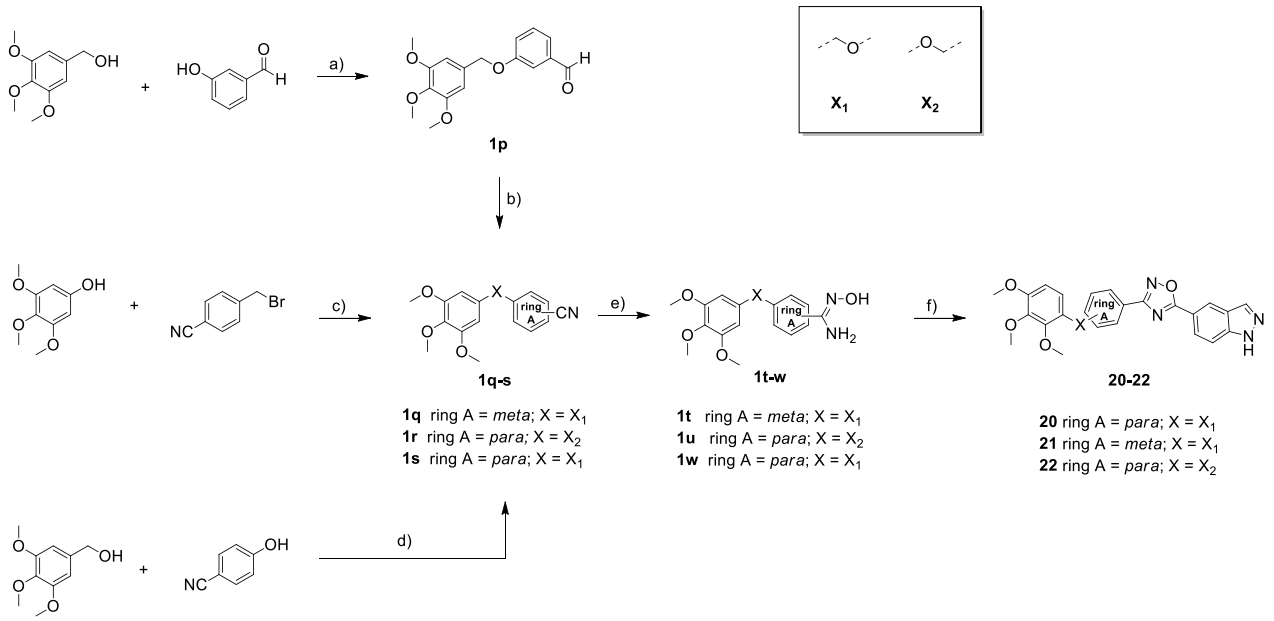

Scheme 4. Synthesis of final compounds **20**-**22**. Reagents and conditions: a) PPh_3, ADDP, anhydrous THF, room temperature, 72 h; b) for **1q**: Et_3N, NH_2OH·HCl, phthalic anhydride, anhydrous acetonitrile, room temperature to Δ, 18 h; c) for **1r**: K_2CO_3, absolute ethanol, room temperature, overnight; d) for **1s**: PPh_3, DIAD, anhydrous THF, room temperature, 72 h; e) NH_2OH 50% wt. in H_2O, ethanol, room temperature, 72 h; f) for **20**: i) 1*H*-indazole-5-carboxylic acid, $SOCl_2$, anhydrous dichloromethane, Δ, 4 h; ii) from **1w**: 1*H*-indazole-5-carbonyl chloride, anhydrous pyridine, Δ, 5 h; for **21**-**22**: **1t** or **1u**, 1*H*-indazole-5-carboxylic acid, EDC·HCl, HOBt, anhydrous DMF, 170 °C, 30 min, MW.

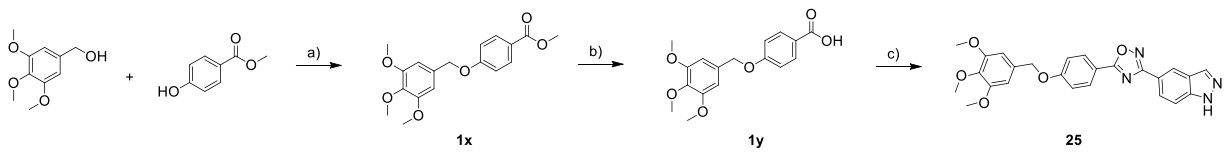

Scheme 5. Synthesis of final compound **25**. Reagents and conditions: a) PPh_3, ADDP, anhydrous THF, room temperature, overnight; b) LiOH·H_2O, THF/H_2O (3/1, v/v), 24 h; c) **1k**, EDC·HCl, HOBt, anhydrous DMF, 170 °C, 30 min, MW.

3. Results and discussion

3.1 Structure-activity relationships (SAR)

The entire subset of newly prepared 1*H*-indazoles was tested for the ability to inhibit human recombinant MAO A and B by using already reported spectrofluorimetric procedures based on the detection of kynuramine oxidative deamination to 4-hydroxyquinoline [27]. Three B-rings were initially investigated, differing for their stereo-electronic, lipophilic and hydrogen bonding (HB) properties (3,5-difluorophenyl: unhindered, lipophilic and electron-poor ring; 3,4,5-trimethoxyphenyl: hindered, polar, HB acceptor and electron-rich ring; 4-cyanophenyl: polar, HB acceptor and electron-poor ring). The hindered and slightly acidic sulphonamide linker was not tolerated in both MAO isoforms, thus all three congeneric entries **2**-**4** (Table 1) showed a percentage of inhibition at 10 μM lower than 50% regardless of ring B substituents. More interesting IC_{50} values were returned by the compounds bearing an amide as the linker between the heteroaromatic and the biphenyl core. In both *para*- and *meta*-substituted subset, the electron-donating 3,4,5-triMeO substitution pattern provided the most active compounds in comparison to 3,5-diF and 4-CN groups (entry **5** > **6**, **7**; entry **8** > **9**, **10**). This trend was confirmed also in more flexible analogues (entry **11**-**13**) upon inserting an oxymethylene bridge disrupting the biphenyl core planarity (entry **11** > **12**, **13**). Based on these preliminary SAR, we decided to maintain the 3,4,5-triMeOPh substituent and focus the attention on the effect of linker type and size as well as on the central ring A geometry (*meta* vs. *para* substitution). Amide group reversal produced an opposite effect as function of ring A substitution, thus decreasing the activity in *para*-substituted analogues (**14** < **5**) while returning a potent *meta*-derivative (**15**) with IC_{50} = 204 nM toward MAO B (40-fold higher than analogue **8**). It is worth noting that **15** proved to be also the most potent MAO A inhibitor (IC_{50} = 2.70 μM) for this class of molecules thus returning a poor B/A selectivity (SI = 13). The replacement of the rigid amide linker with a more flexible oxymethylene bridge provided low micromolar MAO B inhibitors **16**-**17** (IC_{50} = 1.01 and 1.74 μM, respectively) without improving the inhibitory potencies at a remarkable level. Slightly better results were scored by *para*-analogue **16** compared to amides **5** and **14**. In derivatives **18**-**25** the connecting bridges between the lipophilic and the indazole fragment bear 3,5-disubstituted-1,2,4-oxadiazoles as cyclic bioisosteric replacement for the amide group, retaining close HB acceptor properties. Within the oxadiazole series, both in planar biphenyl-substituted compounds (**18**, **19**, **23**, **24**) and in less rigid derivatives (**20**, **21**) the 1,4-geometry of ring A was preferred to 1,3-disubstitution by MAO B (**18** > **19**, **20** > **21**, **23** > **24**). Planarity disruption obtained by inserting an -OCH_2- linker between the two aromatic rings (A and B) improved MAO B inhibition (**20** > **18**; **21** > **19**; **25** > **23**). Looking at regioisomeric *para*-substituted 1,2,4-oxadiazoles, bioisosteres **18**, **20**, and **23** were equipotent or

more potent than the corresponding amides / reverse amides: **18** ≈ **5**, **14**; **23** > **5**, **14**; **20** > **11**; **25** > **11**.

Table 1. Inhibition data toward human MAO A and B for compounds **2**−**26**

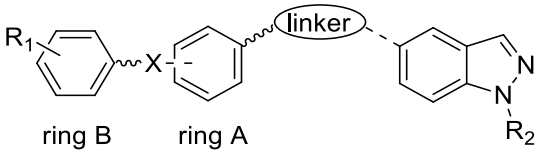

cmpd	R_1	Ring A[a]	X	LINKER	R_2	IC_{50} (μM) or % inhibition at 10 μM[b]	
						*h*MAO A[c]	*h*MAO B[c]
2	3,4,5-triMeO	*p*	--	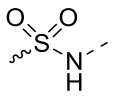	H	43±3%	16±4%
3	3,5-diF				H	38±4%	40±3%
4	4-CN				H	39±4%	31±3%
5	3,4,5-triMeO			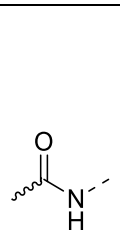	H	25±5%	1.25±0.20
6	3,5-diF				H	17±2%	4.35±0.74
7	4-CN				H	18±3%	33±3%
8	3,4,5-triMeO	*m*			H	5.32±0.08	8.41±1.16
9	3,5-diF				H	22±4%	30±4%
10	4-CN				H	12.2±1.3	9.10±0.29
11	3,4,5-triMeO	*p*	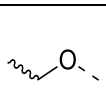		H	38±4%	2.50±0.23
12	3,5-diF				H	9±2%	26±2%
13	4-CN				H	15±2%	47±1%
14	3,4,5-triMeO	*p*	--	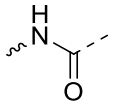	H	21±3%	2.02±0.27
15	3,4,5-triMeO	*m*			H	2.70±0.22	0.204±0.043
16	3,4,5-triMeO	*p*		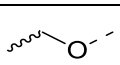	H	15±3%	1.01±0.083
17	3,4,5-triMeO	*m*			H	33±3%	1.74±0.07
18	3,4,5-triMeO	*p*	--	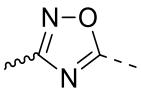	H	16±4%	1.58±0.19
19	3,4,5-triMeO	*m*			H	25±4%	35±3%
20	3,4,5-triMeO	*p*	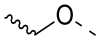		H	14±5%	0.0521±0.0113
21	3,4,5-triMeO	*m*			H	9±1%	2.89±0.43
22	3,4,5-triMeO	*p*	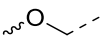		H	38±4%	43±4%
23	3,4,5-triMeO	*p*	--	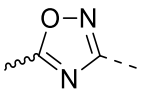	H	21±4%	0.597±0.088
24	3,4,5-triMeO	*m*			H	15±3%	1.81±0.04
25	3,4,5-triMeO	*p*			H	<5%	0.308±0.032
26	--	--	--	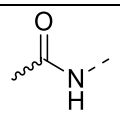	3,4,5-triMeOPh	13±4%	1.32±0.21
safinamide						18±3%	0.0282±0.0015
clorgyline						0.00238±0.00014	2.48±0.43

[a] Substitution pattern for phenyl ring A (*meta*, *para*). [b] Values are the mean of three independent experiments ± SEM. [c] Human recombinant MAOs on Supersomes.

As a main result, compound **20**, combining all these favourable structural motifs (1,4-geometry of ring A; flexible -OCH_2- bridge between ring A and B; 1,2,4-oxadiazole as the linker), proved to be the most potent MAO B inhibitor of the whole series with an IC_{50} = 52 nM along with an outstanding MAO B/A selectivity (SI > 192). Interestingly, the inversion of the linker between ring A and B produced a dramatic affinity drop toward MAO B in compound **21**.

The comparison between rigid regioisomeric 1,2,4-oxadiazoles (**18**-**19** and **23**-**24**) highlighted the preference within MAO B enzymatic cleft for 1*H*-indazole as the substituent at position 3 (**23** > **18**; **24** > **19**). Upon applying a substituent-walking approach, shifting the 3,4,5-trimethoxyphenyl ring at indazole-*N*1 furnished a moderate MAO B inhibitor (**26**) active at the micromolar level (IC_{50} = 1.32 μM).

To rule out false positives due to intrinsic fluorescence properties, the most potent inhibitor (**20**) was also assayed in a similar spectrophotometric protocol, where it returned close IC_{50} values (IC_{50} = 52 nM and 69 nM in spectrofluorimetric and direct absorbance test, respectively).

3.2 Cytotoxicity and neuroprotection studies

Except for **19** and **22**, all compounds bearing the oxadiazole-based linker were endowed with potent MAO B inhibitory activities, being low micromolar (**18**, **21**, **24**) or submicromolar to nanomolar (**20**, **23**, **25**). Taking into account the promising *in vitro* inhibitory potencies displayed by 1,2,4-oxadiazoles prototypes, some of them were advanced to cell-based assays according to the following criteria. Within each *meta*/*para* regioisomeric pair, we selected the most active *para*-derivatives (**18**, **20**, **23**, **25**) and then, for comparative purposes, we enrolled some amide congeners (**5** and **14**, both *para*-substituted) together with *meta*-substituted 1*H*-indazole **15**, showing the lowest IC_{50} value (204 nM toward MAO B). After the evaluation of inherent cytotoxicity against human neuroblastoma cell line SH-SY5Y (figure 2), the safest compounds (**5**, **18**, **20**, **23**, **25**) were tested for their ability to counteract the cytotoxic damage and ROS production on SH-SY5Y line insulted by hydrogen peroxide [37]. Neuroprotection data have been reported in Figure 3, compared with quercetin as effective positive control. This plant flavonoid has been proved to protect SH-SY5Y cells against H_2O_2-mediated apoptosis [38] and counteract oxidative stress in different neurodegenerative diseases (ND) through different mechanisms [39,40], including radical scavenging.

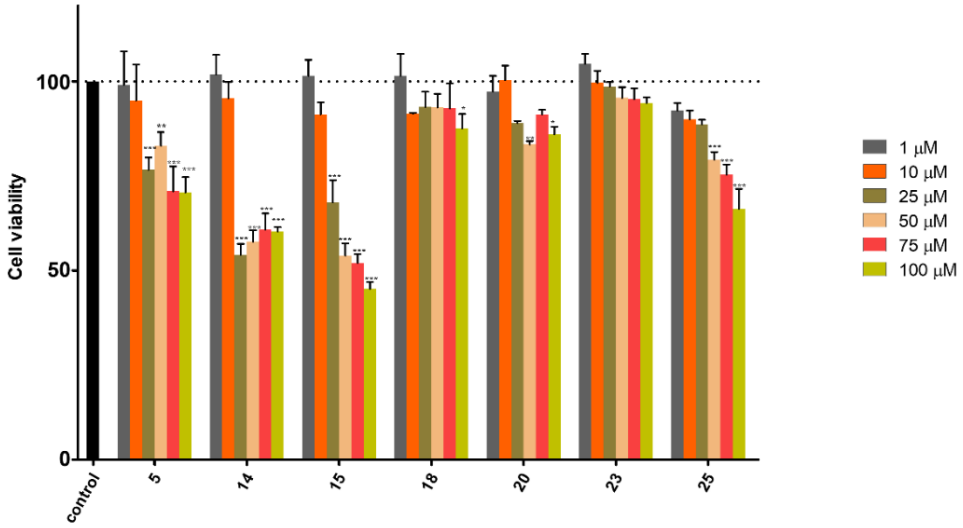

Figure 2. Viability of SH-SY5Y cells in the presence of compounds **5**, **14**, **15**, **18**, **20**, **23**, and **25** at different concentrations (1, 10, 25, 50, 75, 100 µM) measured through MTT assay and showed as means ± SD of three independent experiments, each performed in triplicates and referred to untreated control cells (control, 100% values, in the absence of compound). Statistical significance was calculated using a one-way analysis of variance (ANOVA) followed by the Dunnett's multiple comparison post-hoc test (GraphPad Prism version 5); * $p < 0.05$, ** $p < 0.01$, *** $p < 0.001$.

As illustrated in figure 3, all indazoles under investigation were able to increase the percentage of viable cells at 0.1-5 µM concentrations compared with SH-SY5Y co-incubated with H_2O_2 alone (400 µM). The highest neuroprotection activity was scored by **5** at the highest concentration applied, whereas it is worth noting that **20** returned the most promising viability gain even at low doses (0.1 µM).

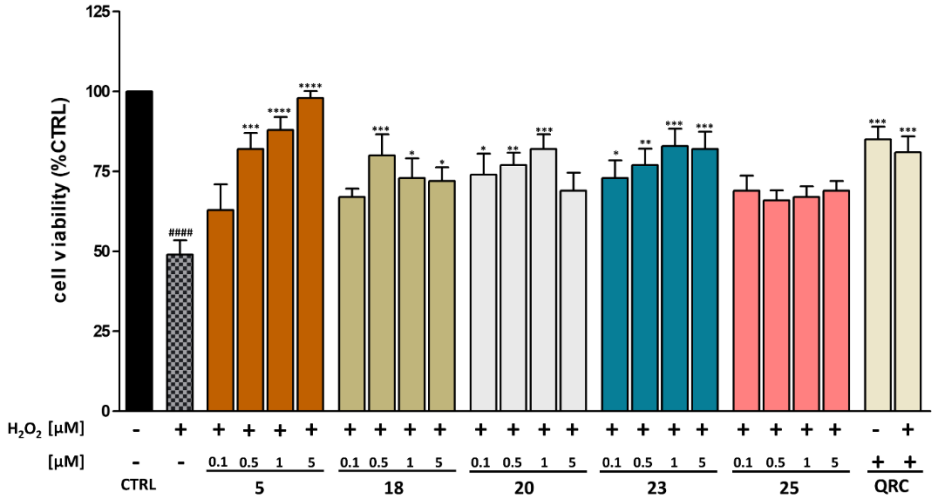

Figure 3. Cytoprotective effect on SH-SY5Y cell viability of compounds **5**, **18**, **20**, **23**, and **25** at different concentrations (0.1-5 µM range) co-incubated with H_2O_2 (400 µM) for 24 h. Results are expressed as cell viability measured through MTT test and showed as means ± SD of three

independent experiments, each performed in triplicates and referred to untreated control cells (CTRL, 100% values). Quercetin (QRC) at 75 μM was used as standard. Statistical significance was calculated using a one-way analysis of variance (ANOVA) followed by Dunnett's multiple comparison test. Levels of significance: referred to H_2O_2 **** $p < 0.0001$, *** $p < 0.001$, ** $p < 0.01$, * $p < 0.05$; referred to control #### $p < 0.0001$.

At low concentration (0.1-5 μM) compounds **5**, **18**, and **20** proved to be able to protect neuroblastoma cells from pro-oxidant insults through ROS-scavenging pathways at a moderate level (figure 4). As expected, these figures were much lower than those exerted by the well-known antioxidant quercetin, used as positive control at higher concentration (75 μM).

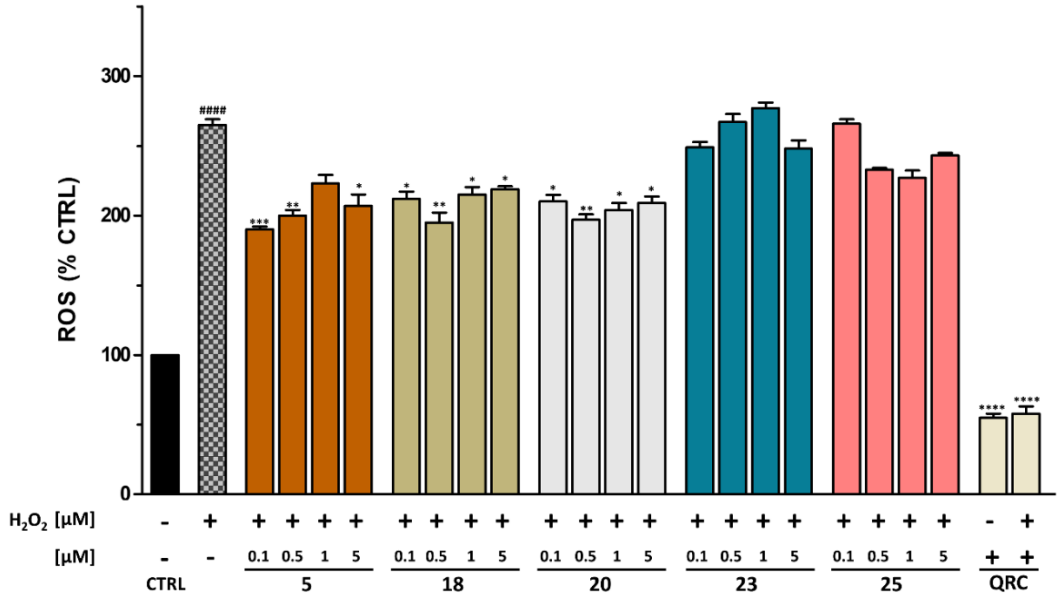

Figure 4. ROS level determination in SH-SY5Y cells measured through DCFH-DA assay after incubation with H_2O_2 (400 μM) in the absence and presence of indazole compound **5**, **18**, **20**, **23**, and **25** at different concentration (0.1, 0.5, 1, 5 μM). Results are expressed as % of ROS production referred to control cells treated only with DCFH-DA. Quercetin (QRC, 75 μM) was used as standard antioxidant. Statistical significance was calculated using a one-way analysis of variance (ANOVA) followed by Dunnett's multiple comparison test. Levels of significance: referred to H_2O_2 **** $p < 0.0001$, *** $p < 0.001$, ** $p < 0.01$, *$p < 0.05$; referred to control #### $p < 0.0001$.

Encouraged by these results, compounds **5** and **20** underwent a further neuroprotection study engaging astrocytes as cell model. Preliminarily, their cytotoxicity was assessed through MTT assay (figure 5A). Interestingly, when co-incubated at 5 μM with hydrogen peroxide (400 μM), derivative **20** maintained viable cells at a level comparable to that of quercetin used as positive control at higher doses (75 μM, figure 5B).

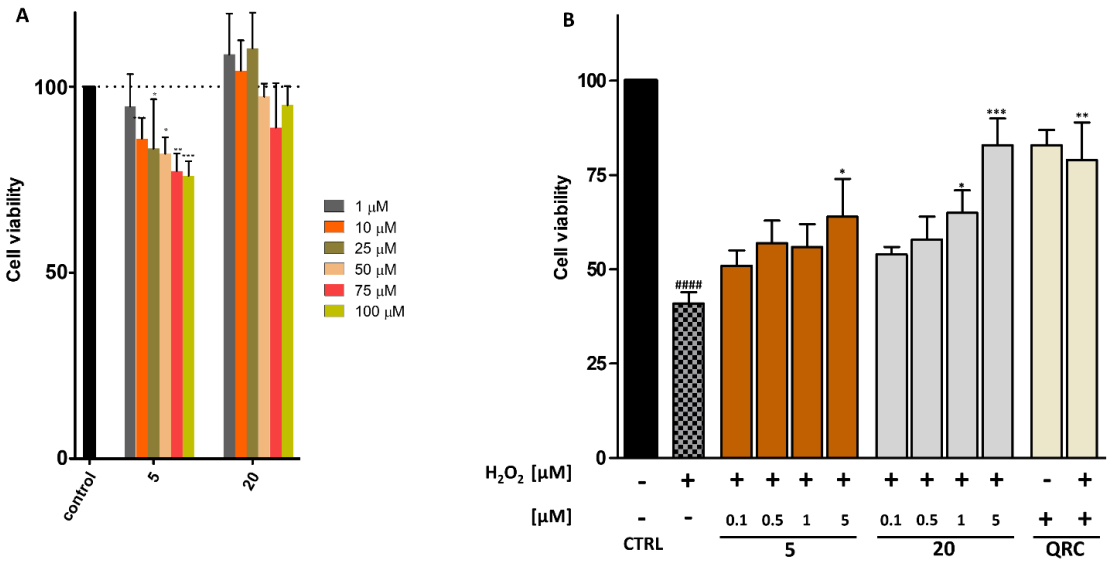

Figure 5. (A) Viability of DI TNC1 astrocyte cell line in the presence of compounds **5** and **20** (1-100 μM range) and (B) upon co-incubation with H_2O_2 (400 μM; compounds **5** and **20** at 0.1-5 μM range) measured through MTT assay. Data are means ± SD of three independent experiments, each performed in triplicates and referred to untreated cells (CTRL, 100% values, in the absence of compound). Quercetin (QRC, 75 μM) was used as standard. For cytotoxicity assay, statistical significance was calculated using a one-way analysis of variance (ANOVA) followed by the Dunnett's multiple comparison test (GraphPad Prism version 5); * $p < 0.05$, ** $p < 0.01$, *** $p < 0.001$. For protection assay, statistical analysis was performed by applying one-way ANOVA followed by Dunnett's multiple comparison test. Levels of significance: referred to H_2O_2 *** $p < 0.001$, ** $p < 0.01$, *$p < 0.05$; referred to control #### $p < 0.0001$.

3.3 Drug-likeness evaluation

A major reason for the high attrition rate of drug discovery programs relies on the selection of non "lead-like" candidates after hit discovery campaigns. Accordingly, the preliminary assessment of drug-like properties should be anticipated in the earliest stages. By applying RP-HPLC based protocols we measured the aqueous solubility at physiological pH (7.4, phosphate buffer) and the hydrolytic stability at two different buffering conditions (acidic pH 2.0 and physiological pH 7.4) of eight indazole analogues. Basically, selected samples were prioritized from the whole indazole subset with the aim of investigating the impact of the bioisostere replacement based on 1,2,4-oxadiazoles, in comparison to amide analogues, as well as the structural requirements for good solubility and chemical stability. To this extent, amides **5**, **8**, **14**, and **15** along with oxadiazoles **18**, **20**, **23**, and **24** were shortlisted for this study as shown in table 2. All compounds returned from low to moderate values likely dependent on their polyaromatic structures. As expected, symmetry/planarity disruption favours solubility. As a matter of fact, less symmetric *meta*-isomers were more soluble than *para*-analogues (**8** > **5**, **15** > **14**, **24** > **23**). Moreover **18** displayed lower

solubility values than **20**, where the –OCH_2– bridge disrupted the planarity of the biphenyl portion. The introduction of cyclic bioisosteres was able to improve aqueous solubility compared to amides (*para*: **18** and **23** > **5** and **14**; *meta*: **24** > **8** and **15**), even if at a mild extent.

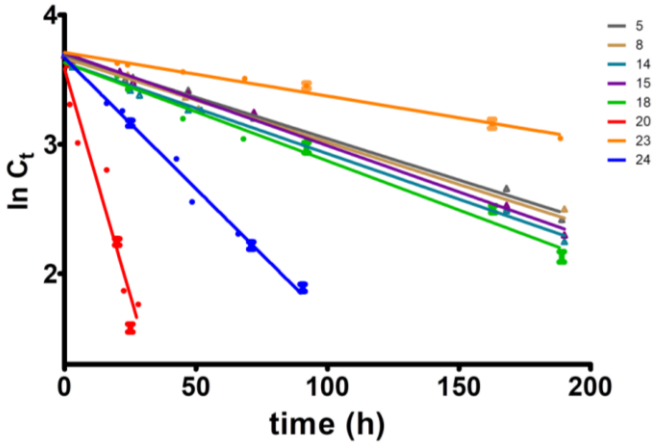

Figure 6. Plots of pseudo-first order kinetics for hydrolytic stability of amides (▲) **5**, **8**, **14**, and **15**, and 1,2,4-oxadiazoles (●) **18**, **20**, **23**, and **24** at pH 2.0 at 37 °C. Time-dependent disappearance was measured under hydrolytic conditions in acidic buffer (10 mM HCl, pH 2.0, 0.15 M KCl) at 37 °C. Compounds were incubated at initial concentration equal to 40 µM and concentration at various time points was determined by RP-HPLC. Data points represent means ± SD of three independent measurements.

All compounds were stable at physiological pH (7.4) and after 72 h incubation in the dark at 37 °C, compounds' residuals were detected higher than 90%. Amide derivatives were unaffected also by acidic conditions (buffered at pH 2.0), simulating gastric pH, with half-lives between 96 h and 112 h from pseudo-first order degradation kinetics. Oxadiazoles **18** and **23** displayed $t_{1/2}$ values comparable (**18**) or superior (**23**, $t_{1/2}$ = 200 h) to that of amides, whereas **20** and **24** were considerably more acid-labile, even though at an acceptable level. The lowest acid-resistant molecule was **20** ($t_{1/2}$ = 10 h), whose chemical integrity at acidic pH is strongly affected by the presence of 3,4,5-trimethoxybenzyl ether group prone to hydrolysis under acid catalysis.

Table 2. Kinetic solubility and hydrolytic stability data for compounds **5**, **8**, **14**-**15**, **18**, **20**, **23**-**24**

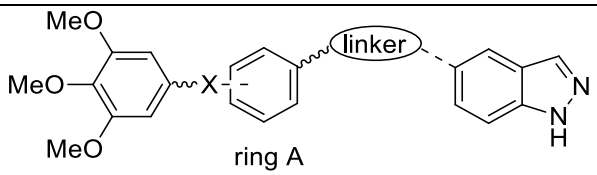

cmpd	linker	ring A[a]	X	$S_{pH7.4}$[b,c]	Hydrolytic stability	
					pH 2, $t_{1/2}$ (h)[c,d]	pH 7.4, residual (%) after 72h[e]
5	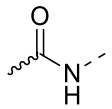	*p*	--	3.2±0.3	112±3	> 98%
8		*m*	--	12±1	101±2	> 98%
15	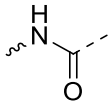		--	15±1	96±4	> 98%
14		*p*	--	7.4±0.4	102±2	> 95%
18	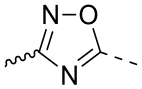		--	9.1±0.5	82±1	> 98%
20			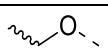	17±1	10±1	> 95%
23	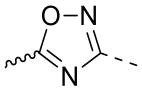		--	7.8±0.6	200±1	> 90%
24		*m*	--	19±1	29±2	> 98%

[a] Substitution pattern for phenyl ring A (*meta*, *para*). [b] Kinetic solubility (μM) measured in phosphate buffer (50 mM, pH 7.4) by RP-HPLC. [c] Values are the mean of three independent experiments ± SEM. [d] Half-lives calculated from pseudo-first order kinetics of chemical stability plots in acidic conditions (10 mM HCl, pH 2, 0.15 M KCl) at 37 °C. Starting compound concentration = 40 μM. Compound concentrations measured at different time-points by RP-HPLC. [e] Percentage of compound concentration after 72 h (initial concentration = 40 μM) in phosphate buffer (40 mM, pH 7.4, 0.15 M KCl) at 37 °C measured by RP-HPLC.

3.4 Molecular docking simulations

Molecular docking simulations were run to gain insights into plausible binding poses of the most potent *h*MAO B inhibitor **20** (IC_{50} = 52 nM) and to better rationalize the activity cliff displayed by its rigid congener **18** (IC_{50} = 1580 nM). Noteworthy, several X-ray structures of *h*MAO B are available within the Protein Data Bank, including binary complexes with both covalent and reversible inhibitors. The choice of crystal structure displaying the most suitable binding site conformation for docking calculations represents a crucial step in affording more reliable predictions [41,42]. In particular, our choice fell on the structure published in 2012 by Binda *et al.*

(PDB code: 4A79) [43] showing *h*MAO B in high resolution complex (1.89 Å) with a reversible inhibitor (pioglitazone, Figure 7A) sharing the size and poly-aromatic skeleton of **18** and **20**. The top MM-GBSA scored docking pose returned by **20** is shown in Figure 7B. The inhibitor was predicted to mimicking the binding mode observed for pioglitazone, stabilized by a well-oriented arene-arene stacking involving the 1,2,4-oxadiazole ring facing Y326 and several hydrophobic contacts with the side-chains of F103, L164, I199. Additional π-π interactions with Y398 (with the 1*H*-indazole core) and W119 (with the terminal phenyl ring) were also detected. According to this observation, computed docking and MM-GBSA scores for **20** (-10.05 kcal/mol and -63.61 kcal/mol, respectively) were close to those returned by the cognate ligand (-10.22 kcal/mol and -55.27 kcal/mol), hence supporting the reliability of the performed docking study. On the contrary, the same docking protocol produced no poses for derivative **18**, thus suggesting that the flexibility allowed by -OCH_2- linker (between rings A and B, see general structure in table 1) might return a better shape complementarity underlying more efficient target recognition. Intrigued by this hypothesis, we performed a conformational study of **18** in the same binding site used for docking simulation (PDB code: 4A79) by employing Confgen, a tool available within the Schrödinger suite 2022-4 [44]. Noteworthy, a close binding mode was supposed for **18** and **20**, building on the high structural similarity between the two ligands. All the generated conformers were subjected to a rigid body superposition on the top MM-GBSA scored pose of **20** as displayed in Figure 7C. Similarly, all the conformations projected the 3,4,5-trimethoxyphenyl motif toward a binding site region hindered by W119 and L164 side chains, where steric clashes hampered complex stabilization (figure 7C). Upon comparing figure 7B and figure 7C, the insertion of an oxymethylene bridge for **20** enabled a different orientation of the 3,4,5-trimethoxyphenyl fragment thus evading the bulky pocket lined by W119 and L164.

Additionally, we performed molecular docking simulations for compound **18** by adopting the structure of *h*MAO B in complex with a potent coumarin inhibitor (coded as inhibitor 1 in ref. [45] , PDB code: 7P4F) as crystallographic template. In this X-ray structure, atypical conformations are experienced by the side chains of both W119 and L164 shaping a wider entrance cavity. Remarkably, this protocol allowed us to obtain docking poses for **18**, further supporting the crucial role of W119 and L164 conformations in accommodating this inhibitor within MAO B. Figure 7D shows the top MM-GBSA scored docking pose, where complex stabilization was predicted to be the result of π-π (Y398) and hydrophobic (F103, W119, L164, I199, Y326) interactions. More importantly, the computed MM-GBSA binding free energy of **18** (-29.04 kcal/mol) was significantly lower than **20** within 4A79 binding site (-63.61 kcal/mol). These data are in full agreement with in vitro inhibition data showing ≈30-fold activity difference for **18** and **20**, despite

quite high structural similarity.

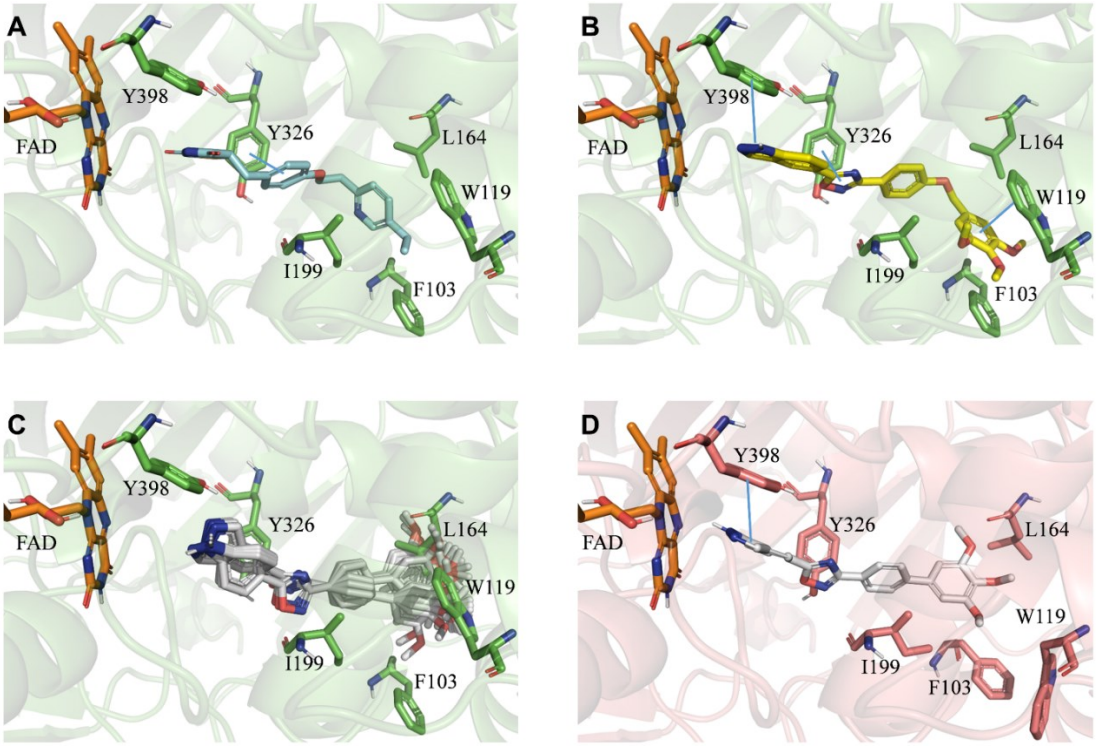

Figure 7. Molecular docking simulations for compounds **18** and **20** with *h*MAO B. A) X-ray coordinates of pioglitazone within the MAO B binding site (PDB code: 4A79, green); B) Top MM-GBSA scored docking pose returned by **20** within the binding site of MAO B (PDB code: 4A79, green). C) Conformers of **18** generated by *Confgen* within the binding site of MAO B (PDB code: 4A79, green). D) Top MM-GBSA scored docking pose returned by **18** within the binding site of MAO B (PDB code: 7P4F, red). A) B) C) D) FAD, ligands and important residues are rendered as sticks, the protein as cartoon and its binding pocket as surface. Carbon atoms of FAD coenzyme are coloured in orange. Arene-arene interactions are itemized by blue lines. For the sake of clarity, only polar hydrogen atoms are shown.

Remarkably, docking simulations of **20** on the binding site of MAO A in complex with harmine (PDB code: 2Z5X, [46]) produced no poses in full agreement with the experimental inhibitory data in Table 1, thus putting forward the herein adopted docking protocol as valuable tool for providing reliable predictions of MAO B selectivity.

3.5 Binding mode analysis of 20 to *h*MAO B

The mechanism of *h*MAO B inhibition of compound **20** was deeply investigated. Since this compound seemed to interfere with the horseradish peroxidase-coupled assay, we employed a direct assay based on 1-methyl-4-(1-methyl-1*H*-pyrrol-2-yl)-1,2,3,6-tetrahydropyridine (MMTP) as

substrate. The measurement of *h*MAO B activity in steady-state conditions showed a linear profile only in the first few seconds, reaching a plateau after 4-5 minutes. This behavior has been previously observed for other tight-binding inhibitors of *h*MAO B [45]. Aiming at studying tight-binding inhibition mechanism, IC_{50} values were determined at four different enzyme concentrations. The IC_{50} vs. [enzyme] plot showed a linear trend (figure 8A), thus confirming the tight-binding behavior. Therefore, K_i value was determined using the Morrison's equation, which returned K_i = 6.8 ± 0.3 μM (figure 8B). This micromolar value appears inconsistent with the nanomolar IC_{50} value determined during *in vitro* screenings (Table 1), likely because tight-binding inhibitors are often reported to be slow binders [47]. To address this issue, we evaluated the effect of incubation interval by determining the Michaelis-Menten curve of *h*MAO B activity in the presence of **20** (100 μM) in both steady-state and after 30 minutes of pre-incubation (figure 8C). As a matter of fact, after incubation the enzyme is almost inactive, suggesting that **20** is a potent *h*MAO B inhibitor although it has a slow binding kinetics.

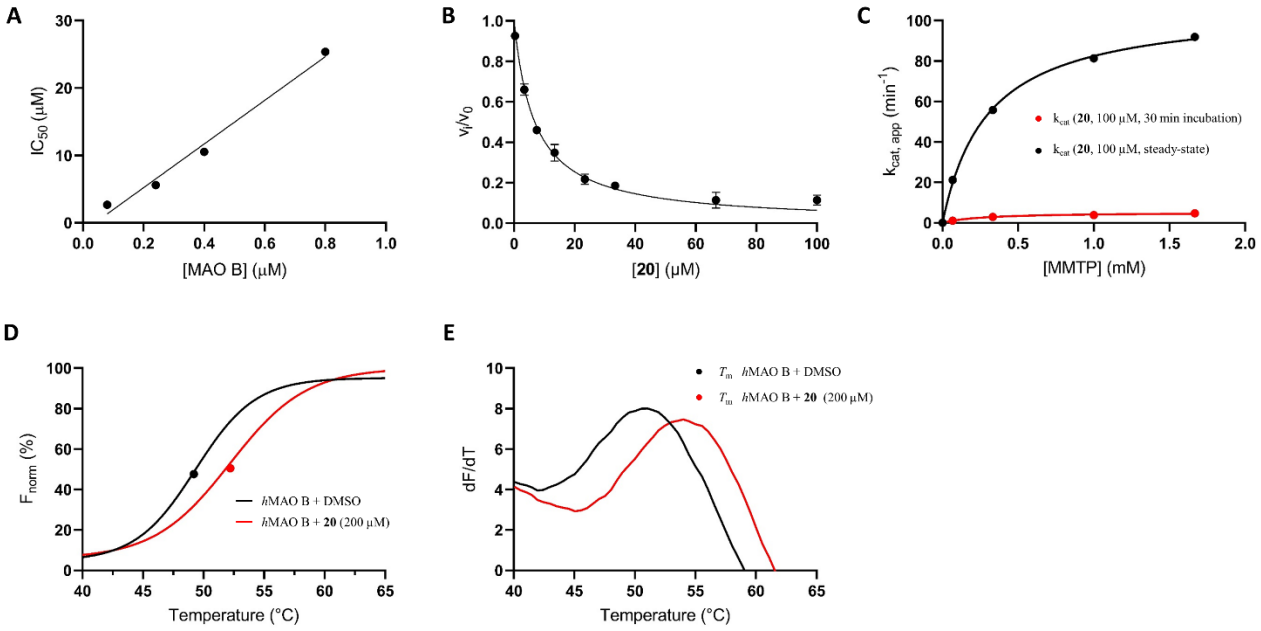

Figure 8. (A) Linear trend of IC_{50} values determined at increasing enzyme concentrations, suggesting a tight-binding inhibition mechanism; (B) Plot of residual enzyme velocity data points as a function of inhibitor concentration, fitted to the Morrison's equation. On y axis, v_i and v_0 are the initial velocity values in the presence and absence of **20**, respectively; (C) Michaelis-Menten curves determined in the presence of **20** (100 μM), in steady-state (black) and after 30 minutes of incubation (red); (D) Boltzmann function fitting of thermal stability curves, plotted as normalized fluorescence signal. The inflection points corresponding to T_m values are indicated with black (DMSO) and red (**20**) dots; (E) Graphs showing the first derivative of the sigmoidal curves showed in figure D, whose maximum peaks correspond to the unfolding temperature values (T_m). Data were first normalized by setting the highest and lowest fluorescence intensity value in each set to 100 and 0%, respectively. Protein melting temperatures were calculated based on a Boltzmann function

fitting to experimental data with GraphPad Prism™ (Inc., San Diego, CA). *h*MAOB concentration: 8.5 μM.

Moreover, thermal stability curves were recorded by measuring the fluorescence intensity of the enzyme flavin cofactor [48], used as an intrinsic probe during a temperature gradient from 40 to 65 °C in the presence of DMSO or **20** (200 μM). During the unfolding process, a remarkable T_m shift (+2.9 °C, figure 8D and 8E) was observed in the presence of compound **20**, which is consistent with the stabilization provided by tight-binders.

4. Conclusion

Recently, MAOs have been reconsidered as valuable targets for the cure of several pathologies. In particular, B isoenzyme has received great attention as ROS source in the field of neurodegenerative disorders including AD. In the present work, we described a hybridization strategy providing novel 5-susbtituted-1*H*-indazoles as potent and selective inhibitors of *h*MAO B. Structural exploration mainly addressed the bridge linking the heterocyclic core with a lipophilic motif. SAR analysis revealed the key role played by molecular flexibility within the terminal biphenyl fragment in improving MAO B activity and selectivity. The bioisosteric introduction of 1,2,4-oxadiazole cycle as the linker led us identifying several submicromolar compounds (**20**, **23**, **25**), which also scored a mild aqueous solubility enhancement compared to amide analogues. Compound **20** emerged as the most potent *h*MAO B inhibitor with an IC_{50} = 52 nM and a great selectivity over MAO A. Moreover, it was endowed with a good chemical stability in different hydrolytic conditions. **20** enabled promising cytoprotective effects against hydrogen peroxide insults in neuroblastoma and, more remarkably, in astrocytes cultures. Computational analysis based on molecular docking simulations indicated the main molecular determinants for the binding of this class of compounds with target enzyme (MAO B). The conformational flexibility of inhibitor **20**, arising from a $–OCH_2–$ bridge, allowed a proper orientation of the 3,4,5-trimethoxyphenyl motif, escaping steric hindrance of W119 and L164 side chains. This rotational feature is essential for obtaining higher shape complementarity with MAO B as compared to more rigid and less active analogue **18**. Steady-state kinetics coupled with thermal shift curves highlighted a tight-binding behaviour for **20**. This prototype herein described could be considered a promising starting hit, deserving further optimization to develop therapeutic small molecules based on the reversible and selective inhibition of MAO B.

5. Experimental section

5.1 Chemistry. General methods

Starting materials, reagents, and analytical grade solvents were purchased from Sigma-Aldrich, Alfa-Aesar or Fluorochem (Europe). The purity of all the intermediates, checked by RP-HPLC, was always better than 95%. RP-HPLC analyses were performed on an Analytic Agilent 1260 Infinity multidetector system equipped with automatic sampler and a 1200 series UV-diode array detector using a Gemini 3 μm C18 column (150 mm × 4.6 mm I. D.). The UV detection was measured at 220 and 254 nm. Each tested compound was analysed by isocratic elution with a different mobile phase system: methanol/ammonium formate buffer (15 mM, pH 5.0) mixtures (composition ranging from 80% to 60% methanol) or acetonitrile/ammonium formate buffer (15 mM, pH 5.0) mixtures (from 80% to 65% acetonitrile) at a flow rate of 0.3 or 0.5 mL/min. All the newly prepared and tested compounds showed purity higher than 95% (elemental analysis). Elemental analyses were performed on the EuroEA 3000 analyzer only on the final compounds tested as MAOs inhibitors. The measured values for C, H, and N agreed to within ± 0.40% of the theoretical values. Microwave reactions were performed in a Milestone MicroSynth apparatus, setting temperature and hold times, fixing maximum irradiation power to 500 W and heating ramp times to 2 minutes. Column chromatography was performed using Merck silica gel 60 (0.063-0.200 mm, 70-230 mesh). Flash chromatographic separations were performed on Biotage SP1 purification system using flash cartridges prepacked with KP-Sil 32-63 μm, 60 Å silica. All reactions were routinely checked by TLC using Merck Kieselgel 60 F_{254} aluminum plates and visualized by UV light. Regarding the reaction requiring the use of anhydrous solvents, the glassware was flame-dried and then cooled under a stream of dry argon before the use. Nuclear magnetic resonance spectra were recorded on a Varian Mercury 300 instrument (at 300 MHz) or on an Agilent Technologies 500 apparatus (at 500 MHz) at ambient temperature in the specified deuterated solvent. Chemical shifts (δ) are quoted in parts per million (ppm) and are referenced to the residual solvent peak. The coupling constants *J* are given in Hertz (Hz). The following abbreviations were used: s (singlet), d (doublet), dd (doublet of doublets), t (triplet), dt (doublet of triplets), ddd (doublet of doublet of doublets), tt (triplet of triplets), m (multiplet), br s (broad signal); signals due to OH and NH protons were located by deuterium exchange with D_2O. HRMS experiments were performed with a dual electrospray interface (ESI) and a quadrupole time-of-flight mass spectrometer (Q-TOF, Agilent 6530 Series Accurate-Mass Quadrupole Time-of-Flight LC/MS, Agilent Technologies Italia S.p.A., Cernusco sul Naviglio, Italy). Full-scan mass spectra were recorded in the mass/charge (m/z) range 50-3000 Da. Melting points for solid final compounds were determined by the capillary method on a Stuart

Scientific SMP3 electrothermal apparatus and are uncorrected.

*5.1.2 Synthesis of intermediates **1a-j***

*5.1.2.1 4-Bromo-N-(1H-indazol-5-yl)benzenesulfonamide (**1a**)*

5-Aminoindazole (2.5 mmol, 0.34 g) was dissolved in THF (20 mL), followed by the addition of DIPEA (3.8 mmol, 0.65 mL) and 4-bromosulfonyl chloride (2.5 mmol, 0.65 g). The reaction mixture was stirred at room temperature for 4 h. The mixture was then concentrated and purified through column chromatography (gradient eluent: ethyl acetate in dichloromethane, 0% → 20%). Yield: 61%. ^{1}H NMR (500 MHz, DMSO-d_6) δ: 13.03 (s, 1H, dis. with D_2O), 10.12 (s, 1H, dis. with D_2O), 7.98 (s, 1H), 7.71 (d, J = 8.6 Hz, 2H), 7.57 (d, J = 8.6 Hz, 2H), 7.44 – 7.37 (m, 2H), 7.04 (dd, J = 8.9, 1.8 Hz, 1H).

*5.1.2.2 General procedure for the synthesis of amides **1b-1e, 1i***

The commercially available carboxylic acid (2.0 mmol) was dissolved in anhydrous DMF (16 mL). 1-Hydroxybenzotriazole (HOBt, 5.0 mmol, 0.77 g) and *N*-(3- dimethylaminopropyl)-*N*′-ethylcarbodiimide hydrochloride (EDC·HCl, 5.0 mmol, 0.96 g) were added to the solution and the reaction mixture was left under magnetic stirring for 30 minutes. After this time, appropriate ammine (4.0 mmol) was added and the reaction was stirred at room temperature overnight. To obtain amides **1d**-**e**, the reaction mixture was poured onto ice and filtered. The precipitate was collected and thorough washed with water, followed by Et_2O/*n*-hexane (4.5/0.5 v/v) mixture and $CHCl_3$, thus furnishing desired products as solids. In all other cases, the reaction mixture was purified as detailed below.

*5.1.2.2.1 N-(1H-indazol-5-yl)-4-iodobenzamide (**1b**)*

Prepared from 4-iodobenzoic acid (2.0 mmol, 0.50 g) and 5-aminoindazole (4.0 mmol, 0.53 g). Purification procedure: the reaction mixture was diluted with water (100 mL) and then filtered. The solid was collected and washed with methanol affording the desired amide as an off-white solid. Yield: 81%. ^{1}H NMR (500 MHz, DMSO-d_6) δ: 13.00 (s, 1H, dis. with D_2O), 10.28 (s, 1H, dis. with D_2O), 8.21 (s, 1H), 8.04 (s, 1H), 7.91 (d, J = 8.4 Hz, 2H), 7.75 (d, J = 8.4 Hz, 2H), 7.60 (dd, J = 8.9, 1.7 Hz, 1H), 7.50 (d, J = 8.9 Hz, 1H).

*5.1.2.2.2 N-(1H-indazol-5-yl)-3-iodobenzamide (**1c**)*

Prepared from 3-iodobenzoic acid (2.0 mmol, 0.50 g) and 5-aminoindazole (4.0 mmol, 0.53 g). Purification procedure: the reaction mixture was poured onto ice. The resulting precipitate was collected after filtration and washed with water followed by methanol, thus furnishing the desired product as a dark pink solid that was used without further purification. Yield: 86%. ^{1}H NMR (500 MHz, DMSO-d_6) δ: 13.00 (s, 1H, dis. with D_2O), 10.31 (s, 1H, dis. with D_2O), 8.30 (t, J = 1.5 Hz, 1H), 8.21 (s, 1H), 8.05 (s, 1H), 7.97 (dt, J = 7.8, 1.5 Hz, 1H), 7.93 (ddd, J = 7.8, 1.5, 1.0 Hz, 1H), 7.61 (dd, J = 8.9, 1.8 Hz, 1H), 7.51 (d, J = 8.9 Hz, 1H), 7.33 (t, J = 7.8 Hz, 1H).

*5.1.2.2.3 N-(4-Bromophenyl)-1H-indazole-5-carboxamide (**1d**)*

Prepared from 1*H*-indazole-5-carboxylic acid (2.0 mmol, 0.32 g) and 4-bromoaniline (4.0 mmol, 0.68 g). Yield: 63%. ^{1}H NMR (300 MHz, DMSO-d_6) δ: 13.32 (s, 1H, dis. with D_2O), 10.36 (s, 1H, dis. with D_2O), 8.45 (s, 1H), 8.25 (s, 1H), 7.92 (dd, J = 8.9, 1.1 Hz, 1H), 7.77 (d, J = 8.7 Hz, 2H), 7.62 (d, J = 8.9 Hz, 1H), 7.52 (d, J = 8.7 Hz, 2H).

*5.1.2.2.4 N-(3-bromophenyl)-1H-indazole-5-carboxamide (**1e**)*

Prepared from 1*H*-indazole-5-carboxylic acid (2.0 mmol, 0.32 g) and 3-bromoaniline (4.0 mmol, 0.68 g). Yield: 43%. ^{1}H NMR (500 MHz, DMSO-d_6) δ: 13.34 (s, 1H, dis. with D_2O), 10.38 (s, 1H, dis. with D_2O), 8.47 (s, 1H), 8.26 (s, 1H), 8.13 (s, 1H), 8.02 – 7.54 (m, 3H), 7.39 – 7.19 (m, 2H).

*5.1.2.2.5 N-(1H-indazol-5-yl)-4-methoxybenzamide (**1i**)*

Prepared from 4-methoxybenzoic acid (4.0 mmol, 0.60 g), 5-aminoindazole (8.0 mmol, 1.1 g), HOBt (10 mmol, 1.4 g), EDC·HCl (10 mmol, 1.9 g) in anhydrous DMF (30 Ml). Purification procedure: the reaction mixture was poured onto ice and filtered. The resulting precipitate was collected and washed with water followed by methanol, giving the desired product as a grey solid. Yield: 90%. ^{1}H NMR (500 MHz, DMSO-d_6) δ: 12.97 (s, 1H, dis. with D_2O), 10.08 (s, 1H, dis. with D_2O), 8.20 (d, J = 1.7 Hz, 1H), 8.03 (s, 1H), 7.97 (d, J = 8.9 Hz, 2H), 7.61 (dd, J = 8.9, 1.7 Hz, 1H), 7.49 (d, J = 8.9 Hz, 1H), 7.05 (d, J = 8.9 Hz, 2H), 3.82 (s, 3H).

*5.1.2.3 General procedure for the synthesis of intermediates **1f-g***

5-Hydroxyindazole (1.4 mmol, 0.19 g) was dissolved in absolute EtOH (for **1f**, 10 mL) or DMF (for **1g**, 10 mL), before the addition of K_2CO_3 (4.6 mmol, 0.44 g), 4-bromobenzyl bromide (for **1f**, 2.0 mmol, 0.50 g) or 3-bromobenzyl bromide (for **1g**, 2.0 mmol, 0.50 g) and a catalytic amount of KI (for **1f**). The reaction mixture was heated (16 h under reflux for **1f**; 48 h at 90 °C for **1g**), then cooled to room temperature and concentrated to dryness. The resulting crude solid was purified as indicated below.

*5.1.2.3.1 5-[(4-Bromobenzyl)oxy]-1H-indazole (**1f**)*

Purified by column chromatography (gradient eluent: ethyl acetate in dichloromethane, 1% → 5%). Yield: 34%. ^{1}H NMR (300 MHz, $CDCl_3$) δ: 8.01 (s, 1H), 7.53 (d, *J* = 8.2 Hz, 2H), 7.47 (d, *J* = 9.1 Hz, 1H), 7.34 (d, *J* = 8.2 Hz, 2H), 7.18 (dd, *J* = 9.1, 2.2 Hz, 1H), 7.14 (d, *J* = 2.2 Hz, 1H), 5.06 (s, 2H), NH not detected.

*5.1.2.3.2 5-[(3-Bromobenzyl)oxy]-1H-indazole (**1g**)*

Purification procedure: the mixture was suspended in water (50 mL), then extracted with $CHCl_3$ (3 x 30 mL). The collected organic layers were dried over anhydrous Na_2SO_4, concentrated under rotatory evaporation and purified by column chromatography (eluent: methanol in dichloromethane, 2%). Yield: 45%. ^{1}H NMR (300 MHz, DMSO-d_6) δ: 12.90 (s, 1H, dis. with D_2O), 7.93 (s, 1H), 7.66 (t, *J* = 1.6 Hz, 1H), 7.51 (ddd, *J* = 7.8, 2.0, 1.2 Hz, 1H), 7.49 – 7.45 (m, 1H), 7.44 (d, *J* = 8.9 Hz, 1H), 7.34 (t, *J* = 7.8 Hz, 2H), 7.23 (d, *J* = 2.2 Hz, 1H), 7.07 (dd, *J* = 8.9, 2.2 Hz, 1H), 5.12 (s, 2H).

*5.1.2.4 N-(1H-indazol-5-yl)benzamide (**1h**)*

1*H*-Indazol-5-amine (1.0 mmol, 0.13 g) was suspended in THF (7 mL) followed by the addition of DIEA (1.0 mmol, 0.17 mL). After cooling at 0 °C, a solution of benzoyl chloride (1.0 mmol, 0.12 mL) in THF (1 mL) was added dropwise to the mixture, that was kept under magnetic stirring overnight. The solvent was removed under reduced pressure and the resulting crude was crystallized from ethanol. Yield: 56%. ^{1}H NMR (500 MHz, DMSO-d_6) δ: 12.99 (s, 1H, dis. with D_2O), 10.24 (s,

1H, dis. with D_2O), 8.23 (d, *J* = 1.8 Hz, 1H), 8.04 (s, 1H), 7.99 – 7.94 (m, 2H), 7.62 (dd, *J* = 8.9, 1.8 Hz, 1H), 7.60 – 7.55 (m, 1H), 7.54 – 7.49 (m, 3H).

*5.1.2.5 4-Hydroxy-N-(1H-indazol-5-yl)benzamide (**1j**)*

Anhydrous $AlCl_3$ (13 mmol, 1.8 g) was added to a suspension of intermediate **1i** (3.3 mmol, 0.90 g) in *o*-xylene (13 mL). The reaction mixture was refluxed for 9 h. After cooling to room temperature, the solvent was evaporated under reduced pressure and aq. 1 N HCl (50 mL) was added to the resulting crude. The precipitate was collected after thoroughly washing with H_2O until neutral pH, thus yielding the desired product. Yield: 41%. ^{1}H NMR (300 MHz, DMSO-d_6) δ: 12.95 (s, 1H, dis. with D_2O), 10.03 (s, 1H, dis. with D_2O), 9.97 (s, 1H, dis. with D_2O), 8.18 (s, 1H), 8.01 (s, 1H), 7.84 (d, *J* = 8.5 Hz, 2H), 7.59 (d, *J* = 8.9 Hz, 1H), 7.47 (d, *J* = 8.9 Hz, 1H), 6.84 (d, *J* = 8.5 Hz, 2H).

5.1.3 Synthesis of 1H-indazole-5-carbonitrile

$Pd_2(dba)_3$ (0.32 mmol, 0.26 g), 2-dicyclohexylphosphino-2′,4′,6′-triisopropylbiphenyl (XPhos, 0.65 mmol, 0.32 g) and $Zn(CN)_2$ (8.0 mmol, 0.95 g) were added to a solution of 5-bromo-1*H*-indazole (6.5 mmol, 1.3 g) in a DMF/H_2O mixture (30 mL, 99/1, v/v). The vessel was placed in a microwave apparatus and irradiated at 160 °C for 30 minutes. The reaction was then cooled to room temperature. This protocol was repeated twice on the same reaction scale, then the reaction mixtures were collected and the work-up was carried out as follows. After dilution with 200 mL of aq. 1 N NaOH and extraction with ethyl acetate (3 x 150 mL), the organic phases were combined, washed with brine (2 x 80 mL) and dried over anhydrous Na_2SO_4. The solvent was evaporated under reduced pressure and the resulting dark oil residue was purified by flash chromatography (gradient eluent: ethyl acetate in *n*-hexane, 5% → 30%) yielding the desired product as a white solid. Yield: 71%. ^{1}H NMR (300 MHz, DMSO-d_6): δ 13.58 (s, 1H, dis. with D_2O), 8.39 (s, 1H), 8.25 (s, 1H), 7.70 (d, *J* = 8.6 Hz, 1H), 7.64 (d, *J* = 8.6 Hz, 1H).

5.1.4 Synthesis of amidoxime intermediates

5.1.4.1 General procedure for the synthesis of amidoximes

The appropriate nitrile (1 eq) was dissolved in absolute ethanol (0.3 M nitrile concentration). Hydroxylamine (50% wt. in water, 8 eq) was then added and the mixture was stirred at room

temperature for 72 hours. The solvent was evaporated under vacuum, furnishing desired products as white solids that were used without further purification.

5.1.4.1.1 N'-hydroxy-3-iodobenzenecarboximidamide

Prepared from 3-iodobenzonitrile (9.0 mmol, 2.1 g) and hydroxylamine (50% wt. in water, 72 mmol, 4.5 mL). Quantitative yield. ^{1}H NMR (300 MHz, DMSO-d_6) δ: 9.73 (s, 1H, dis. with D_2O), 8.00 (t, J = 1.7 Hz, 1H), 7.71 (ddd, J = 7.8, 1.7, 1.1 Hz, 1H), 7.67 (ddd, J = 7.8, 1.7, 1.1 Hz, 1H), 7.16 (t, J = 7.9 Hz, 1H), 5.85 (s, 2H, dis. with D_2O).

5.1.4.1.2 N'-hydroxy-4-iodobenzenecarboximidamide

Prepared from 4-iodobenzonitrile (9.0 mmol, 2.1 g) and hydroxylamine (50% wt. in water, 72 mmol, 4.5 mL). Quantitative yield. ^{1}H NMR (300 MHz, DMSO-d_6) δ: 9.69 (s, 1H, dis. with D_2O), 7.71 (d, J = 8.2 Hz, 2H), 7.45 (d, J = 8.2 Hz, 2H), 5.82 (s, 2H, dis. with D_2O).

*5.1.4.1.3 N'-hydroxy-1H-indazole-5-carboximidamide (**1k**)*

Prepared from 1*H*-indazol-5-carbonitrile (9.0 mmol, 1.3 g) and hydroxylamine (50% wt. in water, 72 mmol, 4.5 mL). Yield: 97%. ^{1}H NMR (300 MHz, DMSO-d_6) δ: 13.09 (s, 1H, dis. with D_2O), 9.52 (s, 1H, dis. with D_2O), 8.08 (s, 1H), 8.03 (s, 1H), 7.70 (d, J = 8.8 Hz, 1H), 7.48 (d, J = 8.8 Hz, 1H), 5.79 (s, 2H, dis. with D_2O).

*5.1.4.1.4 N'-hydroxy-3-[(3,4,5-trimethoxybenzyl)oxy]benzenecarboximidamide (**1t**)*

Prepared from **1q** (0.90 mmol, 0.28 g) and hydroxylamine (50% wt. in water, 7.2 mmol, 0.45 mL). Yield: 96%. ^{1}H NMR (300 MHz, $CDCl_3$) δ: 7.33 – 7.26 (m, 2H), 7.19 (dt, J = 7.5, 1.3 Hz, 1H), 7.04 (ddd, J = 8.1, 2.5, 0.9 Hz, 1H), 6.66 (s, 2H), 5.37 (s, 2H, dis. with D_2O), 5.00 (s, 2H), 3.85 (s, 6H), 3.84 (s, 3H), OH not detected.

*5.1.4.1.4.1 3-[(3,4,5-Trimethoxybenzyl)oxy]benzaldehyde (**1p**)*

3-Hydroxybenzaldehyde (8.0 mmol, 0.98 g) was dissolved in anhydrous THF (25 mL) before adding 3,4,5-trimethoxybenzyl alcohol (4.0 mmol, 0.48 mL) and PPh_3 (8.8 mmol, 2.4 g). Diisopropyl azodicarboxylate (DIAD, 8.0 mmol, 1.6 mL), previously dissolved in THF (5 mL), was added dropwise while cooling at 0-5 °C with an external ice bath. The reaction mixture was kept under magnetic stirring at room temperature for 72 h, then concentrated under reduced pressure and purified by column chromatography (gradient eluent: dichloromethane in *n*-hexane,

40% → 100%). Yield: 70%. ^{1}H NMR (500 MHz, $CDCl_3$) δ: 9.99 (s, 1H), 7.52–7.43 (m, 3H), 7.31 – 7.20 (m, 1H), 6.67 (s, 2H), 5.05 (s, 2H), 3.88 (s, 6H), 3.86 (s, 3H).

*5.1.4.1.4.2 3-[(3,4,5-Trimethoxybenzyl)oxy]benzonitrile (**1q**)*

Intermediate **1p** (1.8 mmol, 0.56 g) and triethylamine (2.0 mmol, 0.28 mL) were added to a suspension of hydroxylamine hydrochloride (1.8 mmol, 0.13 g) in anhydrous acetonitrile (8 mL) while cooling at 0-5 °C through an external ice bath. The reaction mixture was kept under magnetic stirring at room temperature for 1 h. Then phthalic anhydride (1.9 mmol, 0.28 g) was added portionwise to the mixture and the reaction was refluxed for 18 h. After cooling to room temperature, the solvent was removed under rotary evaporation. The resulting crude was dissolved in dichloromethane (120 mL) and washed with 5% ammonia solution (3 x 40 mL). The organic layer was dried over anhydrous Na_2SO_4 and then concentrated under reduced pressure. The resulting crude solid was purified by flash chromatography (gradient eluent: ethyl acetate in *n*-hexane, 10% → 30%). Yield: 56%. ^{1}H NMR (500 MHz, $CDCl_3$) δ: 7.39 (t, J = 7.9 Hz, 1H), 7.29 – 7.26 (m, 1H), 7.23 – 7.18 (m, 2H), 6.64 (s, 2H), 5.00 (s, 2H), 3.88 (s, 6H), 3.86 (s, 3H).

*5.1.4.1.5 N'-hydroxy-4-[(3,4,5-trimethoxybenzyl)oxy]benzenecarboximidamide (**1w**)*

Prepared from **1s** (1.0 mmol, 0.30 g) and hydroxylamine (50% wt. in water, 8.0 mmol, 0.50 mL) in ethanol (3 mL). Yield: 98%. ^{1}H NMR (300 MHz, DMSO-d_6) δ: 9.43 (s, 1H, dis. with D_2O), 7.58 (d, J = 8.7 Hz, 2H), 6.98 (d, J = 8.7 Hz, 2H), 6.75 (s, 2H), 5.69 (s, 2H, dis. with D_2O), 5.00 (s, 2H), 3.75 (s, 6H), 3.62 (s, 3H).

*5.1.4.1.5.1 4-[(3,4,5-Trimethoxybenzyl)oxy]benzonitrile (**1s**)*

4-Cyanophenol (4.0 mmol, 0.48 g) was dissolved in anhydrous THF (15 mL) before adding (3,4,5-trimethoxyphenyl)methanol (2.0 mmol, 0.24 mL) and PPh_3 (4.4 mmol, 1.2 g). DIAD (4.0 mmol, 0.78 mL), previously dissolved in THF (2 mL), was added dropwise while cooling with an external ice bath at 0-5 °C. The reaction mixture was kept under magnetic stirring at room temperature for 72 h, then concentrated under reduced pressure and purified by column chromatography (gradient eluent: dichloromethane in *n*-hexane, 40% → 100%). Yield: 70%. ^{1}H NMR (300 MHz, $CDCl_3$) δ: 7.60 (d, J = 8.8 Hz, 2H), 7.03 (d, J = 8.8 Hz, 2H), 6.63 (s, 2H), 5.03 (s, 2H), 3.87 (s, 6H), 3.85 (s, 3H).

*5.1.4.2 Synthesis of amidoxime **1u***

*5.1.4.2.1 4-[(3,4,5-Trimethoxyphenoxy)methyl]benzonitrile (**1r**)*

3,4,5-Trimethoxyphenol (1.5 mmol, 0.28 g), 4-(bromomethyl)benzonitrile (1.7 mmol, 0.32 g) and K_2CO_3 (2.0 mmol, 0.28 g) were suspended in absolute ethanol (7 mL). Then, the reaction mixture was stirred at room temperature overnight. The mixture was filtered and the precipitate was thoroughly washed with dichloromethane. The resulting solution was concentrated to dryness and the resulting crude solid was purified by flash chromatography (gradient eluent: dichloromethane in *n*-hexane, 50% → 100%), yielding a white solid. Yield: 63%. ^{1}H NMR (500 MHz, $CDCl_3$) δ: 7.69 (d, *J* = 8.3 Hz, 2H), 7.55 (d, *J* = 8.3 Hz, 2H), 6.20 (s, 2H), 5.08 (s, 2H), 3.83 (s, 6H), 3.79 (s, 3H).

*5.1.4.2.2 N'-hydroxy-4-[(3,4,5-trimethoxyphenoxy)methyl]benzenecarboximidamide (**1u**)*

Intermediate **1r** (0.87 mmol, 0.26 g) was dissolved in absolute ethanol (4 mL) before adding hydroxylamine (50% wt. in water, 11 mmol, 0.72 mL). The mixture was stirred at room temperature for 72 h. The mixture was concentrated to dryness, furnishing desired product that was used without further purification. Yield: 95%. ^{1}H NMR (500 MHz, $CDCl_3$) δ: 7.65 (d, *J* = 8.2 Hz, 2H), 7.45 (d, *J* = 8.2 Hz, 2H), 6.20 (s, 2H), 5.31 (s, 2H, dis. with D_2O), 5.02 (s, 2H), 3.81 (s, 6H), 3.78 (s, 3H), OH not detected.

5.1.5 Synthesis of 1,2,4-oxadiazole intermediates

*5.1.5.1 General procedure for the cyclization to 1,2,4-oxadiazoles **1l-o***

In a flame-dried round-bottom flask, suitable carboxylic acid (3.0 mmol) was suspended in anhydrous dichloromethane (3 mL) followed by the addition of thionyl chloride (40 mmol, 3.0 mL). The reaction mixture was refluxed for 2 hours until a clear solution was obtained. After cooling to room temperature, the mixture was concentrated to dryness and the resulting residue was dissolved in anhydrous pyridine (20 mL) before adding an appropriate amidoxime (3.6 mmol). The reaction was refluxed for 5-20 hours until the disappearance of acyl chloride's spot in TLC control. After cooling to room temperature ethanol was added, yielding a white precipitate which was collected after filtration.

*5.1.5.1.1 5-[3-(3-Iodophenyl)-1,2,4-oxadiazol-5-yl]-1H-indazole (**1l**)*

Prepared from 1*H*-indazol-5-carboxylic acid (3.0 mmol, 0.48 g) and *N*'-hydroxy-3-iodobenzenecarboximidamide (3.6 mmol, 0.95 g). Yield: 63%. ^{1}H NMR (500 MHz, DMSO-d_6) δ:

13.53 (s, 1H, dis. with D_2O), 8.69 (s, 1H), 8.37 (t, *J* = 1.5 Hz, 1H), 8.30 (s, 1H), 8.11 – 8.05 (m, 2H), 7.96 (d, *J* = 7.9 Hz, 1H), 7.75 (d, *J* = 8.7 Hz, 1H), 7.38 (t, *J* = 7.9 Hz, 1H).

*5.1.5.1.2 5-[3-(4-Iodophenyl)-1,2,4-oxadiazol-5-yl]-1H-indazole (**1m**)*

Prepared from 1*H*-indazol-5-carboxylic acid (3.0 mmol, 0.48 g) and *N*'-hydroxy-4-iodobenzenecarboximidamide (3.6 mmol, 0.95 g). Yield: 68%. ^{1}H NMR (300 MHz, DMSO-d_6) δ: 13.54 (s, 1H, dis. with D_2O), 8.69 (s, 1H), 8.32 (s, 1H), 8.09 (d, *J* = 7.4 Hz, 1H), 7.97 (d, *J* = 6.7 Hz, 2H), 7.86 (d, *J* = 6.7 Hz, 2H), 7.77 (d, *J* = 7.4 Hz,1H).

*5.1.5.1.3 5-[5-(3-Iodophenyl)-1,2,4-oxadiazol-3-yl]-1H-indazole (**1n**)*

Prepared from 3-iodobenzoic acid (3.0 mmol, 0.75 g) and intermediate **1k** (3.6 mmol, 0.65 g). Yield: 75%. ^{1}H NMR (500 MHz, DMSO-d_6) δ: 13.39 (s, 1H, dis. with D_2O), 8.57 (s, 1H), 8.48 (t, *J* = 1.6 Hz, 1H), 8.25 (s, 1H), 8.20 (dt, *J* = 7.8, 1.6 Hz, 1H), 8.08 (ddd, *J* = 7.8, 1.6, 1.0 Hz, 1H), 8.03 (dd, *J* = 8.7, 1.5 Hz, 1H), 7.71 (d, *J* = 8.7 Hz, 1H), 7.45 (t, *J* = 7.8 Hz, 1H).

*5.1.5.1.4 5-[5-(4-Iodophenyl)-1,2,4-oxadiazol-3-yl]-1H-indazole (**1o**)*

Prepared from 4-iodobenzoic acid (3.0 mmol, 0.75 g) and intermediate **1k** (3.6 mmol, 0.65 g). Yield: 80%. ^{1}H NMR (300 MHz, DMSO-d_6) δ: 13.39 (s, 1H, dis. with D_2O), 8.55 (s, 1H), 8.25 (s, 1H), 8.04 (d, *J* = 8.3 Hz, 2H), 8.03 – 7.98 (m, 1H), 7.93 (d, *J* = 8.3 Hz, 2H), 7.71 (d, *J* = 8.7 Hz, 1H).

*5.1.6 Synthesis of final compounds **2-10, 14-19, 23-24***

*5.1.6.1 General procedure for the synthesis of final compounds **2-10, 14-19, 23-24***

In a pyrex vessel charged with a magnetic stirring bar, appropriate bromo- or iodo-intermediate (0.40 mmol; **1a**-**g**, **1l-o**) was suspended in a dioxane/water (3.2 mL/0.8 mL, 4/1, v/v) mixture. After 5 minutes, $Pd(PPh_3)_4$ (0.040 mmol, 0.046 g) and K_2CO_3 (0.80 mmol, 0.11 g) were added followed by the addition of a suitable boronic acid (0.80 mmol). The vessel was placed in the microwave apparatus and irradiated for 30 min at 150 °C. After cooling to room temperature, the mixture was

purified as detailed below.

*5.1.6.1.1 N-(1H-indazol-5-yl)-3',4',5'-trimethoxybiphenyl-4-sulfonamide (**2**)*

Prepared from **1a** (0.40 mmol, 0.14 g) and 3,4,5-trimethoxyphenylboronic acid (0.80 mmol, 0.17 g). Purification procedure: the mixture was concentrated under vacuum and purified by column chromatography (eluent: ethyl acetate in dichloromethane, 20%). The resulting solid was crystallized from ethanol. Yield: 68%; bright yellow solid; m.p.: 190-1 °C. ^{1}H NMR (500 MHz, DMSO-d_6) δ: 13.00 (s, 1H, dis. with D_2O), 10.12 (s, 1H, dis. with D_2O), 7.97 (s, 1H), 7.82 (d, J = 8.5 Hz, 2H), 7.72 (d, J = 8.5 Hz, 2H), 7.46 (d, J = 1.9 Hz, 1H), 7.41 (d, J = 8.9 Hz, 1H), 7.12 (dd, J = 8.9, 1.9 Hz, 1H), 6.92 (s, 2H), 3.82 (s, 6H), 3.66 (s, 3H). ^{13}C NMR (126 MHz, DMSO-d_6) δ: 153.70 (s), 144.58 (s), 138.43 (s), 138.35 (s), 138.02 (s), 134.32 (s), 133.87 (s), 130.72 (s), 127.71 (s), 127.59 (s), 123.28 (s), 122.38 (s), 112.85 (s), 111.17 (s), 104.98 (s), 60.50 (s), 56.45 (s). Anal. ($C_{22}H_{21}N_3O_5S$) calcd % C, 60.13; H, 4.82; N, 9.56; found % C, 60.01; H, 4.84; N, 9.31. HRMS (ESI) Calcd for ($C_{22}H_{21}N_3O_5S$): $[M-H]^-$ m/z: 438.1129, found 438.1120; $[M+Na]^+$ m/z: 462.1094, found 462.1097.

*5.1.6.1.2 3',5'-Difluoro-N-(1H-indazol-5-yl)biphenyl-4-sulfonamide (**3**)*

Prepared from intermediate **1a** (0.40 mmol, 0.14 g) and 3,5-difluorophenylboronic acid (0.80 mmol, 0.28 g). Purification procedure: the reaction mixture was suspended in water (10 mL) and extracted with $CHCl_3$ (3 x 20 mL). The collected organic layers were dried over Na_2SO_4. The solvent was removed under rotary evaporation and the resulting crude was purified by column chromatography (eluent: ethyl acetate in dichloromethane, 10%) affording a solid that was further crystallized from ethanol. Yield: 43%; yellow crystals; m.p.: 204-7 °C. ^{1}H NMR (300 MHz, acetone-d_6) δ: 12.22 (s, 1H, dis. with D_2O), 8.96 (s, 1H, dis. with D_2O), 7.98 (s, 1H), 7.90 – 7.77 (m, 4H), 7.61 (d, J = 1.9 Hz, 1H), 7.50 (d, J = 8.9 Hz, 1H), 7.41 – 7.32 (m, 2H), 7.25 (dd, J = 8.9, 1.9 Hz, 1H), 7.08 (tt, J = 9.0, 2.2 Hz, 1H). ^{13}C NMR (126 MHz, acetone-d_6) δ: 163.39 (dd, J = 247.0, 13.3 Hz), 142.69 (t, J = 9.7 Hz), 142.22 (t, J = 2.5 Hz), 139.90 (s), 138.40 (s), 133.84 (s), 130.38 (s), 127.83 (s), 127.51 (s), 123.49 (s), 122.91 (s), 114.01 (s), 110.53 (s), 110.20 (dd, J = 20.1, 6.4 Hz), 103.33 (t, J = 25.8 Hz). Anal. ($C_{19}H_{13}F_2N_3O_2S$) calcd % C, 59.22; H, 3.40; N, 10.90; found % C, 58.96; H, 3.55; N, 10.63. HRMS (ESI) Calcd for ($C_{19}H_{13}F_2N_3O_2S$): $[M-H]^-$ m/z: 384.0624, found 384.0635.

*5.1.6.1.3 4'-Cyano-N-(1H-indazol-5-yl)biphenyl-4-sulfonamide (**4**)*

Prepared from intermediate **1a** (0.40 mmol, 0.14 g) and 4-cyanophenylboronic acid (0.40 mmol, 0.141 g). Purification procedure: the mixture was concentrated under rotatory evaporation and purified by column chromatography (eluent: ethyl acetate in dichloromethane, 10%). Yield: 32%; white solid; m.p.: > 230 °C. ^{1}H NMR (500 MHz, acetone-d_6) δ: 12.21 (s, 1H, dis. with D_2O), 8.96 (s, 1H, dis. with D_2O), 7.98 (s, 1H), 7.90 (d, J = 8.8 Hz, 2H), 7.88 (d, J = 8.8 Hz, 2H), 7.87 – 7.83 (m, 4H), 7.61 (d, J = 1.8 Hz, 1H), 7.49 (d, J = 8.9 Hz, 1H), 7.25 (dd, J = 8.9, 1.8 Hz, 1H). ^{13}C NMR (126 MHz, DMSO-d_6) δ: 143.14 (s), 142.51 (s), 139.88 (s), 138.09 (s), 133.90 (s), 133.38 (s), 130.48 (s), 128.42 (s), 128.28 (s), 127.90 (s), 123.28 (s), 122.56 (s), 119.06 (s), 113.23 (s), 111.51 (s), 111.20 (s). Anal. ($C_{20}H_{14}N_4O_2S$) calcd % C, 64.16; H, 3.77; N, 14.96; found % C, 64.21; H, 3.80; N, 14.68. HRMS (ESI) Calcd for ($C_{20}H_{14}N_4O_2S$): $[M-H]^-$ m/z: 373.0765, found 373.0760; $[M+Na]^+$ m/z: 397.0730, found 397.0733.

*5.1.6.1.4 N-(1H-indazol-5-yl)-3',4',5'-trimethoxybiphenyl-4-carboxamide (**5**)*

Prepared from intermediate **1b** (0.40 mmol, 0.15 g) and 3,4,5-trimethoxyphenylboronic acid (0.80 mmol, 0.17 g). Purification procedure: the reaction mixture was suspended in brine (25 mL) and extracted with $CHCl_3$ (3 x 25 mL). The collected organic phases were dried over anhydrous Na_2SO_4 and concentrated to dryness. The corresponding crude was suspended in chloroform and the resulting precipitate was collected after filtration. This solid precipitate was then crystalized from absolute ethanol yielding the desired product as a white solid. Yield: 50%; white solid; m.p.: 229-231 °C (dec). ^{1}H NMR (500 MHz, DMSO-d_6) δ: 13.00 (s, 1H, dis. with D_2O), 10.28 (s, 1H, dis. with D_2O), 8.25 (s, 1H), 8.05 (s, 1H), 8.05 (d, J = 8.3 Hz, 2H), 7.85 (d, J = 8.3 Hz, 2H), 7.65 (dd, J = 8.9, 1.6 Hz, 1H), 7.52 (d, J = 8.9 Hz, 1H), 7.00 (s, 2H), 3.88 (s, 6H), 3.70 (s, 3H). ^{13}C NMR (126 MHz, DMSO-d_6) δ: 165.47 (s), 153.74 (s), 143.50 (s), 138.13 (s), 137.57 (s), 135.30 (s), 134.10 (s), 133.93 (s), 132.50 (s), 128.53 (s), 127.06 (s), 123.14 (s), 121.98 (s), 111.70 (s), 110.41 (s), 104.87 (s), 60.54 (s), 56.50 (s). Anal. ($C_{23}H_{21}N_3O_4$) calcd % C, 68.47; H, 5.25; N, 10.42; found % C, 68.22; H, 5.40; N, 10.09. HRMS (ESI) Calcd for ($C_{23}H_{21}N_3O_4$): $[M-H]^-$ m/z: 402.1459, found 402.1458.

*5.1.6.1.5 3',5'-Difluoro-N-(1H-indazol-5-yl)biphenyl-4-carboxamide (**6**)*

Prepared from intermediate **1b** (0.40 mmol, 0.14 g) and 3,5-difluorophenylboronic acid (0.80 mmol, 0.28 g). Purification procedure: the reaction mixture was diluted with brine (25 mL) and extracted

with $CHCl_3$ (3 x 25 mL). The collected organic phases were dried over anhydrous Na_2SO_4 and concentrated under rotary evaporation. The corresponding crude was suspended in chloroform and the precipitate was collected after filtration. The obtained solid was further crystallized from methanol furnishing the desired product as a white solid. Yield: 24%; white solid; m.p.: > 230 °C. ^{1}H NMR (300 MHz, DMSO-*d*$_6$) δ: 13.00 (s, 1H, dis. with D_2O), 10.33 (s, 1H, dis. with D_2O), 8.25 (s, 1H), 8.08 (d, *J* = 8.4 Hz, 2H), 8.05 (s, 1H), 7.92 (d, *J* = 8.4 Hz, 2H), 7.64 (dd, *J* = 8.9, 1.7 Hz, 1H), 7.59 – 7.54 (m, 2H), 7.51 (d, *J* = 8.9 Hz, 1H), 7.29 (tt, *J* = 9.4, 2.3 Hz, 1H). ^{13}C NMR (126 MHz, DMSO-*d*$_6$) δ 165.19 (s), 163.35 (dd, *J* = 245.9, 13.7 Hz), 143.13 (t, *J* = 9.9 Hz), 140.62 (t, *J* = 2.5 Hz), 137.59 (s), 135.40 (s), 133.94 (s), 132.43 (s), 128.76 (s), 127.31 (s), 123.13 (s), 121.90 (s), 111.69 (s), 110.52 (dd, *J* = 19.8, 6.2 Hz), 110.43 (s), 103.82 (t, *J* = 25.5 Hz). Anal. ($C_{20}H_{13}F_2N_3O$) calcd % C, 68.76; H, 3.75; N, 12.03; found % C, 68.63; H, 3.61; N, 11.90. HRMS (ESI) Calcd for ($C_{20}H_{13}F_2N_3O$): $[M-H]^-$ m/z: 348.0954, found 348.0950.

5.1.6.1.6 4'-Cyano-N-(1H-indazol-5-yl)biphenyl-4-carboxamide (7)

Prepared from intermediate **1b** (0.40 mmol, 0.14 g) and 4-cyanophenylboronic acid (0.80 mmol, 0.12 g). Purification procedure: the reaction mixture was partitioned between H_2O (25 mL) and $CHCl_3$, then extracted with $CHCl_3$ (3 x 25 mL). The collected organic layers were dried over anhydrous Na_2SO_4 and concentrated under rotary evaporation. The resulting crude was suspended in chloroform and the precipitate was collected after filtration. The solid was purified by column chromatography (gradient eluent: methanol in dichloromethane 2% → 3%), furnishing the desired product as a yellow solid. Yield: 22%; yellow solid; m.p.: > 230°C. ^{1}H NMR (300 MHz, DMSO-*d*$_6$) δ: 13.00 (s, 1H, dis. with D_2O), 10.34 (s, 1H, dis. with D_2O), 8.25 (br s, 1H), 8.11 (d, *J* = 8.4 Hz, 2H), 8.05 (s, 1H), 8.00 – 7.95 (m, 4H), 7.92 (d, *J* = 8.4 Hz, 2H), 7.65 (dd, *J* = 8.9, 1.5 Hz, 1H), 7.52 (d, *J* = 8.9 Hz, 1H). ^{13}C NMR (75 MHz, DMSO-*d*$_6$) δ: 165.23 (s), 144.04 (s), 141.35 (s), 137.60 (s), 135.49 (s), 133.94 (s), 133.39 (s), 132.43 (s), 128.87 (s), 128.27 (s), 127.50 (s), 123.13 (s), 121.89 (s), 119.21 (s), 111.69 (s), 111.10 (s), 110.44 (s). Anal. ($C_{21}H_{14}N_4O$) calcd % C, 74.54; H, 4.17; N, 16.56; found % C, 74.28; H, 4.33; N, 16.20. HRMS (ESI) Calcd for ($C_{21}H_{14}N_4O$): $[M-H]^-$ m/z: 337.1095, found 337.1091.

*5.1.6.1.7 N-(1H-indazol-5-yl)-3',4',5'-trimethoxybiphenyl-3-carboxamide (**8**)*

Prepared from **1c** (0.40 mmol, 0.15 g) and 3,4,5-trimethoxyphenylboronic acid (0.80 mmol, 0.17 g).

Purification procedure: the reaction mixture was diluted with H_2O (25 mL) and extracted with $CHCl_3$ (3 x 25 mL). The collected organic layers were dried over anhydrous Na_2SO_4 and concentrated under reduced pressure. The corresponding crude was suspended in chloroform and then the precipitate was filtered off. The solution was concentrated to dryness and the resulting crude was purified by column chromatography (gradient eluent: methanol in dichloromethane 2% → 3%), yielding a solid that was crystallized from $CHCl_3$/*n*-hexane. Yield: 58%; white solid; m.p.: 190-1 °C. ^{1}H NMR (500 MHz, acetone-d_6) δ: 12.20 (s, 1H, dis. with D_2O), 9.64 (s, 1H, dis. with D_2O), 8.40 (d, *J* = 1.8 Hz, 1H), 8.25 (s, 1H), 8.05 (s, 1H), 7.98 (d, *J* = 7.8 Hz, 1H), 7.86 (d, *J* = 7.8 Hz, 1H), 7.72 (dd, *J* = 8.9, 1.8 Hz, 1H), 7.59 (t, *J* = 7.8 Hz, 1H), 7.57 (d, *J* = 8.9 Hz, 1H), 7.03 (s, 2H), 3.94 (s, 6H), 3.79 (s, 3H). ^{13}C NMR (126 MHz, acetone-d_6) δ: 165.35 (s), 153.91 (s), 141.37 (s), 138.40 (s), 137.67 (s), 136.19 (s), 135.92 (s), 133.79 (s), 132.58 (s), 129.71 (s), 128.84 (s), 126.24 (s), 125.83 (s), 123.38 (s), 121.17 (s), 111.03 (s), 109.91 (s), 104.76 (s), 59.73 (s), 55.73 (s). Anal. ($C_{23}H_{21}N_3O_4$) calcd % C, 68.47; H, 5.25; N, 10.42; found % C, 68.19; H, 5.38; N, 10.17. HRMS (ESI) Calcd for ($C_{23}H_{21}N_3O_4$): $[M-H]^-$ m/z: 402.1459, found 402.1457.

*5.1.6.1.8 3',5'-Difluoro-N-(1H-indazol-5-yl)biphenyl-3-carboxamide (**9**)*

Prepared from **1c** (0.40 mmol, 0.15 g) and 3,5-difluorophenylboronic acid (0.80 mmol, 0.28 g). Purification procedure: the reaction mixture was partitioned between brine (25 mL) and $CHCl_3$, then extracted with $CHCl_3$ (3 x 25 mL). The collected organic layers were dried over anhydrous Na_2SO_4 and concentrated under rotary evaporation. The resulting crude was suspended in chloroform and the precipitate was collected after filtration. The obtained solid was crystallized from hot methanol furnishing the desired product as a white solid. Yield: 18%; white crystals; m.p: > 230 °C. ^{1}H NMR (500 MHz, DMSO-d_6) δ: 13.02 (s, 1H, dis. with D_2O), 10.34 (s, 1H, dis. with D_2O), 8.29 (t, *J* = 1.6 Hz, 1H), 8.23 (d, *J* = 1.2 Hz, 1H), 8.06 (s, 1H), 7.99 (dt, *J* = 7.8, 1.6 Hz, 1H), 7.95 (ddd, *J* = 7.8, 1.6, 1.1 Hz, 1H), 7.65 (d, *J* = 8.9 Hz, 1H), 7.64 (t, *J* = 7.8 Hz, 1H), 7.58 (dd, *J* = 9.0, 2.3 Hz, 2H), 7.53 (d, *J* = 8.9 Hz, 1H), 7.28 (tt, *J* = 9.3, 2.3 Hz, 1H). ^{13}C NMR (126 MHz, DMSO-d_6) δ: 165.42 (s), 163.36 (dd, *J* = 245.7, 13.6 Hz), 143.63 (t, *J* = 9.8 Hz), 138.09 (t, *J* = 2.4 Hz), 137.64 (s), 136.32 (s), 133.94 (s), 132.32 (s), 130.25 (s), 129.72 (s), 128.54 (s), 126.27 (s), 123.14 (s), 122.04 (s), 111.89 (s), 110.72 – 110.47 (m), 110.46 (s), 103.56 (t, *J* = 25.9 Hz). Anal. ($C_{20}H_{13}F_2N_3O$) calcd % C, 68.76; H, 3.75; N, 12.03; found % C, 69.13; H, 4.10; N, 11.77. HRMS (ESI) Calcd for ($C_{20}H_{13}F_2N_3O$): $[M-H]^-$ m/z: 348.0954, found 348.0948; $[M+Na]^+$ m/z: 372.0919, found 372.0929.

*5.1.6.1.9 4'-Cyano-N-(1H-indazol-5-yl)biphenyl-3-carboxamide (**10**)*

Prepared from intermediate **1c** (0.40 mmol, 0.15 g) and 4-cyanophenylboronic acid (0.80 mmol, 0.28 g). Purification procedure: the reaction mixture was poured onto ice. The resulting precipitate was collected after filtration, washed with chloroform and then crystallized from absolute ethanol. Yield: 22%; pink solid; m.p.: > 230 °C. ^{1}H NMR (500 MHz, DMSO-d_6) δ: 13.01 (s, 1H, dis. with D_2O), 10.37 (s, 1H, dis. with D_2O), 8.31 (t, J = 1.9 Hz, 1H), 8.24 (d, J = 1.6 Hz, 1H), 8.06 (s, 1H), 8.04 – 7.94 (m, 6H), 7.67 (t, J = 7.8 Hz, 1H), 7.63 (dd, J = 8.9, 1.6 Hz, 1H), 7.53 (d, J = 8.9 Hz, 1H). ^{13}C NMR (126 MHz, DMSO-d_6) δ: 165.46 (s), 144.46 (s), 138.79 (s), 137.62 (s), 136.43 (s), 133.95 (s), 133.39 (s), 132.35 (s), 130.41 (s), 129.83 (s), 128.50 (s), 128.29 (s), 126.55 (s), 123.14 (s), 121.96 (s), 119.26 (s), 111.82 (s), 110.88 (s), 110.47 (s). Anal. ($C_{21}H_{14}N_4O$) calcd % C, 74.54; H, 4.17; N, 16.56; found % C, 74.46; H, 4.11; N, 16.23. HRMS (ESI) Calcd for ($C_{21}H_{14}N_4O$): $[M-H]^-$ m/z: 337.1095, found 337.1094; $[M+Na]^+$ m/z: 361.1060, found 361.1066.

*5.1.6.1.10 N-(3',4',5'-trimethoxybiphenyl-4-yl)-1H-indazole-5-carboxamide (**14**)*

Prepared from intermediate **1d** (0.40 mmol, 0.13 g) and 3,4,5-trimethoxyphenylboronic acid (0.80 mmol, 0.17 g). Purification procedure: the reaction mixture was diluted with brine (25 Ml) and extracted with $CHCl_3$ (3 x 25 Ml). The collected organic layers were dried over anhydrous Na_2SO_4 and concentrated under reduced pressure. The corresponding crude solid was suspended in chloroform. The precipitate was collected after filtration and then crystallized from absolute ethanol furnishing the desired product as a white solid. Yield: 40%; white solid; m.p.: > 230 °C. ^{1}H NMR (500 MHz, DMSO-d_6) δ: 13.33 (s, 1H, dis. with D_2O), 10.33 (s, 1H, dis. with D_2O), 8.49 (s, 1H), 8.26 (s, 1H), 7.96 (dd, J = 8.8, 1.4 Hz, 1H), 7.88 (d, J = 8.7 Hz, 2H), 7.68 (d, J = 8.7 Hz, 2H), 7.64 (d, J = 8.8 Hz, 1H), 6.91 (s, 2H), 3.86 (s, 6H), 3.68 (s, 3H). ^{13}C NMR (126 MHz, DMSO-d_6) δ: 166.20 (s), 153.64 (s), 141.46 (s), 139.25 (s), 137.31 (s), 136.02 (s), 135.64 (s), 135.42 (s), 127.67 (s), 127.27 (s), 126.13 (s), 122.78 (s), 121.66 (s), 120.81 (s), 110.39 (s), 104.21 (s), 60.51 (s), 56.40 (s). Anal. ($C_{23}H_{21}N_3O_4$) calcd % C, 68.47; H, 5.25; N, 10.42; found % C, 68.62; H, 5.44; N, 10.05. HRMS (ESI) Calcd for ($C_{23}H_{21}N_3O_4$): $[M-H]^-$ m/z: 402.1459, found 402.1448.

*5.1.6.1.11 N-(3',4',5'-trimethoxybiphenyl-3-yl)-1H-indazole-5-carboxamide (**15**)*

Prepared from intermediate **1e** (0.40 mmol, 0.13 g) and 3,4,5-trimethoxyphenylboronic acid (0.80 mmol, 0.17 g). Purification procedure: the solvent was evaporated under vacuum. The resulting solid was suspended in brine (20 mL) and then extracted with ethyl acetate (3 x 20 mL). The combined organic layers were washed with water (1 x 20 mL) and brine (1 x 10 mL), then dried over anhydrous Na_2SO_4 and concentrated under rotatory evaporation. The resulting crude was purified through flash chromatography (gradient eluent: ethyl acetate in dichloromethane, 10% → 40%). Yield: 55%; dark yellow solid; m.p.: 119-121 °C. ^{1}H NMR (300 MHz, DMSO-*d*$_6$) δ: 13.34 (s, 1H, dis. with D_2O), 10.31 (s, 1H, dis. with D_2O), 8.49 (s, 1H), 8.26 (s, 1H), 8.03 – 7.98 (m, 1H), 7.96 (dd, *J* = 8.7, 1.5 Hz, 1H), 7.89 – 7.81 (m, 1H), 7.63 (d, *J* = 8.7 Hz, 1H), 7.42 (t, *J* = 7.6 Hz, 1H), 7.41 – 7.36 (m, 1H), 6.88 (s, 2H), 3.85 (s, 6H), 3.69 (s, 3H). ^{13}C NMR (126 MHz, DMSO-*d*$_6$) δ: 166.36 (s), 153.65 (s), 141.48 (s), 141.20 (s), 140.22 (s), 137.68 (s), 136.48 (s), 135.44 (s), 129.49 (s), 127.65 (s), 126.11 (s), 122.77 (s), 122.48 (s), 121.68 (s), 119.75 (s), 119.13 (s), 110.42 (s), 104.58 (s), 60.55 (s), 56.42 (s). Anal. ($C_{23}H_{21}N_3O_4$) calcd % C, 68.47; H, 5.25; N, 10.42; found % C, 68.16; H, 5.48; N, 10.10. HRMS (ESI) Calcd for ($C_{23}H_{21}N_3O_4$): [M-H]- m/z: 402.1459, found 402.1453.

*5.1.6.1.12 5-[(3',4',5'-Trimethoxybiphenyl-4-yl)methoxy]-1H-indazole (**16**)*

Prepared from intermediate **1f** (0.40 mmol, 0.12 g) and 3,4,5-trimethoxyphenylboronic acid (0.80 mmol, 0.17 g). Purification procedure: the reaction mixture was concentrated under rotatory evaporation. The resulting crude was suspended in $CHCl_3$. The inorganic solid was filtered off and the solution was purified by flash chromatography (eluent: ethyl acetate in dichloromethane, 20%). Yield: 72%; white solid; m.p.: 185-8 °C. ^{1}H NMR (500 MHz, $CDCl_3$) δ: 9.97 (s, 1H, dis. with D_2O), 7.99 (s, 1H), 7.59 (d, *J* = 8.1 Hz, 2H), 7.53 (d, *J* = 8.1 Hz, 2H), 7.42 (d, *J* = 8.8 Hz, 1H), 7.20 (s, 1H), 7.18 (dd, *J* = 8.8, 2.2 Hz, 1H), 6.79 (s, 2H), 5.15 (s, 2H), 3.93 (s, 6H), 3.90 (s, 3H). ^{13}C NMR (126 MHz, DMSO-*d*$_6$) δ: 149.07 (s), 148.72 (s), 136.30 (s), 132.99 (s), 132.00 (s), 131.35 (s), 131.28 (s), 129.74 (s), 123.17 (s), 122.57 (s), 118.78 (s), 114.85 (s), 105.95 (s), 99.70 (s), 96.94 (s), 65.60 (s), 56.20 (s), 51.46 (s). Anal. ($C_{23}H_{22}N_2O_4$) calcd % C, 70.75; H, 5.68; N, 7.17; found % C, 70.68; H, 5.71; N, 7.02. HRMS (ESI) Calcd for ($C_{23}H_{22}N_2O_4$): $[M-H]^-$ m/z: 389.1507, found 389.1501; $[M+Na]^+$ m/z: 413.1472, found 413.1474.

*5.1.6.1.13 5-[(3',4',5'-Trimethoxybiphenyl-3-yl)methoxy]-1H-indazole (**17**)*

Prepared from intermediate **1g** (0.40 mmol, 0.12 g) and 3,4,5-trimethoxyphenylboronic acid (0.80 mmol, 0.17 g). Purification procedure: the mixture was concentrated to dryness and the resulting crude was suspended in $CHCl_3$. The inorganic residue was filtered off and the solution was purified by column chromatography (gradient eluent: ethyl acetate in chloroform, 0% → 5%). Yield: 67%; pale yellow solid; m.p.: 189-192 °C. ^{1}H NMR (500 MHz, DMSO-*d*$_6$) δ: 12.90 (s, 1H, dis. with D_2O), 7.93 (s, 1H), 7.76 (s, 1H), 7.65 – 7.60 (m, 1H), 7.48 – 7.40 (m, 3H), 7.29 (s, 1H), 7.09 (d, *J* = 8.9 Hz, 1H), 6.90 (s, 2H), 5.18 (s, 2H), 3.84 (s, 6H), 3.68 (s, 3H). ^{13}C NMR (126 MHz, DMSO-*d*$_6$) δ: 153.64 (s), 153.20 (s), 140.91 (s), 138.27 (s), 137.57 (s), 136.24 (s), 133.28 (s), 129.33 (s), 127.16 (s), 126.72 (s), 126.67 (s), 123.49 (s), 118.85 (s), 111.53 (s), 104.60 (s), 101.81 (s), 93.19 (s), 70.06 (s), 60.51 (s), 56.38 (s). Anal. ($C_{23}H_{22}N_2O_4$) calcd % C, 70.75; H, 5.68; N, 7.18; found % C, 70.37; H, 5.50; N, 6.77. HRMS (ESI) Calcd for ($C_{23}H_{22}N_2O_4$): $[M-H]^-$ m/z: 389.1507, found 389.1504; $[M+Na]^+$ m/z: 413.1472, found 413.1479.

*5.1.6.1.14 5-[3-(3',4',5'-Trimethoxybiphenyl-4-yl)-1,2,4-oxadiazol-5-yl]-1H-indazole (**18**)*

Prepared from intermediate **1m** (0.40 mmol, 0.16 g) and 3,4,5-trimethoxyphenylboronic acid (0.80 mmol, 0.17 g). Purification procedure: the solvent was evaporated under reduced pressure thus furnishing a solid that was partitioned between brine (50 mL) and ethyl acetate (3 x 30 mL). The combined organic phases were dried over anhydrous Na_2SO_4 and the solvent was removed under rotary evaporation. The resulting crude was purified by column chromatography (gradient eluent: ethyl acetate in dichloromethane, 0% → 20%), yielding a solid that was crystallized from absolute ethanol to give pale yellow crystals. Yield: 20%; pale yellow crystals; m.p.: > 230 °C. ^{1}H NMR (500 MHz, DMSO-*d*$_6$) δ: 13.57 (s, 1H, dis. with D_2O), 8.74 (s, 1H), 8.35 (s, 1H), 8.17 (d, *J* = 8.4 Hz, 2H), 8.15 (dd, *J* = 8.9, 1.5 Hz, 1H), 7.94 (d, *J* = 8.4 Hz, 2H), 7.80 (d, *J* = 8.9 Hz, 1H), 7.03 (s, 2H), 3.89 (s, 6H), 3.71 (s, 3H). ^{13}C NMR (126 MHz, DMSO-*d*$_6$) δ: 176.56 (s), 168.39 (s), 153.76 (s), 143.67 (s), 141.92 (s), 138.13 (s), 135.92 (s), 135.20 (s), 128.00 (s), 127.95 (s), 125.54 (s), 125.52 (s), 123.40 (s), 123.04 (s), 116.12 (s), 111.97 (s), 104.76 (s), 60.55 (s), 56.48 (s). Anal. ($C_{24}H_{20}N_4O_4$) calcd % C, 67.28; H, 4.71; N, 13.08; found % C, 66.96; H, 4.93; N, 12.81. HRMS (ESI) Calcd for ($C_{24}H_{20}N_4O_4$): $[M-H]^-$ m/z: 427.1412, found 427.1408; $[M+Na]^+$ m/z: 451.1377, found 451.1378.

*5.1.6.1.15 5-[3-(3',4',5'-Trimethoxybiphenyl-3-yl)-1,2,4-oxadiazol-5-yl]-1H-indazole (**19**)*

Prepared from intermediate **1l** (0.40 mmol, 0.16 g) and 3,4,5-trimethoxyphenylboronic acid (0.80 mmol, 0.17 g). Purification procedure: the solvent was removed under rotary evaporation, thus obtaining a solid that was suspended with brine (50 mL) and extracted with ethyl acetate (3 x 30 mL). The combined organic phases were dried over anhydrous Na_2SO_4 and concentrated under reduced pressure. The resulting crude was purified by column chromatography (gradient eluent: ethyl acetate in dichloromethane, 0% → 20%), yielding a solid that was crystallized from absolute ethanol. Yield: 25%; white crystals; m.p.: > 230 °C. ^{1}H NMR (500 MHz, DMSO-*d*$_6$) δ: 13.57 (s, 1H, dis. with D_2O), 8.75 (br s, 1H), 8.34 (s, 1H), 8.31 (s, 1H), 8.15 (dd, *J* = 8.8, 1.5 Hz, 1H), 8.08 (d, *J* = 7.8 Hz, 1H), 7.93 (d, *J* = 7.8 Hz, 1H), 7.79 (d, *J* = 8.8 Hz, 1H), 7.69 (t, *J* = 7.8 Hz, 1H), 6.98 (s, 2H), 3.90 (s, 6H), 3.71 (s, 3H). ^{13}C NMR (126 MHz, DMSO-*d*$_6$) δ: 176.61 (s), 168.63 (s), 153.78 (s), 141.89 (s), 141.87 (s), 137.94 (s), 135.89 (s), 135.64 (s), 130.67 (s), 130.25 (s), 127.35 (s), 126.49 (s), 125.68 (s), 125.56 (s), 123.39 (s), 123.07 (s), 116.09 (s), 111.99 (s), 104.87 (s), 60.55 (s), 56.51 (s). Anal. ($C_{24}H_{20}N_4O_4$) calcd % C, 67.28; H, 4.71; N, 13.08; found % C, 66.96; H, 5.02; N, 12.71. HRMS (ESI) Calcd for ($C_{24}H_{20}N_4O_4$): $[M-H]^-$ m/z: 427.1412, found 427.1405; $[M+Na]^+$ m/z: 451.1377, found 451.1379.

*5.1.6.1.16 5-[5-(3',4',5'-Trimethoxybiphenyl-4-yl)-1,2,4-oxadiazol-3-yl]-1H-indazole (**23**)*

Prepared from intermediate **1o** (0.40 mmol, 0.16 g) and 3,4,5-trimethoxyphenylboronic acid (0.80 mmol, 0.17 g). Purification procedure: the solvent was evaporated under reduced pressure and the resulting crude solid was suspended with brine (50 mL) and extracted with ethyl acetate (3 x 30 mL). The combined organic phases were washed with H_2O (2 x 25 mL), dried over anhydrous Na_2SO_4 and concentrated under rotary evaporation. The resulting crude was purified by column chromatography (gradient eluent: ethyl acetate in dichloromethane, 0% → 20%), yielding the desired product as an off-white solid. Yield: 35%; off-white solid; m.p.: 195-8 °C. ^{1}H NMR (500 MHz, DMSO-*d*$_6$) δ: 13.39 (s, 1H, dis. with D_2O), 8.60 (s, 1H), 8.27 (s, 1H), 8.25 (d, *J* = 8.4 Hz, 2H), 8.06 (dd, *J* = 8.7, 1.1 Hz, 1H), 8.01 (d, *J* = 8.4 Hz, 2H), 7.73 (d, *J* = 8.7 Hz, 1H), 7.05 (s, 2H), 3.89 (s, 6H), 3.71 (s, 3H). ^{13}C NMR (126 MHz, DMSO-*d*$_6$) δ: 175.43 (s), 169.21 (s), 153.81 (s), 145.20 (s), 141.39 (s), 138.43 (s), 135.39 (s), 134.72 (s), 128.79 (s), 128.22 (s), 124.94 (s), 123.41 (s), 122.55 (s), 121.39 (s), 118.84 (s), 111.63 (s), 104.92 (s), 60.56 (s), 56.50 (s).). Anal. ($C_{24}H_{20}N_4O_4$) calcd % C, 67.28; H, 4.71; N, 13.08; found % C, 67.39; H, 4.75; N, 12.92. HRMS (ESI) Calcd for ($C_{24}H_{20}N_4O_4$): $[M-H]^-$ m/z: 427.1412, found 427.1409; $[M+Na]^+$ m/z: 451.1377, found 451.1377.

*5.1.6.1.17 5-[5-(3',4',5'-Trimethoxybiphenyl-3-yl)-1,2,4-oxadiazol-3-yl]-1H-indazole (**24**)*

Prepared from intermediate **1n** (0.40 mmol, 0.16 g) and 3,4,5-trimethoxyphenylboronic acid (0.80 mmol, 0.17 g). Purification procedure: the solvent was removed under rotary evaporation and the resulting solid was suspended with brine (50 mL) and extracted with ethyl acetate (3 x 30 mL). The combined organic phases were washed with H_2O (2 x 20 mL), dried over anhydrous Na_2SO_4 and concentrated under reduced pressure. The resulting oil was purified by column chromatography (gradient eluent: ethyl acetate in dichloromethane, 0% → 20%), yielding the desired product as a pale-yellow solid. Yield: 35%; pale-yellow solid; m.p.: 209-212 °C. ^{1}H NMR (500 MHz, DMSO-*d*$_6$) δ: 13.39 (s, 1H, dis. with D_2O), 8.61 (s, 1H), 8.41 (s, 1H), 8.27 (s, 1H), 8.18 (d, *J* = 7.8 Hz, 1H), 8.07 (d, *J* = 8.8 Hz, 1H), 8.04 (d, *J* = 7.8 Hz, 1H), 7.75 (t, *J* = 7.8 Hz, 1H), 7.73 (d, *J* = 8.8 Hz, 1H), 7.02 (s, 2H), 3.90 (s, 6H), 3.71 (s, 3H). ^{13}C NMR (126 MHz, DMSO-*d*$_6$) δ: 175.62 (s), 169.23 (s), 153.82 (s), 142.15 (s), 141.40 (s), 138.09 (s), 135.37 (s), 135.10 (s), 132.28 (s), 130.54 (s), 127.23 (s), 126.39 (s), 124.96 (s), 124.51 (s), 123.40 (s), 121.43 (s), 118.81 (s), 111.64 (s), 104.97 (s), 60.55 (s), 56.54 (s). Anal. ($C_{24}H_{20}N_4O_4$) calcd % C, 67.28; H, 4.71; N, 13.08; found % C, 67.40; H, 5.07; N, 12.66. HRMS (ESI) Calcd for ($C_{24}H_{20}N_4O_4$): $[M-H]^-$ m/z: 427.1412, found 427.1403; $[M+Na]^+$ m/z: 451.1377, found 451.1390.

*5.1.7 N-(1H-indazol-5-yl)-4-[(3,4,5-trimethoxybenzyl)oxy]benzamide (**11**)*

3,4,5-Trimethoxybenzyl alcohol (0.27 mmol, 0.12 g) and PPh_3 (0.39 mmol, 0.11 g) were added to a suspension of intermediate **1j** (0.39 mmol, 0.10 g) in anhydrous THF (2.5 mL). After cooling the reaction to 0 °C through an external ice bath, diisopropyl azodicarboxylate (DIAD, 0.39 mmol, 0.080 mL) was added dropwise. The reaction was then warmed to room temperature and left under magnetic stirring for 24 h. The inorganic residue was filtered off and the solution was concentrated under rotatory evaporation. The resulting residue was suspended in $CHCl_3$ and filtered. The obtained solution was concentrated under reduced pressure and then purified by flash chromatography (gradient eluent: methanol in dichloromethane, 0 → 5%). Yield: 24%; white solid; m.p.: 201-4 °C (dec). ^{1}H NMR (300 MHz, DMSO-*d*$_6$) δ: 12.97 (s, 1H, dis. with D_2O), 10.08 (s, 1H, dis. with D_2O), 8.20 (s, 1H), 8.02 (s, 1H), 7.96 (d, J = 8.8 Hz, 2H), 7.60 (dd, J = 9.0, 1.4 Hz, 1H), 7.49 (d, J = 9.0 Hz, 1H), 7.13 (d, J = 8.8 Hz, 2H), 6.79 (s, 2H), 5.10 (s, 2H), 3.77 (s, 6H), 3.64 (s, 3H). ^{13}C NMR (126 MHz, DMSO-*d*$_6$) δ: 165.47 (s), 160.85 (s), 153.38 (s), 137.43 (s), 133.83 (s), 132.79 (s), 130.02 (s), 129.91 (s), 126.01 (s), 123.14 (s), 122.00 (s), 115.32 (s), 114.86 (s), 111.41

(s), 110.28 (s), 105.80 (s), 70.13 (s), 60.45 (s), 56.36 (s). Anal. ($C_{24}H_{23}N_3O_5$) calcd % C, 66.50; H, 5.35; N, 9.69; found % C, 66.17; H, 5.44; N, 9.35. HRMS (ESI) Calcd for ($C_{24}H_{23}N_3O_5$): $[M-H]^-$ m/z: 432.1565, found 432.1552; $[M+Na]^+$ m/z: 456.1530, found 456.1533.

5.1.8 Synthesis of final compounds ***12-13***

5.1.8.1 General procedure for the synthesis of final compounds ***12-13***

Intermediate **1j** (0.40 mmol, 0.10 g) was suspended in acetonitrile (4 mL) before adding K_2CO_3 (0.60 mmol, 0.084 g), the appropriate benzyl bromide (0.40 mmol) and KI in catalytic amount. The reaction mixture was refluxed for 7 h. After cooling to room temperature, the solvent was concentrated under rotatory evaporation and the resulting crude solid was suspended in $CHCl_3$. The precipitate was collected after thoroughly washing with water and purified as described below.

*5.1.8.1.1 4-[(3,5-Difluorobenzyl)oxy]-N-(1H-indazol-5-yl)benzamide (**12**)*

Prepared from 3,5-difluorobenzyl bromide (0.40 mmol, 0.052 mL). Purification procedure: the precipitate was washed with hot water (2 x 20 mL) followed by hot methanol (2 x 20 mL), yielding the desired product. Yield: 40%; off-white solid; m.p.: > 230 °C. ^{1}H NMR (300 MHz, DMSO-*d*$_6$) δ: 12.96 (s, 1H, dis. with D_2O), 10.08 (s, 1H, dis. with D_2O), 8.19 (s, 1H), 8.02 (s, 1H), 7.96 (d, *J* = 8.8 Hz, 2H), 7.60 (dd, *J* = 8.9, 1.5 Hz, 1H), 7.48 (d, *J* = 8.9 Hz, 1H), 7.25 – 7.16 (m, 3H), 7.13 (d, *J* = 8.8 Hz, 2H), 5.23 (s, 2H). ^{13}C NMR (126 MHz, DMSO-*d*$_6$) δ: 165.16 (s), 162.87 (dd, *J* = 246.3, 13.1 Hz), 160.75 (s), 141.88 (t, *J* = 9.3 Hz), 137.50 (s), 133.87 (s), 132.63 (s), 129.96 (s), 128.17 (s), 123.14 (s), 121.94 (s), 114.90 (s), 111.50 (s), 110.96 (dd, *J* = 19.6, 6.0 Hz), 110.34 (s), 103.73 (t, *J* = 25.6 Hz), 68.39 (t, *J* = 1.9 Hz). Anal. ($C_{21}H_{15}F_2N_3O_2$) calcd % C, 66.49; H, 3.99; N, 11.08; found % C, 66.14; H, 4.28; N, 10.74. HRMS (ESI) Calcd for ($C_{21}H_{15}F_2N_3O_2$): $[M-H]^-$ m/z: 378.1060, found 378.1059.

*5.1.8.1.2 4-[(4-Cyanobenzyl)oxy]-N-(1H-indazol-5-yl)benzamide (**13**)*

Prepared from 4-cyanobenzyl bromide (0.40 mmol, 0.078 g). Purification procedure: the precipitate was crystallized from THF. Yield: 37%; off-white solid; m.p.: > 230 °C. ^{1}H NMR (500 MHz, DMSO-*d*$_6$) δ: 13.00 (s, 1H, dis. with D_2O), 10.09 (s, 1H, dis. with D_2O), 8.19 (d, *J* = 1.7 Hz, 1H),

8.02 (s, 1H), 7.96 (d, *J* = 8.9 Hz, 2H), 7.88 (d, *J* = 8.3 Hz, 2H), 7.66 (d, *J* = 8.3 Hz, 2H), 7.60 (dd, *J* = 8.9, 1.7 Hz, 1H), 7.49 (d, *J* = 8.9 Hz, 1H), 7.14 (d, *J* = 8.8 Hz, 2H), 5.32 (s, 2H). ^{13}C NMR (126 MHz, DMSO-*d*$_6$) δ: 165.16 (s), 160.83 (s), 142.98 (s), 137.49 (s), 133.87 (s), 132.91 (s), 132.63 (s), 129.97 (s), 128.59 (s), 128.15 (s), 123.13 (s), 121.95 (s), 119.17 (s), 114.90 (s), 111.50 (s), 111.03 (s), 110.34 (s), 68.84 (s). Anal. ($C_{22}H_{16}N_4O_2$) calcd % C, 71.73; H, 4.38; N, 15.21; found % C, 71.30; H, 4.32; N, 14.86. HRMS (ESI) Calcd for ($C_{22}H_{16}N_4O_2$): $[M-H]^-$ m/z: 367.1200, found 367.1195.

*5.1.9 5-(3-{4-[(3,4,5-Trimethoxybenzyl)oxy]phenyl}-1,2,4-oxadiazol-5-yl)-1H-indazole (**20**)*

1*H*-Indazole-5-carboxylic acid (0.45 mmol, 0.073 g) was suspended in anhydrous dichloromethane (2 mL). Thionyl chloride (1.0 mL) was added and then the reaction mixture was refluxed under magnetic stirring for 4 h. After cooling to room temperature, the mixture was concentrated to dryness. A solution of amidoxime **1w** (0.50 mmol, 0.17 g) in anhydrous pyridine (3 mL) was added and the mixture was refluxed for 5 h. Ethanol (12 mL), followed by water (15 mL), was added to the mixture to furnish a precipitate that was collected after filtration. The solution was concentrated, and water was added to obtain a second precipitate. The two precipitates were combined and purified by flash chromatography (gradient eluent: ethyl acetate in dichloromethane, 0 → 10%). Yield: 33%; white solid; m.p.: 189-192 °C. ^{1}H NMR (300 MHz, DMSO-*d*$_6$) δ: 13.52 (s, 1H, dis. with D_2O), 8.68 (br s, 1H), 8.31 (s, 1H), 8.09 (dd, *J* = 8.8, 1.6 Hz, 1H), 8.03 (d, *J* = 8.9 Hz, 2H), 7.76 (d, *J* = 8.8 Hz, 1H), 7.21 (d, *J* = 8.9 Hz, 2H), 6.80 (s, 2H), 5.09 (s, 2H), 3.77 (s, 6H), 3.64 (s, 3H). ^{13}C NMR (126 MHz, DMSO-*d*$_6$) δ: 176.23 (s), 168.28 (s), 161.30 (s), 153.39 (s), 141.82 (s), 137.62 (s), 135.90 (s), 132.51 (s), 129.23 (s), 125.49 (s), 123.38 (s), 122.86 (s), 119.25 (s), 116.22 (s), 115.91 (s), 111.86 (s), 105.85 (s), 70.21 (s), 60.45 (s), 56.35 (s). Anal. ($C_{25}H_{22}N_4O_5$) calcd % C, 65.49; H, 4.84; N, 12.22; found % C, 65.29; H, 4.81; N, 12.04. HRMS (ESI) Calcd for ($C_{25}H_{22}N_4O_5$): $[M-H]^-$ m/z: 457.1517, found 457.1505; $[M+Na]^+$ m/z: 481.1482, found 481.1493.

*5.1.10 Synthesis of final compounds **21-22**, **25***

*5.1.10.1 General procedure for the synthesis of final compounds **21-22**, **25***

In a pyrex vessel charged with a magnetic stirring bar, 1*H*-indazole-5-carboxylic acid (0.75 mmol, 0.12 g, for **21**-**22**) or **1y** (0.75 mmol, 0.24 g, for **25**) was dissolved in anhydrous DMF (2.5 mL) followed by the addition of 1-hydroxybenzotriazole hydrate (HOBt; 0.90 mmol, 0.14 g) and *N*-(3-dimethylaminopropyl)-*N*′-ethylcarbodiimide hydrochloride (EDC·HCl; 0.83 mmol, 0.16 g). This mixture was left under magnetic stirring for 30 minutes and then a solution of intermediate amidoxime (**1t** or **1u** or **1k**, 0.75 mmol) in anhydrous DMF (1.5 mL) was added to the mixture. The vessel was placed in the microwave apparatus and irradiated for 30 min at 170 °C. After cooling to room temperature, the mixture was purified as detailed below.

*5.1.10.1.1 5-(3-{3-[(3,4,5-Trimethoxybenzyl)oxy]phenyl}-1,2,4-oxadiazol-5-yl)-1H-indazole (**21**)*

Prepared from **1t** (0.75 mmol, 0.25 g). Purification procedure: the reaction mixture was poured onto ice (50 mL) and left under magnetic stirring for 30 minutes. The resulting precipitate was collected after filtration and purified by flash chromatography (gradient eluent: ethyl acetate in dichloromethane, 0 → 20%). Yield: 29%; white solid; m.p.: 224-7 °C (dec). ^{1}H NMR (500 MHz, DMSO-d_6) δ: 13.57 (s, 1H, dis. with D_2O), 8.71 (dd, J = 1.6, 0.9 Hz, 1H), 8.33 (d, J = 0.9 Hz, 1H), 8.11 (dd, J = 8.8, 1.6 Hz, 1H), 7.78 (d, J = 8.8 Hz, 1H), 7.74 – 7.66 (m, 2H), 7.52 (t, J = 7.9 Hz, 1H), 7.27 (ddd, J = 7.9, 2.5, 0.9 Hz, 1H), 6.83 (s, 2H), 5.13 (s, 2H), 3.78 (s, 6H), 3.65 (s, 3H). ^{13}C NMR (126 MHz, $CDCl_3$) δ: 181.30 (s), 173.24 (s), 163.96 (s), 158.14 (s), 146.69 (s), 142.31 (s), 140.60 (s), 137.46 (s), 135.77 (s), 132.78 (s), 130.22 (s), 128.13 (s), 127.72 (s), 124.80 (s), 123.51 (s), 120.83 (s), 118.22 (s), 116.72 (s), 110.50 (s), 74.92 (s), 65.20 (s), 61.11 (s). Anal. ($C_{25}H_{22}N_4O_5$) calcd % C, 65.49; H, 4.84; N, 12.22; found % C, 65.24; H, 4.96; N, 11.94. HRMS (ESI) Calcd for ($C_{25}H_{22}N_4O_5$): $[M-H]^-$ m/z: 457.1517, found 457.1508.

*5.1.10.1.2 5-(3-{4-[(3,4,5-Trimethoxyphenoxy)methyl]phenyl}-1,2,4-oxadiazol-5-yl)-1H-indazole (**22**)*

Prepared from **1u** (0.75 mmol, 0.25 g). Purification procedure: the reaction mixture was poured onto ice (50 mL) and left under magnetic stirring for 30 minutes. The resulting precipitate was collected after filtration, washed with methanol and purified by flash chromatography (eluent: ethyl acetate in chloroform, 5%). Yield: 21%; white solid; m.p.: 225-7 °C (dec). ^{1}H NMR (300 MHz, DMSO-d_6) δ: 13.55 (s, 1H, dis. with D_2O), 8.71 (s, 1H), 8.33 (s, 1H), 8.13 (d, J = 8.0 Hz, 2H), 8.12

(d, *J* = 8.8 Hz, 1H), 7.78 (d, *J* = 8.8 Hz, 1H), 7.67 (d, *J* = 8.0 Hz, 2H), 6.36 (s, 2H), 5.18 (s, 2H), 3.74 (s, 6H), 3.56 (s, 3H). ^{13}C NMR (126 MHz, DMSO-*d*$_6$) δ: 176.56 (s), 168.41 (s), 155.19 (s), 153.80 (s), 141.90 (s), 141.28 (s), 135.88 (s), 132.32 (s), 128.70 (s), 127.67 (s), 126.17 (s), 125.49 (s), 123.39 (s), 122.99 (s), 116.11 (s), 111.95 (s), 93.37 (s), 69.53 (s), 60.57 (s), 56.33 (s). Anal. ($C_{25}H_{22}N_4O_5$) calcd % C, 65.49; H, 4.84; N, 12.22; found % C, 65.34; H, 4.74; N, 12.08. HRMS (ESI) Calcd for ($C_{25}H_{22}N_4O_5$): $[M-H]^-$ m/z: 457.1517, found 457.1509; $[M+Na]^+$ m/z: 481.1482, found 481.1496.

*5.1.10.1.3 5-(5-{4-[(3,4,5-Trimethoxybenzyl)oxy]phenyl}-1,2,4-oxadiazol-3-yl)-1H-indazole (**25**)*

Prepared from **1k** (0.75 mmol, 0.13 g). Purification procedure: the reaction mixture was poured onto ice (50 mL) and left under magnetic stirring for 30 minutes. The resulting precipitate was collected after filtration and purified by flash chromatography (gradient eluent: ethyl acetate in dichloromethane, 0 → 20%). Yield: 22%; white solid; m.p.: 173–6 °C. ^{1}H NMR (500 MHz, DMSO-*d*$_6$) δ: 13.38 (s, 1H, dis. with D_2O), 8.55 (br s, 1H), 8.26 (s, 1H), 8.15 (d, *J* = 8.9 Hz, 2H), 8.02 (dd, *J* = 8.7, 1.5 Hz, 1H), 7.71 (d, *J* = 8.7 Hz, 1H), 7.28 (d, *J* = 8.9 Hz, 2H), 6.81 (s, 2H), 5.14 (s, 2H), 3.77 (s, 6H), 3.65 (s, 3H). ^{13}C NMR (126 MHz, DMSO-*d*$_6$) δ: 175.42 (s), 169.01 (s), 162.64 (s), 153.41 (s), 141.42 (s), 137.71 (s), 135.26 (s), 132.25 (s), 130.37 (s), 124.89 (s), 123.36 (s), 121.24 (s), 119.00 (s), 116.46 (s), 116.24 (s), 111.60 (s), 105.95 (s), 70.41 (s), 60.45 (s), 56.37 (s). Anal. ($C_{25}H_{22}N_4O_5$) calcd % C, 65.49; H, 4.84; N, 12.22; found % C, 65.06; H, 5.13; N, 11.84. HRMS (ESI) Calcd for ($C_{25}H_{22}N_4O_5$): $[M-H]^-$ m/z: 457.1517, found 457.1502; $[M+Na]^+$ m/z: 481.1482, found 481.1492.

*5.1.10.1.3.1 Methyl 4-[(3,4,5-trimethoxybenzyl)oxy]benzoate (**1x**)*

3,4,5-Trimethoxybenzyl alcohol (4.0 mmol, 0.66 mL) and methyl *p*-hydroxybenzoate (8.0 mmol, 1.2 g) were dissolved in anhydrous THF (28 mL) before adding ADDP (8.0 mmol, 2.0 g) followed by a solution of PPh_3 (8.8 mmol, 2.4 g) in THF (4 mL) dropwise, while cooling with an external ice bath. The reaction mixture was stirred at room temperature overnight. The resulting precipitate was filtered off, the solution was concentrated under reduced pressure and purified by flash chromatography (eluent: ethyl acetate in dichloromethane, 5%), affording the desired product as a green solid. Yield: 47%. ^{1}H NMR (300 MHz, $CDCl_3$) δ: 8.00 (d, *J* = 8.9 Hz, 2H), 7.00 (d, *J* = 8.9 Hz, 2H), 6.65 (s, 2H), 5.04 (s, 2H), 3.89 (s, 3H), 3.87 (s, 6H), 3.85 (s, 3H).

*5.1.10.1.3.2 4-[(3,4,5-Trimethoxybenzyl)oxy]benzoic acid (**1y**)*

Lithium hydroxide monohydrate (5.5 mmol, 0.22 g), previously dissolved in water (1 mL), was dropped *via* syringe into a solution of intermediate **1x** (1.2 mmol, 0.38 g) in THF (3 mL). The reaction mixture was stirred at room temperature for 24 h. After this time, the mixture was cooled at 0 °C through an external ice bath and acidified with aq. 1 N HCl until pH 2.0. The resulting precipitate was collected after filtration and washed with abundant water, thus furnishing the desired product as a solid that was used without further purification. Yield: 92%. ^{1}H NMR (300 MHz, $CDCl_3$) δ: 8.07 (d, *J* = 8.8 Hz, 2H), 7.03 (d, *J* = 8.8 Hz, 2H), 6.66 (s, 2H), 5.06 (s, 2H), 3.88 (s, 6H), 3.86 (s, 3H), OH not detected.

*5.1.11 N-[1-(3,4,5-Trimethoxyphenyl)-1H-indazol-5-yl]benzamide (**26**)*

In a Pyrex vessel charged with a magnetic bar, intermediate **1h** (0.46 mmol, 0.11 g) was suspended in a anhydrous DMF/dioxane mixture (4 mL, 1/3 v/v) before adding 5-bromo-1,2,3-trimethoxybenzene (1.0 mmol, 0.25 g), K_2CO_3 (2.0 mmol, 0.28 g), CuI (0.10 mmol, 0.019 g) and trans-*N*,*N*'-dimethylcyclohexane-1,2-diamine (0.15 mmol, 0.023 mL). The vessel was heated under microwave irradiation at 150 °C for 1 h. After cooling to room temperature, the reaction mixture was diluted with ethyl acetate (20 mL) and filtered through a pad of celite. The resulting solution was concentrated under rotatory evaporation and purified by flash chromatography (gradient eluent: ethyl acetate in dichloromethane, 10% → 40%). Yield: 21%; off-white solid; m.p.: 82-5 °C. ^{1}H NMR (300 MHz, $CDCl_3$) δ: 8.21 (s, 1H), 8.18 (s, 1H), 7.97 – 7.89 (m, 3H), 7.73 (d, *J* = 8.9 Hz, 1H), 7.62 – 7.48 (m, 4H), 6.94 (s, 2H), 3.94 (s, 6H), 3.92 (s, 3H). ^{13}C NMR (126 MHz, $CDCl_3$) δ: 165.93 (s), 153.80 (s), 136.89 (s), 136.35 (s), 135.04 (s), 134.77 (s), 131.96 (s), 128.86 (s), 127.01 (s), 125.30 (s), 122.17 (s), 112.49 (s), 111.18 (s), 110.86 (s), 108.10 (s), 100.52 (s), 61.06 (s), 56.37 (s). Anal. ($C_{23}H_{21}N_3O_4$) calcd % C, 68.47; H, 5.25; N, 10.42; found % C, 68.59; H, 5.30; N, 10.11**.** HRMS (ESI) Calcd for ($C_{23}H_{21}N_3O_4$): $[M-H]^-$ m/z: 402.1459, found 402.1467.

5.2. Cell-based studies

5.2.1 Materials

Dulbecco's modified Eagle's medium (DMEM), fetal bovine serum (FBS), penicillin and streptomycin (P/S) were provided by GIBCO (Paisley, Scotland). Trypan Blue, 3-(4,5-dimethylthiazol-2-yl)-2.5-diphenyltetrazolium bromide (MTT), 2',7'-dichlorofluorescein diacetate

(DCFH-DA) was from Calbiochem, San Diego, CA, USA. Human Neuroblastoma Cells (SH-SY5Y) and astrocytes DI TNC1 were from American Type Culture Collection (ATCC). Hydrogen peroxide solution 30% stabilized was purchased from Sigma-Aldrich. All aqueous solutions were prepared by using water obtained from a Milli-Q gradient A-10 system (Millipore, 18.2 MΩ·cm, organic carbon content ≥ 4 μg/L).

5.2.2 Cell viability and neuroprotection studies

Human neuroblastoma SH-SY5Y cells were maintained in T-75 flasks (75 cm^2) in Dulbecco's modified Eagle's medium (DMEM) supplemented with 100 U/mL penicillin, 100 μg/mL streptomycin, 10% FBS, at 37 °C, 5% CO_2. At 80% of confluence, cells were detached by mechanical stirring, counted, and plated at $4x10^4$ cells/well in a 96-well plate. To assess the biocompatibility of selected compounds, confluent SH-SY5Y cells were treated with compound **5**, **14**, **15**, **18**, **20**, **23**, and **25** at concentration ranging from 0 to 100 μM in serum-free DMEM medium. After incubation for 24 h at 37 °C, 5% CO_2, the culture medium was removed and the cell viability was evaluated by MTT [3-(4,5-dimethylthiazol-2-yl)-2,5-diphenyl tetrazolium bromide] assay [27].

In another set of experiments, to evaluate the potential neuroprotective effects of less cytotoxic 1*H*-indazoles (**5**, **18**, **20**, **23**, **25**), SH-SY5Y cells were plated in a 96 well/plate and incubated with the compounds at concentrations ranging from 0.1 to 5 μM in the presence of a non-specific cytotoxic stimulus (H_2O_2 at 400 μM) for 24 h, at 37 °C, 5% CO_2. After this treatment, the medium was removed and cytoprotective effects were determined by evaluating cell viability through the MTT assay. Controls were represented by cells treated with H_2O_2 alone, by standard quercetin at 75 μM (QRC) and by untreated cells (CTRL). The results were expressed as percentage of cell survival compared to CTRL. Compounds **5** and **20** were tested also on DI TNC1 astrocyte cell line cultured in DMEM supplemented with 100 U/mL penicillin, 100 μg/mL streptomycin, 10% FBS, at 37 °C, 5% CO_2. After confluence, the cells were detached with trypsin (0.25%), centrifuged at 1500 rpm for 10 min, and plated at 4,5 x 10^4 cells/well in a 96 well/plate for 24 h. The cell viability of astrocytes was assessed by MTT assay after incubation for 24 h with compounds **5** and **20** (concentrations ranging from 0 to 100 μM) in serum-free DMEM at 37 °C, 5% CO_2. The neuroprotection against the pro-oxidant activity of H_2O_2 was evaluated by MTT assay on DI TNC1 cells, after co-incubation (24 h) with compounds **5** and **20** at concentrations ranging from 0.1 to 5 μM. Controls were represented by cells treated with H_2O_2 alone, with standard quercetin at 75 μM (QRC) or by untreated cells (CTRL).

5.2.3 Reactive oxygen species (ROS) detection

The detection of reactive oxygen species (ROS) was performed by loading confluent SH-SY5Y cells with 10 μM of 2′,7′-dichlorofluorescein diacetate (DCFH-DA) in phenol red–free DMEM at 37 °C for 30 min, 5% CO_2 as previously reported [37]. After removing DCFH-DA from plate wells, cells were washed once with phosphate buffer saline (pH 7.2, 10 mM), then incubated for 45 min with H_2O_2 (200 μM) and the tested compound (**5**, **18**, **20**, **23**, and **25**) in the range of concentrations 0-5 μM. Cells were subjected to spectrofluorimetric analysis (excitation wavelength = 485 nm; emission wavelength = 585 nm) using a multi plate reader [37]. Results were expressed as percentage of ROS production compared to the negative control (CTRL) represented by cells treated only with DCFH-DA, which was set as 100%. Cells treated with H_2O_2 represented the positive control and quercetin (QRC) at 75 μM was used as standard antioxidant.

5.2.4 Statistical analysis

Data analysis was performed by using GraphPad Prism 5.0 (GraphPad Software Inc., San Diego, CA, USA). Data were expressed as mean values ± SD of three independent experiments, each performed in triplicates and referred to untreated control cells. Statistical analysis was carried out using one-way analysis of variance (ANOVA) followed by the Dunnett's Multiple Comparison post hoc test for multiple comparison analysis. The levels of significance were reported towards the cytotoxic insult (represented by H_2O_2) and untreated cells.

5.3. Reversed-phase HPLC studies

5.3.1 Stability studies

For hydrolytic stability, 0.12 mL of 1 mM stock solutions in DMSO of compounds under study was added to 0.30 mL of acetonitrile, 0.48 mL of DMSO and 2.10 mL of aqueous buffer solution (40 mM phosphate buffer, pH 7.4, 0.15 M KCl; 10 mM HCl, pH 2, 0.15 M KCl; final compound concentrations 40 μM, co-solvent mixture 30%). Samples were kept in the dark and incubated at 37 ± 0.5 °C until gentle orbital shaking. At appropriate time intervals, aliquots (150 μL) were taken and diluted with cold methanol (600 μL) before injection. Samples were analysed by HPLC using a Gemini C18 4.6 mm × 150 mm, with 3 μm size particles on a Analytic Agilent 1260 Infinity multidetector system equipped with a 1200 series UV-diode array detector. UV spectra were recorded at 220 and 254 nm. Analytes were eluted in isocratic conditions by using mixtures of methanol and ammonium formate buffer (15 mM, pH 5.0), methanol/buffer 15-35% (v/ v), as the mobile phase. The mobile phase was filtered through a Nylon-66 membrane 0.45 μm (Supelco,

USA) before use. Injection volumes were 20 µL and the flow rate was 0.5 mL/min. Data were integrated and reported using OpenLAB software (Agilent Technologies). Standard areas were derived by injecting 20 µL of solutions obtained by adding 20 µL of 10 mM stock solutions (DMSO) to 1.98 mL of a 1/1 (v/v) methanol/acetonitrile mixture and diluting with methanol (150 µL to 750 µL) before injection, measuring the peak area absorbance at 254 nm. Each kinetic experiment was performed in triplicate. Linear and non-linear regression analyses were performed with Prism 5.0. Data are the mean ± SD.

5.3.2 Kinetic solubility determination

For the determination of kinetic solubility, slight modifications to a reported procedure were applied [49]. 20 µL of a 10 mM stock solution (DMSO) was added to 980 µL of phosphate buffer pH 7.4 (50 mM). The suspensions were shaken on an orbital shaker at 250 rpm for 2 h and then centrifuged (2500 rpm for 3 min). After filtration, 500 µL of the filtrate was diluted with a 1:1 (v:v) mixture of DMSO with phosphate buffer pH 7.4. The concentration of the title compound was then determined by HPLC with UV detection at 254 nm as described before. Data were integrated and reported using OpenLAB software (Agilent Technologies). Standard areas were derived as already described. Each experiment was performed in triplicate.

5.4 Molecular docking simulations

Compounds **18** and **20** were subjected to molecular docking simulations. To this aim, the crystal structures of human MAO B in complex with pioglitazone (PDB code: 4A79, [43]) and a coumarin-bearing inhibitor (PDB code: 7P4F, [45]) were employed. Additional docking simulations of compound **20** were performed on the crystal structure of human MAO A in complex with a reversible inhibitor (PDB code: 2Z5X, [46]). The retrieved .pdb files were pre-treated using the Protein Preparation Wizard (PPW) tool available from the Schrödinger suite 2022-4 [50]. This tool allows adding missing hydrogen atoms, reconstructing incomplete side chains, assigning the ionization states at physiological pH, setting the orientation of any misoriented groups, removing water molecules, optimizing the hydrogen bond network and performing a force field-based minimization (OPLS-4) [51] of the 3D protein structures. Both ligands were subjected to LigPrep [52], a tool available from the Schrodinger Suite 2022-4, to build the 3D structures, desalt and generate all tautomers and ionization states at a pH value of 7.0 ± 2.0. A cubic grid was generated

on the centroid of the cognate ligand. In doing that, we obtained an inner box of 10 Å × 10 Å × 10 Å, irrespective of the considered protein structure, and an outer box having an edge of 26.7 Å, 28.0 Å, and 23 Å in 4A79, 7P4F, and 2Z5X, respectively. The obtained files were employed for standard docking simulations performed using Grid-based ligand docking with energetics (GLIDE) [53], available from the Schrodinger Suite 2022-4 as software program. During docking simulations, receptor protein was held fixed, whereas full conformational flexibility was allowed for the ligands. All docking simulations were performed using the default force field OPLS_2005 [54] and the standard precision docking (SP) protocol, keeping 25 poses for the post-docking minimization and finally selecting the top-five poses for each ligand. Importantly, this protocol was validated by re-docking the cognate ligands. The obtained Root-Mean-Square Deviation (RMSD) values, computed based on the heavy atoms only, supported the robustness of the employed docking protocols being equal to 0.50 Å (MAO B structures) and 1.45 Å (MAO A structure).

5.4.1 MM-GBSA calculations

Following a protocol published elsewhere and commonly used for virtual screening procedures [55], we applied the molecular mechanics/generalized Born surface area approach (MM-GBSA [56]) to the five top-scored docking complexes of each ligand, thus providing, for each of them, an estimation of the protein-ligand binding free energy (ΔG). During this calculation, flexibility was allowed for all residues having at least one atom within a distance of 3 Å from the ligand.

5.4.2 Conformational analysis

A conformational study of **18** within the *h*MAO B binding site (PDB code: 4A79 [43]) was carried out using Confgen, available from Schrödinger 2022-4 as tool [44]. In particular, 64 conformers were generated. Subsequently, each of them was subjected to a rigid body superposition on the top MM-GBSA scored pose of **20**.

5.5 MAO inhibition assays

Human recombinant MAO A and B and substrate kynuramine were from Aldrich (Milan, Italy). Experiments were made in 96-well black, flat-bottomed polystyrene plates (Greiner Bio-One

GmbH, Frickenhausen, Germany) with an Infinite M1000 Pro plate reader (Tecan, Cernusco s.N., Italy). The spectrometric assays, quantifying the formation of 4-hydroxyquinoline from substrate oxidation by means of fluorimetric [57] and absorbance [58] measurements, have already been described in quoted references. All incubations were run in triplicate and results obtained as mean ± SEM from 3 independent experiments. Non-linear regressions for IC_{50} calculations were done with Prism 5.0 (GraphPad Software, San Diego, CA, USA).

*5.6 Binding mode analysis of **20** to hMAO B*

5.6.1 Recombinant MAO B expression and purification

Detergent-purified samples of recombinant MAO B were prepared following expression in *P. pastoris* according to established protocols [59]. The concentration of the purified protein sample in potassium phosphate buffer (50 mM, pH 7.5), 0.8% (w/v) β-octylglucoside, 20% (w/v) glycerol was determined by measuring the absorbance of the flavin cofactor (ε_{456} = 12,000 $M^{-1}cm^{-1}$) using a NanoDrop ND-100 spectrophotometer (Thermo Scientific) and adjusted to about 50 µM by concentrating using Amicon30K (Millipore).

5.6.2 Inhibition kinetics

The direct spectrophotometric MMTP assay was used for kinetic experiments [60]. Assays were carried out in 100 µl cuvettes (quartz) at 25 °C using a Cary 100 UV/VIS spectrophotometer (Agilent) in HEPES buffer (50 mM, pH 7.5), 0.25% (v/v) reduced Triton X-100. Measurements were started by adding MAO B (0.07 µM). The rate of oxidation of MMTP substrate (ε_{420} = 25,000 $M^{-1}cm^{-1}$) was determined over time at ranging concentrations of **20** or in the presence of DMSO (1%, v/v) as control. IC_{50} values were determined at different MAO B concentration (8, 24, 40, 80 nM) to verify the tight-binding inhibition mechanism. Activity was measured after 10 minutes incubation on ice with serial diluted concentrations of **20**. Data were plotted with the dose response model using GraphPad Prism 5.0 (GraphPad Software). IC_{50} values were plotted against MAO B concentration and analysed by linear regression with GraphPad Prism 5.0 (GraphPad Software). The K_i value was determined by measuring the activity in steady-state conditions in the presence of **20** (0-100 µM). v_i/v_0 data points (initial velocities in the presence and absence of **20**, respectively) were plotted against inhibitor concentration. The inhibition constant value was obtained by fitting the data with the Morrison's equation model using GraphPad Prism 5.0 (GraphPad Software).

5.6.3 Thermal-shift assay

ThermoFAD experiments were performed with *h*MAO B (8.5 μM), after 15 minutes incubation with **20** (200 μM), in HEPES buffer (50 mM, pH 7.5), 0.25% (v/v) reduced Triton X-100. The temperature gradient was set to 40-65 °C with fluorescence detection at a constant rate every 0.1 °C/s at 450 ± 30 nm excitation and 535 ± 30 nm emission (BioRad MiniOpticon Real-Time PCR System).

Acknowledgments

Thanks are due to Italian MIUR (Ministero dell'Istruzione, dell'Università e della Ricerca) for partial financial support (PRIN2017 to Leonardo Pisani, project code: 2017RPHBCW). This research was also supported within the "Dipartimenti di Eccellenza Program (2018–2022) - Dept. of Biology and Biotechnology – University of Pavia" by the Italian MIUR (to Claudia Binda). Mariagrazia Rullo thanks European Social Found (FSE-FESR; Programma Operativo Nazionale Ricerca e Innovazione 2014-2020) for supporting PhD fellowship.

[1] J.C. Shih, K. Chen, M.J. Ridd, Monoamine Oxidase: from genes to behavior, Annu. Rev. Neurosci. 22 (1999) 197–217.

[2] L. De Colibus, M. Li, C. Binda, A. Lustig, D.E. Edmondson, A. Mattevi, Three-dimensional structure of human monoamine oxidase A (MAO A): Relation to the structures of rat MAO A and human MAO B, Proc. Natl. Acad. Sci. 102 (2005) 12684–12689.

[3] C. Binda, M. Li, F. Hubálek, N. Restelli, D.E. Edmondson, A. Mattevi, Insights into the mode of inhibition of human mitochondrial monoamine oxidase B from high-resolution crystal structures, Proc. Natl. Acad. Sci. U. S. A. (2003).

[4] M.B.H. Youdim, D. Edmondson, K.F. Tipton, The therapeutic potential of monoamine oxidase inhibitors, Nat. Rev. Neurosci. 7 (2006) 295–309.

[5] P.L. Dostert, M. Strolin Benedetti, K.F. Tipton, Interactions of monoamine oxidase with substrates and inhibitors., Med. Res. Rev. 9 (1989) 45–89.

[6] E.M. Milczek, C. Binda, S. Rovida, A. Mattevi, D.E. Edmondson, The 'gating' residues

Ile199 and Tyr326 in human monoamine oxidase B function in substrate and inhibitor recognition, FEBS J. 278 (2011) 4860–4869.

[7] D. Knez, N. Colettis, L.G. Iacovino, M. Sova, A. Pišlar, J. Konc, S. Lešnik, J. Higgs, F. Kamecki, I. Mangialavori, A. Dolšak, S. Žakelj, J. Trontelj, J. Kos, C. Binda, M. Marder, S. Gobec, Stereoselective activity of 1-propargyl-4-styrylpiperidine-like analogues that can discriminate between monoamine oxidase isoforms A and B, J. Med. Chem. 63 (2020) 1361–1387.

[8] P. Guglielmi, S. Carradori, A. Ammazzalorso, D. Secci, Novel approaches to the discovery of selective human monoamine oxidase-B inhibitors: is there room for improvement?, Expert Opin. Drug Discov. 14 (2019) 995–1035.

[9] R. R. Ramsay, Inhibitor design for monoamine oxidases, Curr. Pharm. Des. 19 (2013) 2529–2539.

[10] E.A. Zeller, J. Barsky, In vivo inhibition of liver and brain monoamine oxidase by 1-isonicotinyl-2-isopropyl hydrazine, Exp. Biol. Med. 81 (1952) 459–461.

[11] M. Da Prada, G. Zürcher, I. Wüthrich, W.E. Haefely, On tyramine, food, beverages and the reversible MAO inhibitor moclobemide, J. Neural Transm. Suppl. 26 (1988) 31–56.

[12] H. Sies, Role of metabolic H2O2 generation, J. Biol. Chem. 289 (2014) 8735–8741.

[13] B. Kumar, S. Sheetal, A.K. Mantha, V. Kumar, Recent developments on the structure–activity relationship studies of MAO inhibitors and their role in different neurological disorders, RSC Adv. 6 (2016) 42660–42683.

[14] S. Carradori, D. Secci, J.P. Petzer, MAO inhibitors and their wider applications: a patent review, Expert Opin. Ther. Pat. 28 (2018) 211–226.

[15] S. Manzoor, N. Hoda, A comprehensive review of monoamine oxidase inhibitors as anti-Alzheimer's disease agents: a review, Eur. J. Med. Chem. 206 (2020) 112787.

[16] L.G. Iacovino, N. Manzella, J. Resta, M.A. Vanoni, L. Rotilio, L. Pisani, D.E. Edmondson, A. Parini, A. Mattevi, J. Mialet-Perez, C. Binda, Rational redesign of monoamine oxidase A into a dehydrogenase to probe ROS in cardiac aging, ACS Chem. Biol. 15 (2020) 1795–1800.

[17] C. Datta, A. Bhattacharjee, Role of monoamine oxidase A (MAO-A) in cardiac aging, J.

Cardiol. Cardiovasc. Sci. 4 (2020) 31–40.

[18] A. Lewis, J.H. Miller, R.A. Lea, Monoamine oxidase and tobacco dependence, Neurotoxicology. 28 (2007) 182–195.

[19] C.-P. Liao, T.-P. Lin, P.-C. Li, L.A. Geary, K. Chen, V.P. Vaikari, J.B. Wu, C.-H. Lin, M.E. Gross, J.C. Shih, Loss of MAOA in epithelia inhibits adenocarcinoma development, cell proliferation and cancer stem cells in prostate, Oncogene. 37 (2018) 5175–5190.

[20] J.C. Shih, Monoamine oxidase isoenzymes: genes, functions and targets for behavior and cancer therapy, J. Neural Transm. 125 (2018) 1553–1566.

[21] V. Narayanaswami, L.R. Drake, A.F. Brooks, J.H. Meyer, S. Houle, M.R. Kilbourn, P.J.H. Scott, N. Vasdev, Classics in neuroimaging: development of PET tracers for imaging monoamine oxidases, ACS Chem. Neurosci. 10 (2019) 1867–1871.

[22] T. Behl, D. Kaur, A. Sehgal, S. Singh, N. Sharma, G. Zengin, F.L. Andronie-Cioara, M.M. Toma, S. Bungau, A.G. Bumbu, Role of monoamine oxidase activity in Alzheimer's disease: an insight into the therapeutic potential of inhibitors, Molecules. 26 (2021) 3724.

[23] J. Saura, J.M. Luque, A.M. Cesura, M. Da Prada, V. Chan-Palay, G. Huber, J. Löffler, J.G. Richards, Increased monoamine oxidase b activity in plaque-associated astrocytes of Alzheimer brains revealed by quantitative enzyme radioautography, Neuroscience. 62 (1994) 15–30.

[24] S. Schedin-Weiss, M. Inoue, L. Hromadkova, Y. Teranishi, N.G. Yamamoto, B. Wiehager, N. Bogdanovic, B. Winblad, A. Sandebring-Matton, S. Frykman, L.O. Tjernberg, Monoamine oxidase B is elevated in Alzheimer disease neurons, is associated with γ-secretase and regulates neuronal amyloid β-peptide levels, Alzheimers. Res. Ther. 9 (2017) 57.

[25] J.-H. Park, Y.H. Ju, J.W. Choi, H.J. Song, B.K. Jang, J. Woo, H. Chun, H.J. Kim, S.J. Shin, O. Yarishkin, S. Jo, M. Park, S.K. Yeon, S. Kim, J. Kim, M.-H. Nam, A.M. Londhe, J. Kim, S.J. Cho, S. Cho, C. Lee, S.Y. Hwang, S.W. Kim, S.-J. Oh, J. Cho, A.N. Pae, C.J. Lee, K.D. Park, Newly developed reversible MAO-B inhibitor circumvents the shortcomings of irreversible inhibitors in Alzheimer's disease, Sci. Adv. 5 (2019) eaav0316.

[26] G.F. Mangiatordi, D. Alberga, L. Pisani, D. Gadaleta, D. Trisciuzzi, R. Farina, A. Carotti, G. Lattanzi, M. Catto, O. Nicolotti, A rational approach to elucidate human monoamine oxidase

molecular selectivity, Eur. J. Pharm. Sci. 101 (2017) 90–99.

[27] M. Rullo, M. Cipolloni, M. Catto, C. Colliva, D.V. Miniero, T. Latronico, M. de Candia, T. Benicchi, A. Linusson, N. Giacchè, C.D. Altomare, L. Pisani, Probing fluorinated motifs onto dual AChE-MAO B inhibitors: rational design, synthesis, biological evaluation, and early-ADME studies, J. Med. Chem. 65 (2022) 3962–3977.

[28] L. Pisani, M. Catto, O. Nicolotti, G. Grossi, M. Di Braccio, R. Soto-Otero, E. Mendez-Alvarez, A. Stefanachi, D. Gadaleta, A. Carotti, Fine molecular tuning at position 4 of 2H-chromen-2-one derivatives in the search of potent and selective monoamine oxidase B inhibitors, Eur. J. Med. Chem. 70 (2013) 723–739.

[29] A. Pisani, L.; Muncipinto, G.; Miscioscia, T. F.; Nicolotti, O.; Leonetti, F.; Catto, M.; Caccia, C.; Salvati, P.; Soto-Otero, R.; Mendez-Alvarez, E.; Passeleu, C.; Carotti, Discovery of a novel class of potent coumarin monoamine oxidase B inhibitors: development and biopharmacological profiling of 7-[(3-chlorobenzyl)oxy]-4-[(methylamino)methyl]-2H-chromen-2-one methanesulfonate (NW-1772) as a highly potent, selective, revers, J. Med. Chem. 52 (2009) 6685–6706.

[30] R. Silvestri, G. La Regina, G. De Martino, M. Artico, O. Befani, M. Palumbo, E. Agostinelli, P. Turini, Simple, potent, and selective pyrrole inhibitors of monoamine oxidase types A and B, J. Med. Chem. 46 (2003) 917–920.

[31] N.T. Tzvetkov, S. Hinz, P. Küppers, M. Gastreich, C.E. Müller, Indazole-and indole-5-carboxamides: selective and reversible monoamine oxidase B inhibitors with subnanomolar potency, J. Med. Chem. 57 (2014) 6679–6703.

[32] L.H.A. Prins, J.P. Petzer, S.F. Malan, Inhibition of monoamine oxidase by indole and benzofuran derivatives, Eur. J. Med. Chem. 45 (2010) 4458–4466.

[33] S. Rivara, G. Piersanti, F. Bartoccini, G. Diamantini, D. Pala, T. Riccioni, M.A. Stasi, W. Cabri, F. Borsini, M. Mor, G. Tarzia, P. Minetti, Synthesis of (E)-8-(3-chlorostyryl)caffeine analogues leading to 9-deazaxanthine derivatives as dual A2A antagonists/MAO-B inhibitors, J. Med. Chem. 56 (2013) 1247–1261.

[34] A. Brunschweiger, P. Koch, M. Schlenk, F. Pineda, P. Küppers, S. Hinz, M. Köse, S. Ullrich, J. Hockemeyer, M. Wiese, J. Heer, C.E. Müller, 8-Benzyltetrahydropyrazino[2,1-f]purinediones: water-soluble tricyclic xanthine derivatives as multitarget drugs for

neurodegenerative diseases, ChemMedChem. 9 (2014) 1704–24.

[35] M.V. Berridge, A.S. Tan, Characterization of the Cellular Reduction of 3-(4,5-dimethylthiazol-2-yl)-2,5-diphenyltetrazolium bromide (MTT): Subcellular Localization, Substrate Dependence, and Involvement of Mitochondrial Electron Transport in MTT Reduction, Arch. Biochem. Biophys. 303 (1993) 474–482.

[36] L. Pisani, M. Catto, A. De Palma, R. Farina, S. Cellamare, C.D. Altomare, Discovery of Potent Dual Binding Site Acetylcholinesterase Inhibitors via Homo- and Heterodimerization of Coumarin-Based Moieties, ChemMedChem. 12 (2017) 1349–1358. https://onlinelibrary.wiley.com/doi/10.1002/cmdc.201700282.

[37] L. Pisani, A. De Palma, N. Giangregorio, D. V. Miniero, P. Pesce, O. Nicolotti, F. Campagna, C.D. Altomare, M. Catto, Mannich base approach to 5-methoxyisatin 3-(4-isopropylphenyl)hydrazone: A water-soluble prodrug for a multitarget inhibition of cholinesterases, beta-amyloid fibrillization and oligomer-induced cytotoxicity, Eur. J. Pharm. Sci. 109 (2017) 381–388.

[38] N. Suematsu, M. Hosoda, K. Fujimori, Protective effects of quercetin against hydrogen peroxide-induced apoptosis in human neuronal SH-SY5Y cells, Neurosci. Lett. 504 (2011) 223–227.

[39] P. Dhiman, N. Malik, E. Sobarzo-Sánchez, E. Uriarte, A. Khatkar, Quercetin and related chromenone derivatives as monoamine oxidase inhibitors: Targeting neurological and mental disorders, Molecules. 24 (2019).

[40] B. Salehi, L. Machin, L. Monzote, J. Sharifi-Rad, S.M. Ezzat, M.A. Salem, R.M. Merghany, N.M. El Mahdy, C.S. Kılıç, O. Sytar, M. Sharifi-Rad, F. Sharopov, N. Martins, M. Martorell, W.C. Cho, Therapeutic potential of quercetin: New insights and perspectives for human health, ACS Omega. 5 (2020) 11849–11872.

[41] N. Wang, L. Wang, X.-Q. Xie, ProSelection: a novel algorithm to select proper protein structure subsets for in silico target identification and drug discovery research, J. Chem. Inf. Model. 57 (2017) 2686–2698.

[42] T.M. Creanza, P. Delre, N. Ancona, G. Lentini, M. Saviano, G.F. Mangiatordi, Structure-Based Prediction of hERG-Related Cardiotoxicity: A Benchmark Study, J. Chem. Inf. Model. 61 (2021) 4758–4770.

[43] C. Binda, M. Aldeco, W.J. Geldenhuys, M. Tortorici, A. Mattevi, D.E. Edmondson, Molecular insights into human monoamine oxidase B inhibition by the glitazone antidiabetes drugs, ACS Med. Chem. Lett. 3 (2012) 39–42.

[44] Schrödinger Release 2022-4: ConfGen, Schrödinger, LLC, New York, NY, (2021).

[45] F. Ekström, A. Gottinger, N. Forsgren, M. Catto, L.G. Iacovino, L. Pisani, C. Binda, Dual reversible coumarin inhibitors mutually bound to monoamine oxidase B and acetylcholinesterase crystal structures, ACS Med. Chem. Lett. 13 (2022) 499–506.

[46] S.-Y. Son, J. Ma, Y. Kondou, M. Yoshimura, E. Yamashita, T. Tsukihara, Structure of human monoamine oxidase A at 2.2-Å resolution: the control of opening the entry for substrates/inhibitors, Proc. Natl. Acad. Sci. U. S. A. 105 (2008) 5739–44.

[47] R.A. Copeland, Tight Binding Inhibitors, in: Enzymes, John Wiley & Sons, Inc., New York, USA, 2003: pp. 305–317.

[48] F. Forneris, R. Orru, D. Bonivento, L.R. Chiarelli, A. Mattevi, Thermo FAD, a Thermofluor ® -adapted flavin ad hoc detection system for protein folding and ligand binding, FEBS J. 276 (2009) 2833–2840. https://doi.org/10.1111/j.1742-4658.2009.07006.x.

[49] C. Saal, A.C. Petereit, Optimizing solubility: Kinetic versus thermodynamic solubility temptations and risks, Eur. J. Pharm. Sci. 47 (2012) 589–595.

[50] Schrödinger Release 2022-4: Protein Preparation Wizard; Epik, Schrödinger, LLC, New York, NY, (2022).

[51] C. Lu, C. Wu, D. Ghoreishi, W. Chen, L. Wang, W. Damm, G.A. Ross, M.K. Dahlgren, E. Russell, C.D. Von Bargen, R. Abel, R.A. Friesner, E.D. Harder, OPLS4: improving force field accuracy on challenging regimes of chemical space, J. Chem. Theory Comput. 17 (2021) 4291–4300.

[52] Schrödinger Release 2022-4: c, Schrödinger, LLC, New York, NY, (2022).

[53] Schrödinger Release 2022-4: Glide, Schrödinger, LLC, New York, NY, (2022).

[54] G.A. Kaminski, R.A. Friesner, J. Tirado-Rives, W.L. Jorgensen, Evaluation and reparametrization of the OPLS-AA force field for proteins via comparison with accurate quantum chemical calculations on peptides, J. Phys. Chem. B. 105 (2001) 6474–6487.

[55] P. Delre, F. Caporuscio, M. Saviano, G.F. Mangiatordi, Repurposing known drugs as

covalent and non-covalent inhibitors of the SARS-CoV-2 papain-like protease, Front. Chem. 8 (2020).

[56] S. Genheden, U. Ryde, The MM/PBSA and MM/GBSA methods to estimate ligand-binding affinities, Expert Opin. Drug Discov. 10 (2015) 449–461.

[57] L. Pisani, R. Farina, M. Catto, R.M. Iacobazzi, O. Nicolotti, S. Cellamare, G.F. Mangiatordi, N. Denora, R.R. Soto-Otero, L. Siragusa, C.D. Altomare, A. Carotti, Exploring Basic Tail Modifications of Coumarin-Based Dual Acetylcholinesterase-Monoamine Oxidase B Inhibitors: Identification of Water-Soluble, Brain-Permeant Neuroprotective Multitarget Agents, J. Med. Chem. 59 (2016) 6791–6806.

[58] L. Pisani, R.M. Iacobazzi, M. Catto, M. Rullo, R. Farina, N. Denora, S. Cellamare, C.D. Altomare, Investigating alkyl nitrates as nitric oxide releasing precursors of multitarget acetylcholinesterase-monoamine oxidase B inhibitors, Eur. J. Med. Chem. 161 (2019) 292–309.

[59] P. Newton-Vinson, F. Hubalek, D.E. Edmondson, High-Level Expression of Human Liver Monoamine Oxidase B in Pichia pastoris, Protein Expr. Purif. 20 (2000) 334–345.

[60] P. Bissel, M.C. Bigley, K. Castagnoli, N. Castagnoli Jr, Synthesis and Biological Evaluation of MAO-A Selective 1,4-Disubstituted-1,2,3,6-tetrahydropyridinyl Substrates, Bioorg. Med. Chem. 10 (2002) 3031–3041.

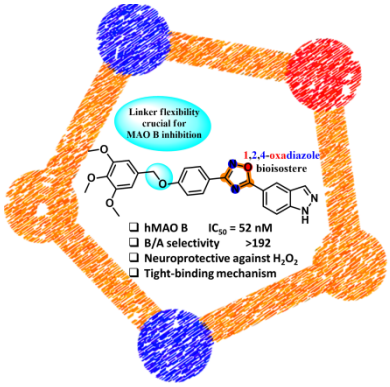

Supporting Information

Bioisosteric replacement based on 1,2,4-oxadiazoles in the discovery of 1*H*-indazole-bearing neuroprotective MAO B inhibitors

Mariagrazia Rullo,[a] Gabriella La Spada,[a,#] Daniela Valeria Miniero,[b,#] Andrea Gottinger,[c] Marco Catto,[a] Pietro Delre,[d] Margherita Mastromarino,[a] Tiziana Latronico,[b] Sara Marchese,[c] Giuseppe Felice Mangiatordi,[d] Claudia Binda,[c] Anna Linusson,[e] Grazia Maria Liuzzi,[b] Leonardo Pisani[a,*]

[a] *Dept. of Pharmacy-Pharmaceutical Sciences, University of Bari Aldo Moro, via E. Orabona 4, 70125 Bari, Italy*

[b] *Dept. of Biosciences, Biotechnologies and Environment, University of Bari Aldo Moro, Via E. Orabona 4, 70125, Bari, Italy*

[c] *Dept. of Biology and Biotechnology, University of Pavia, via Ferrata 9, 27100 Pavia, Italy*

[d] *CNR, Institute of Crystallography, 70126 Bari, Italy*

[e] *Department of Chemistry, Umeå University, 90187, Umeå, Sweden*

[#] *these authors contributed equally*

[*]Corresponding author: Prof. Leonardo Pisani; tel: +390805442803; fax: +390805442230; email: leonardo.pisani@uniba.it

Fig. S1a. ^{1}H NMR spectra (300 MHz, acetone-d_6) for compound **3**

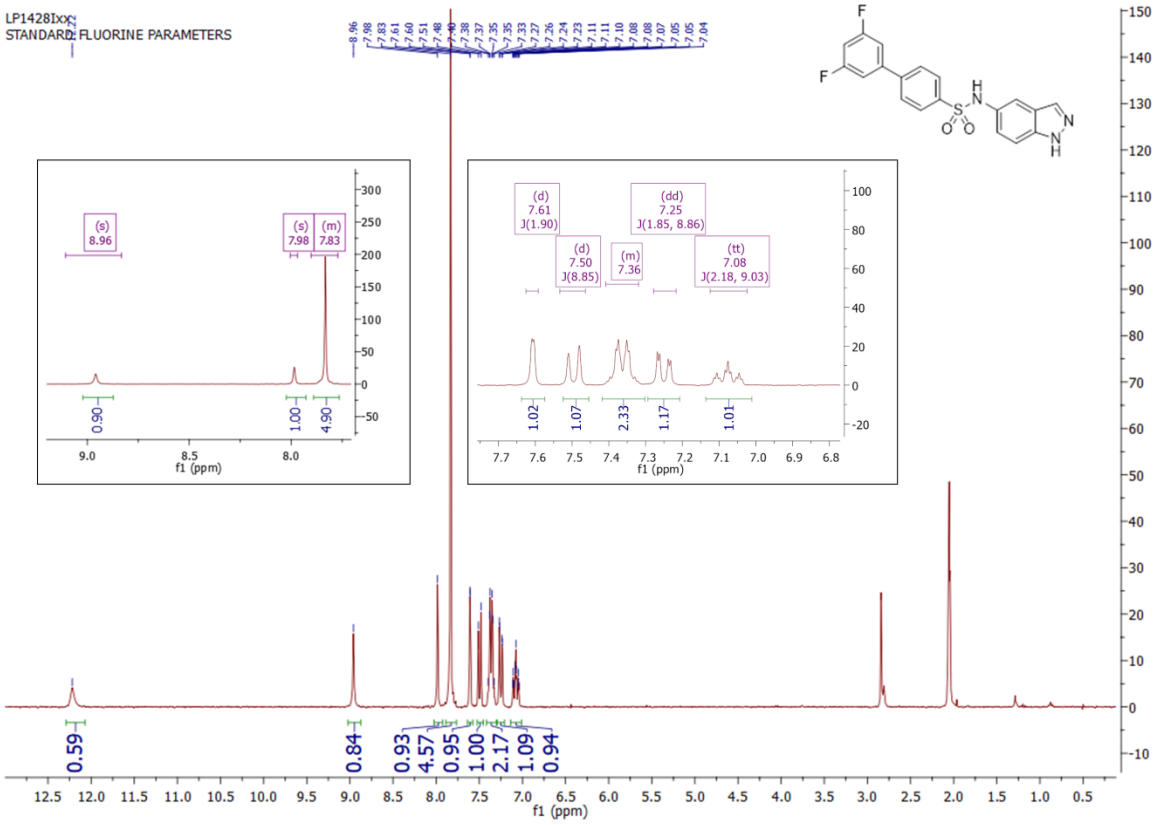

Fig. S1b. ^{13}C NMR spectra (126 MHz, acetone-d_6) for compound **3**

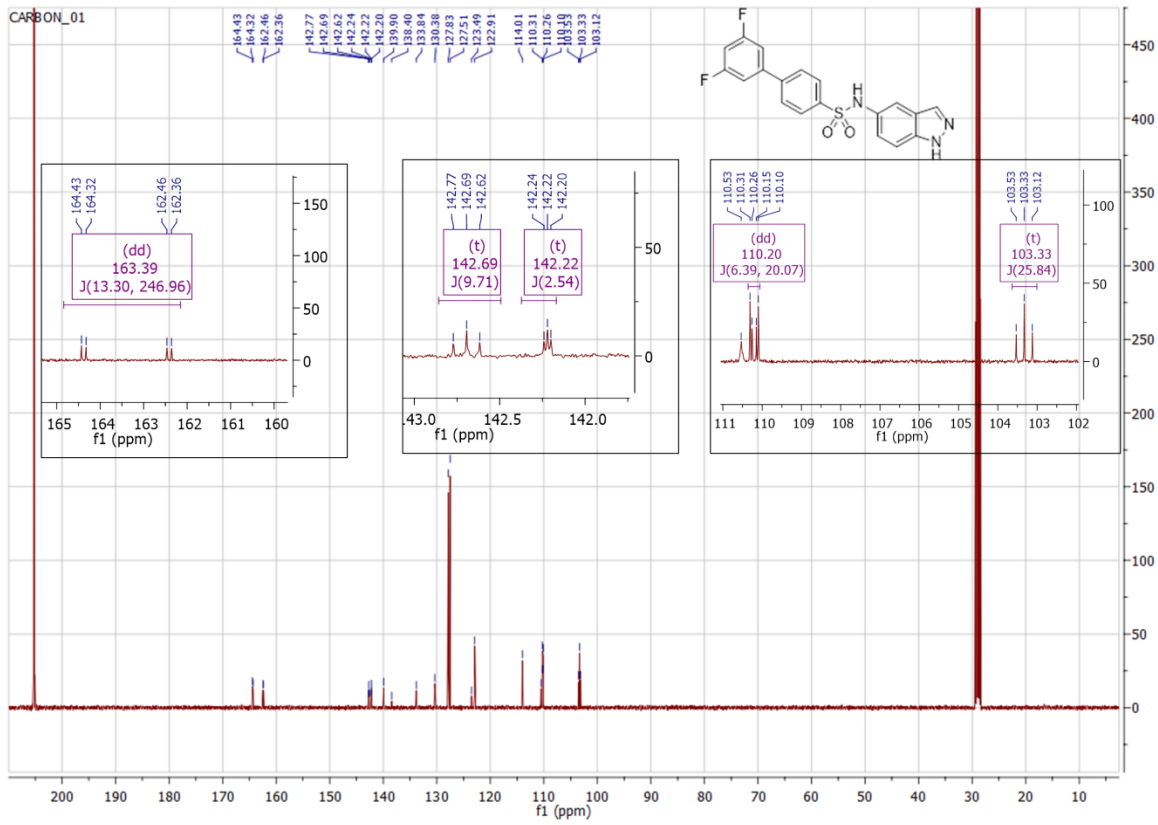

Fig. S2a. ^{1}H NMR spectra (500 MHz, DMSO-d_6) for compound **5**

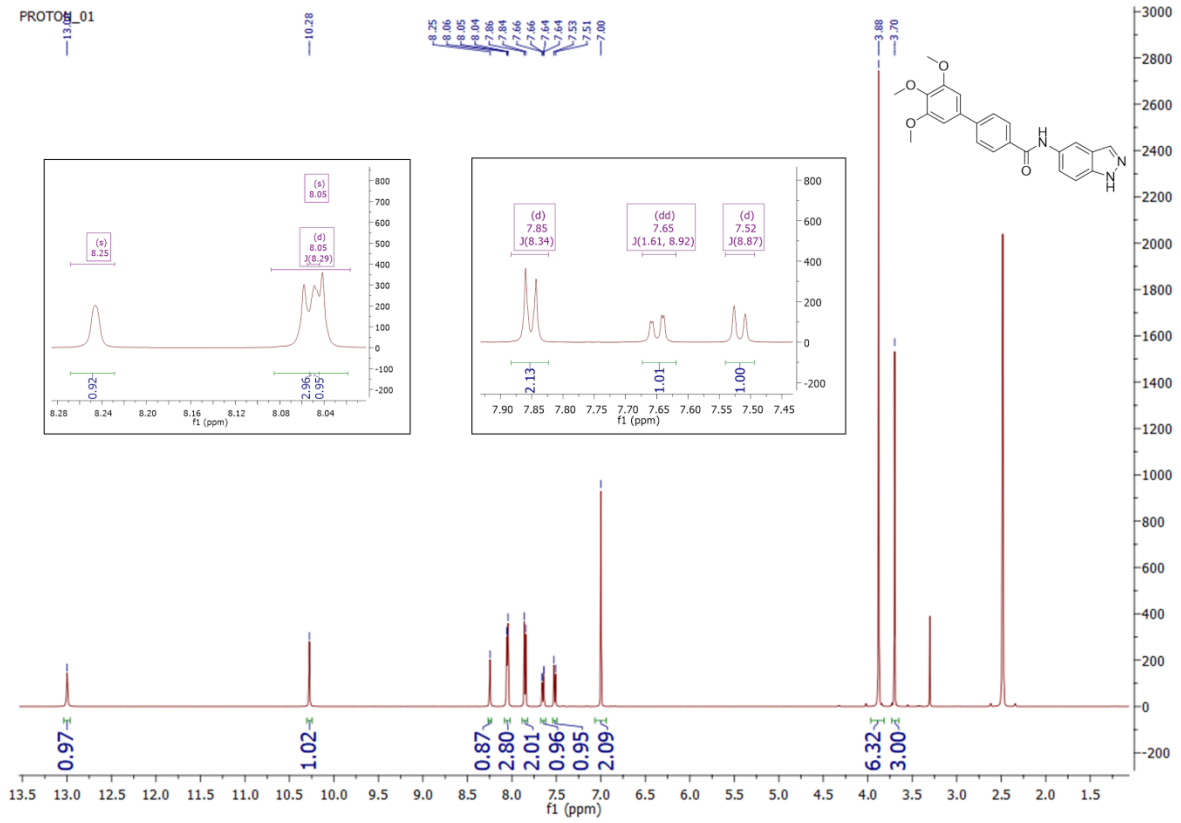

Fig. S2b. ^{13}C NMR spectra (126 MHz, DMSO-d_6) for compound **5**

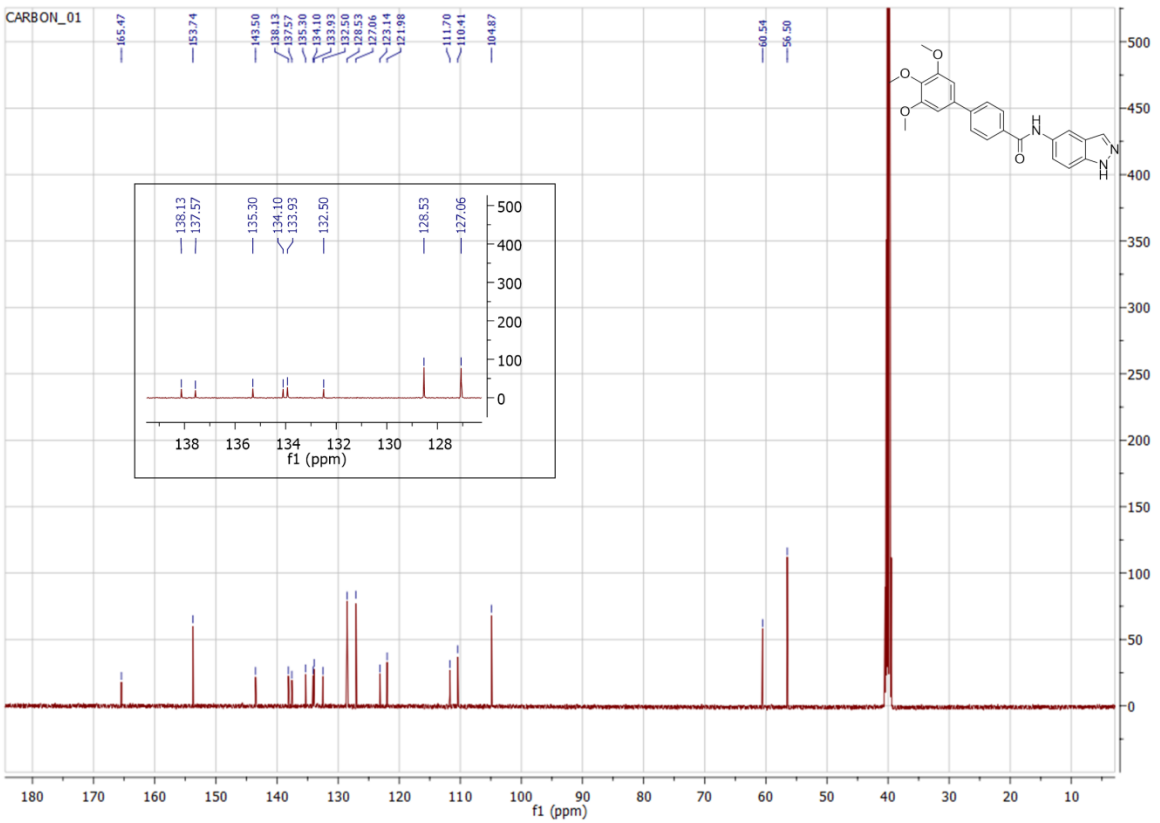

Fig. S3a. [1]H NMR spectra (500 MHz, acetone-d_6) for compound **8**

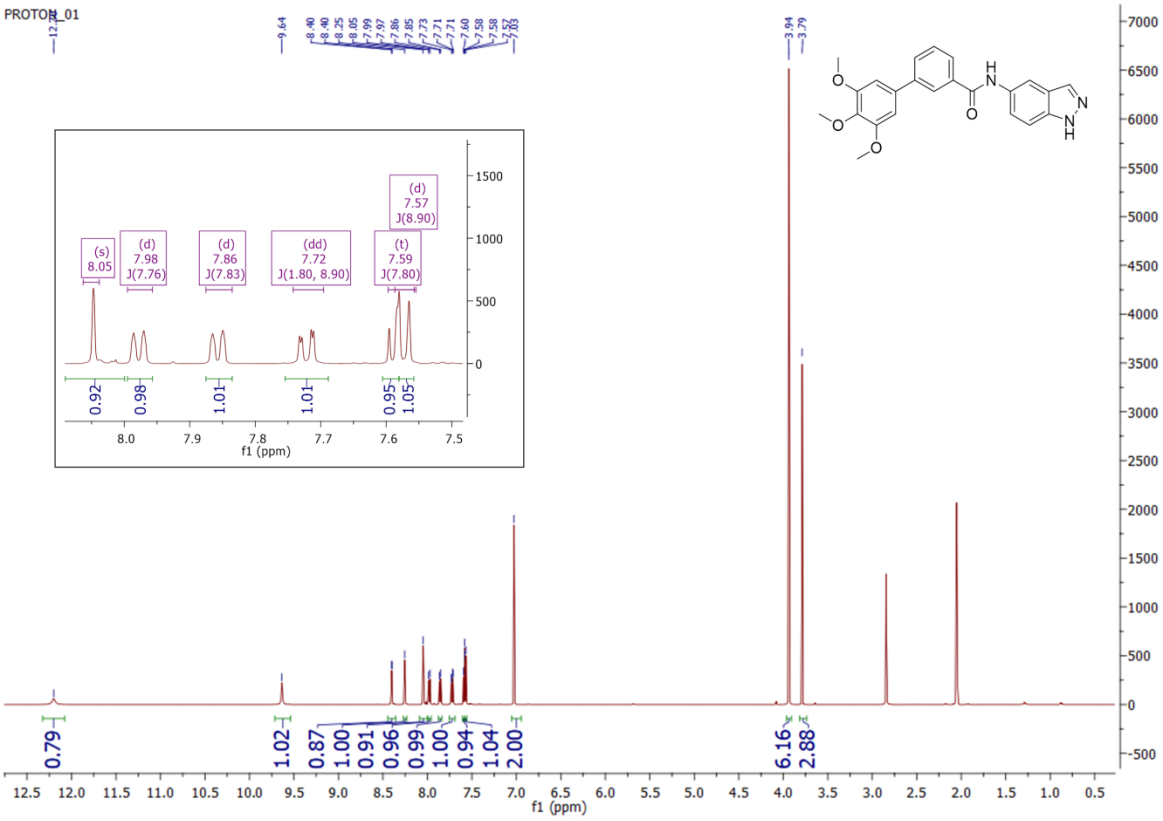

Fig. S3b. [13]C NMR spectra (126 MHz, acetone-d_6) for compound **8**

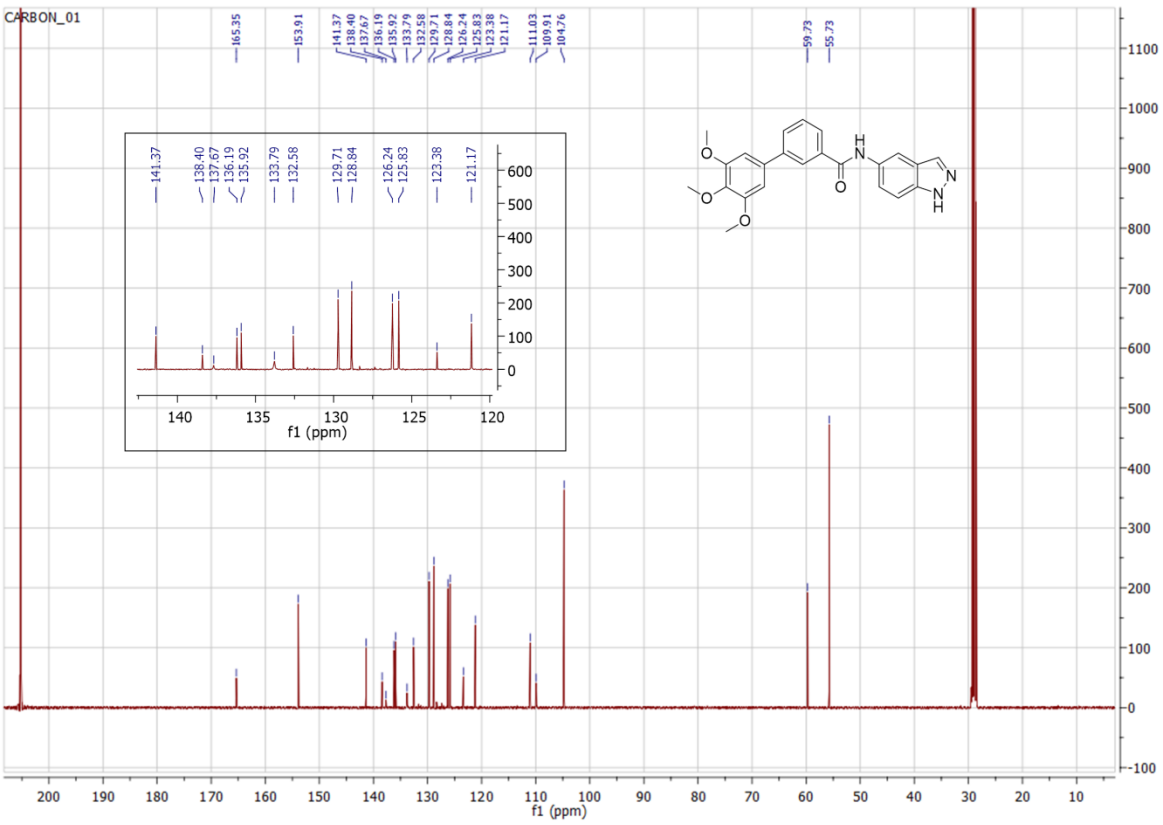

Fig. S4a. ^{1}H NMR spectra (500 MHz, DMSO-d_6) for compound **9**

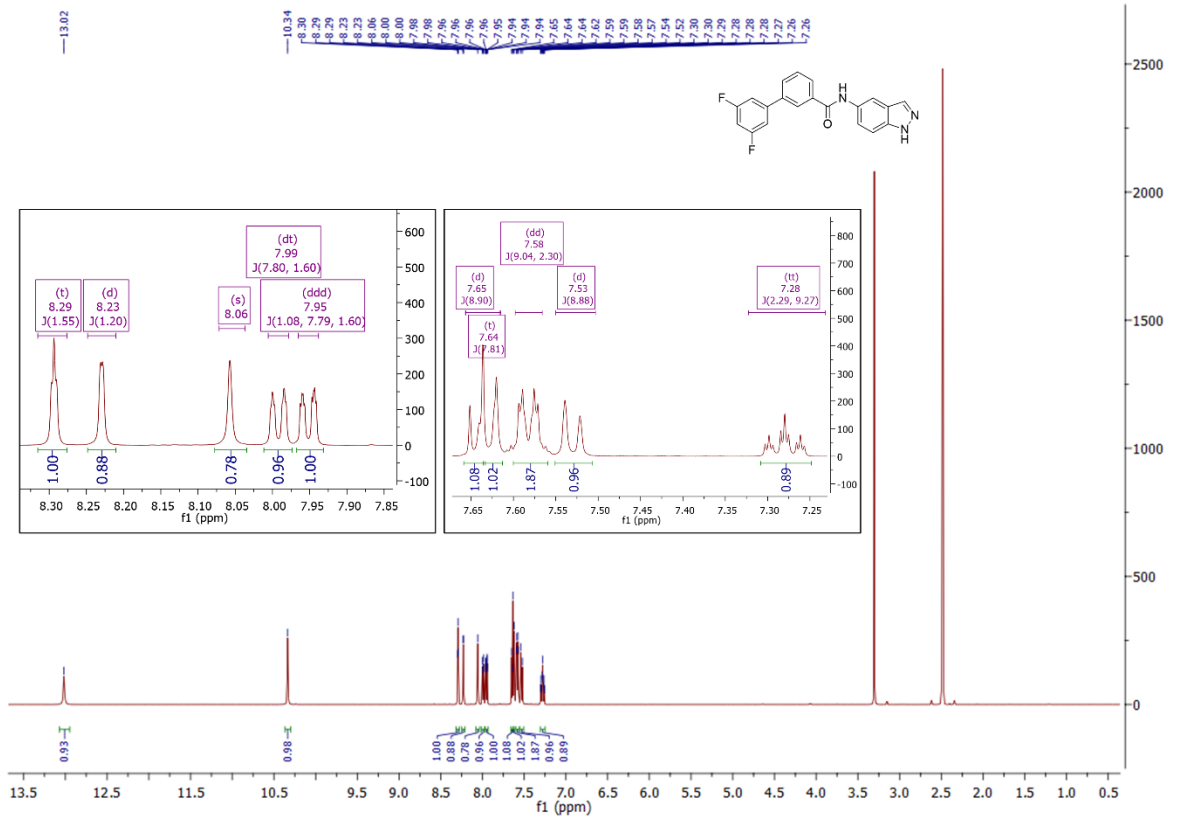

Fig. S4b. ^{13}C NMR spectra (126 MHz, DMSO-d_6) for compound **9**

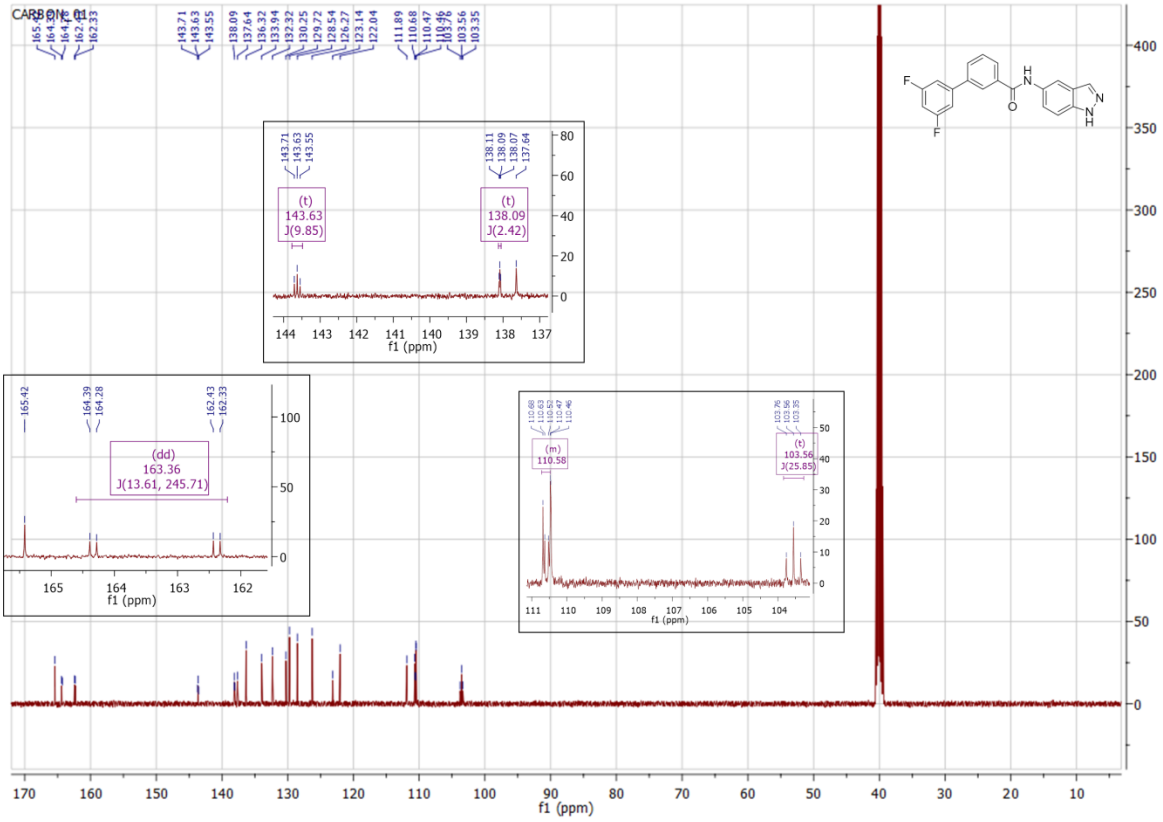

Fig. S5a. [1]H NMR spectra (300 MHz, DMSO-d_6) for compound **12**

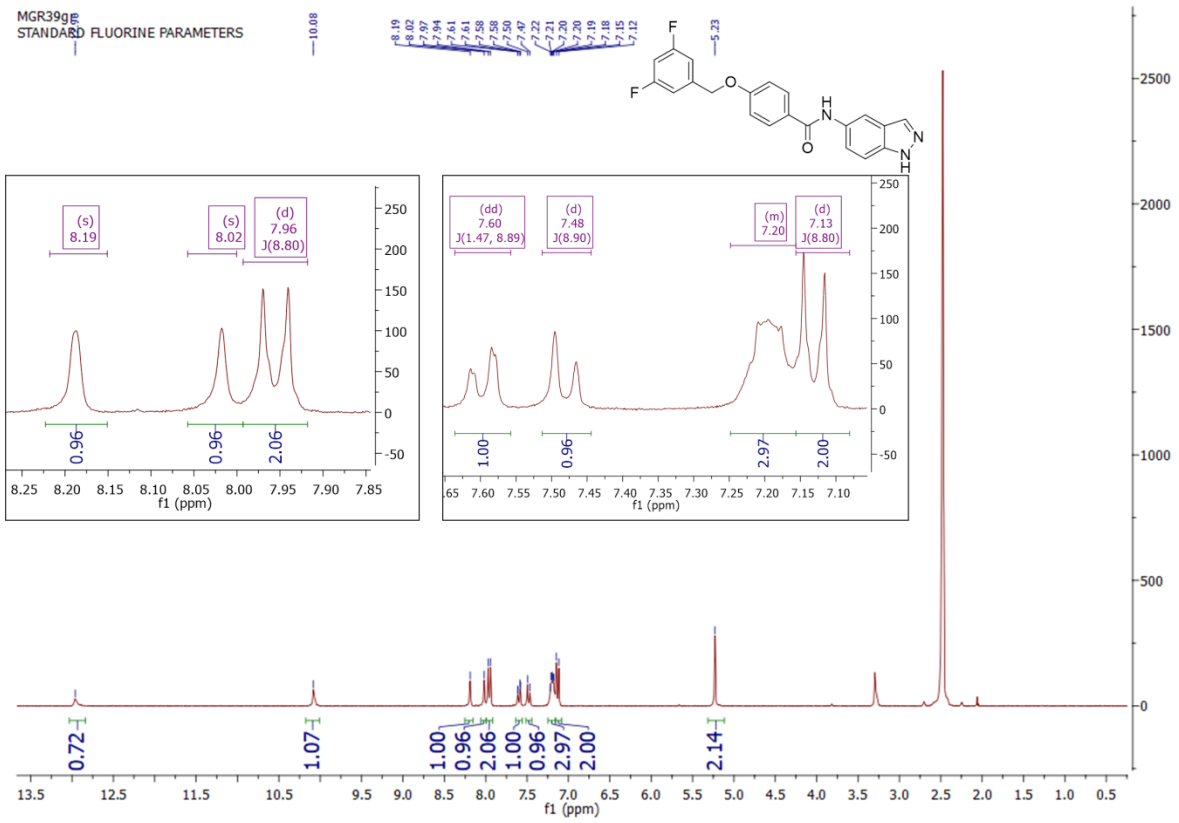

Fig. S5b. [13]C NMR spectra (126 MHz, DMSO-d_6) for compound **12**

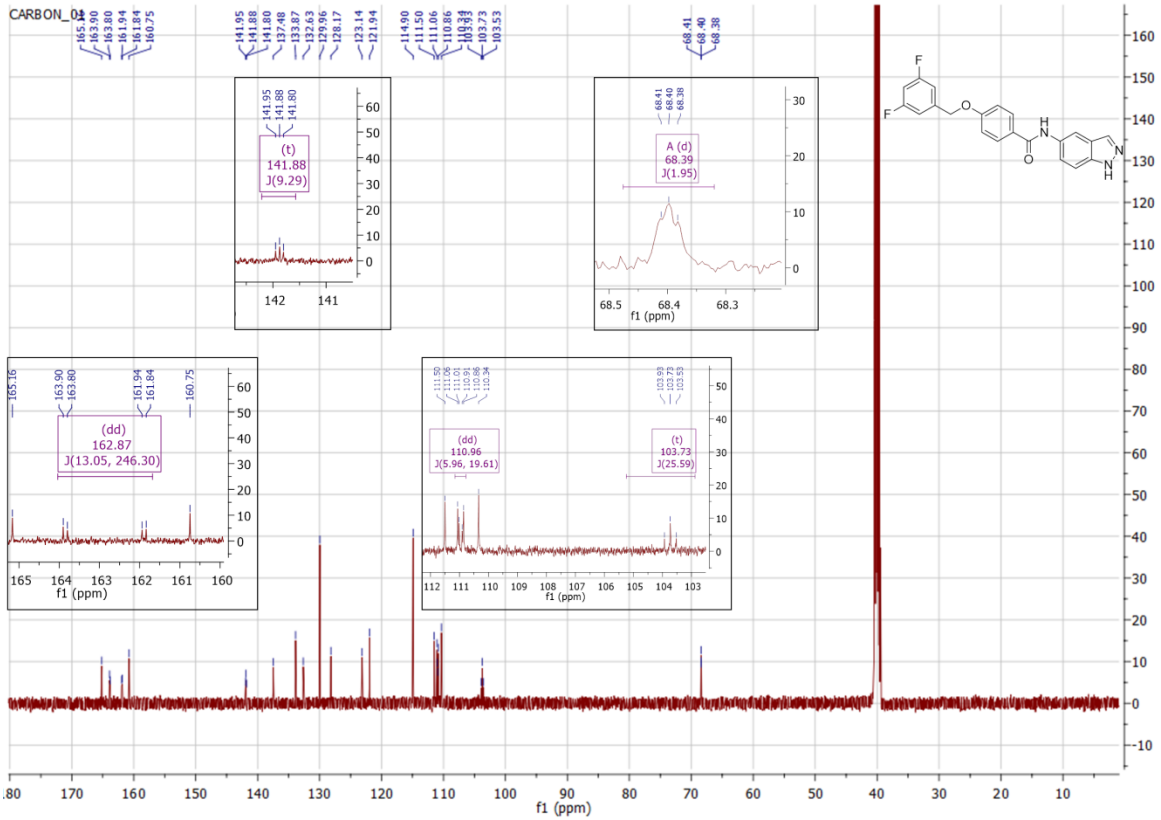

Fig. S6a. [1]H NMR spectra (500 MHz, DMSO-d_6) for compound **14**

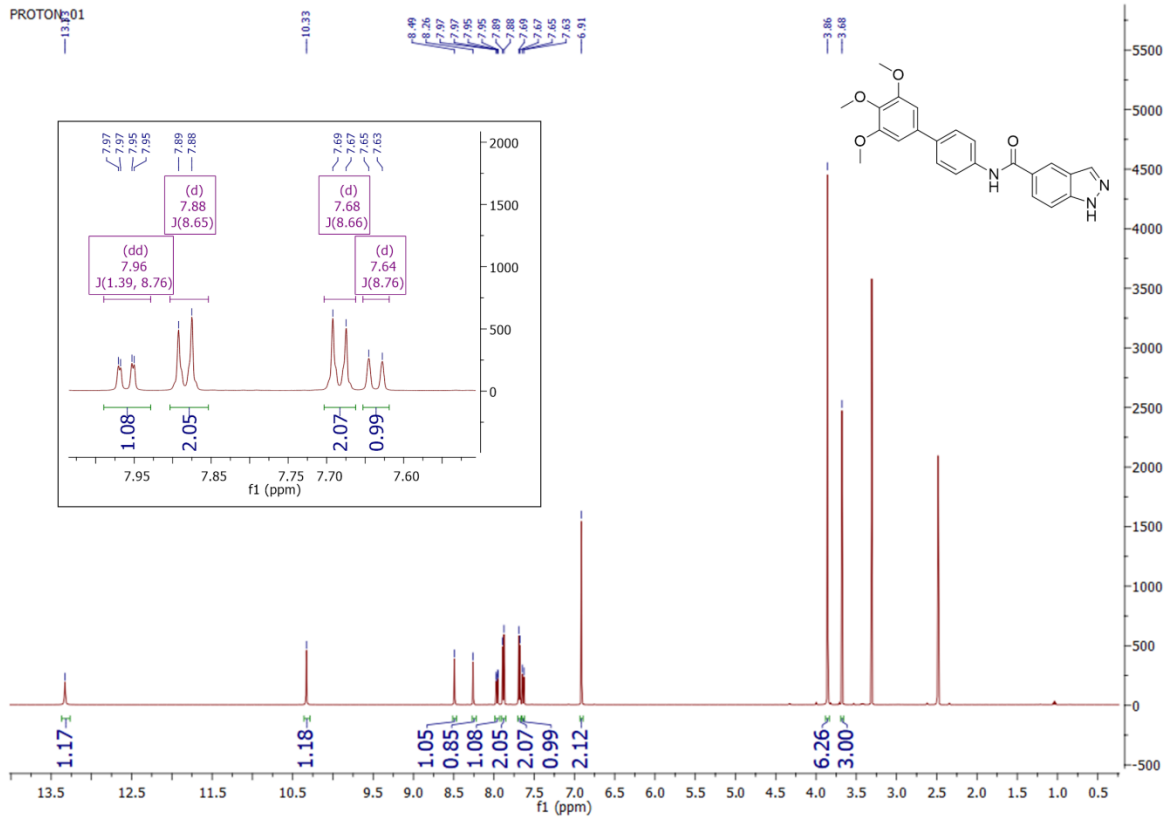

Fig. S6b. [13]C NMR spectra (126 MHz, DMSO-d_6) for compound **14**

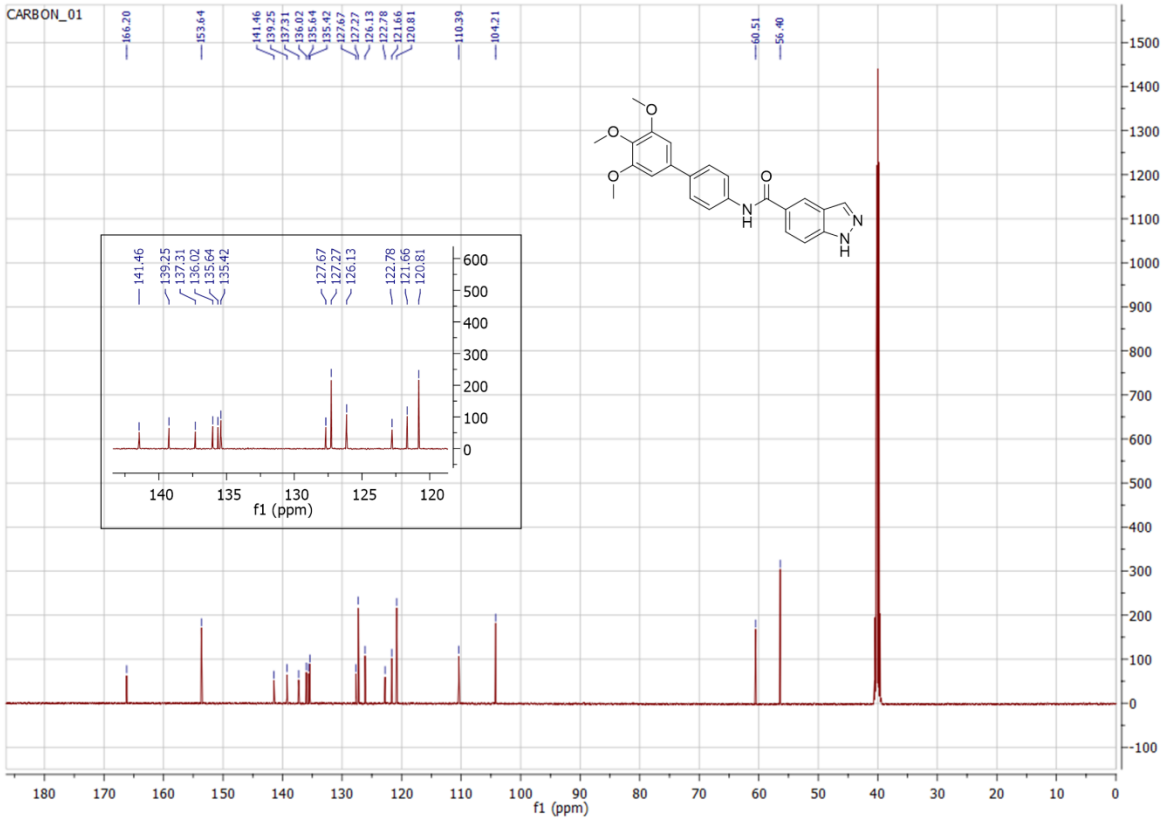

Fig. S7a. [1]H NMR spectra (500 MHz, DMSO-d_6) for compound **18**

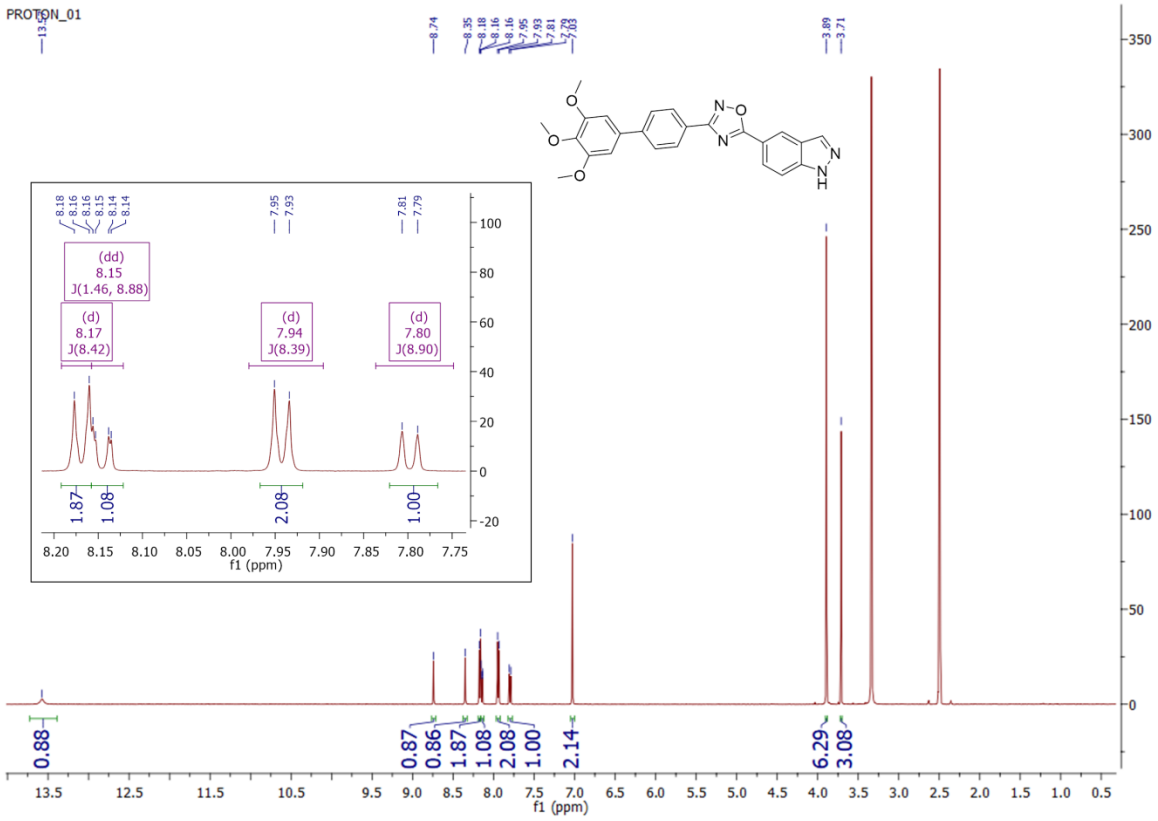

Fig. S7b. [13]C NMR spectra (126 MHz, DMSO-d_6) for compound **18**

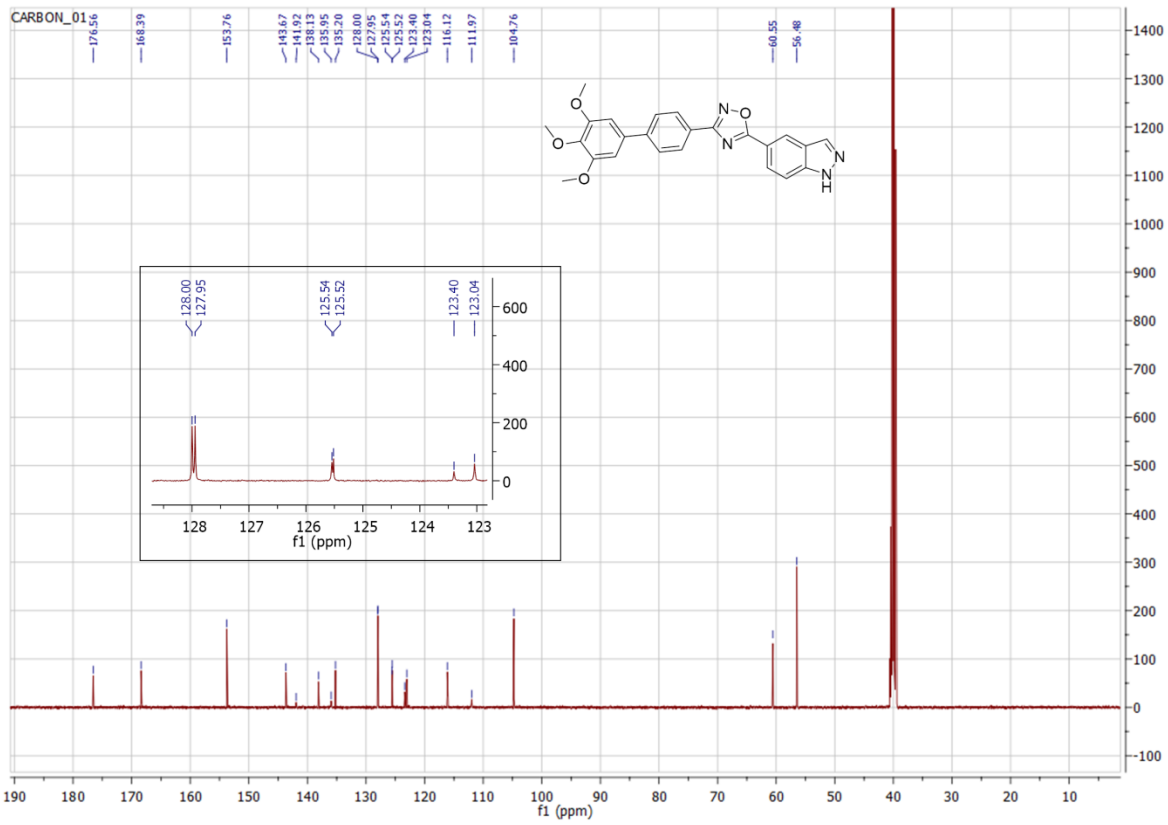

Fig. S8a. [1]H NMR spectra (500 MHz, DMSO-d_6) for compound **19**

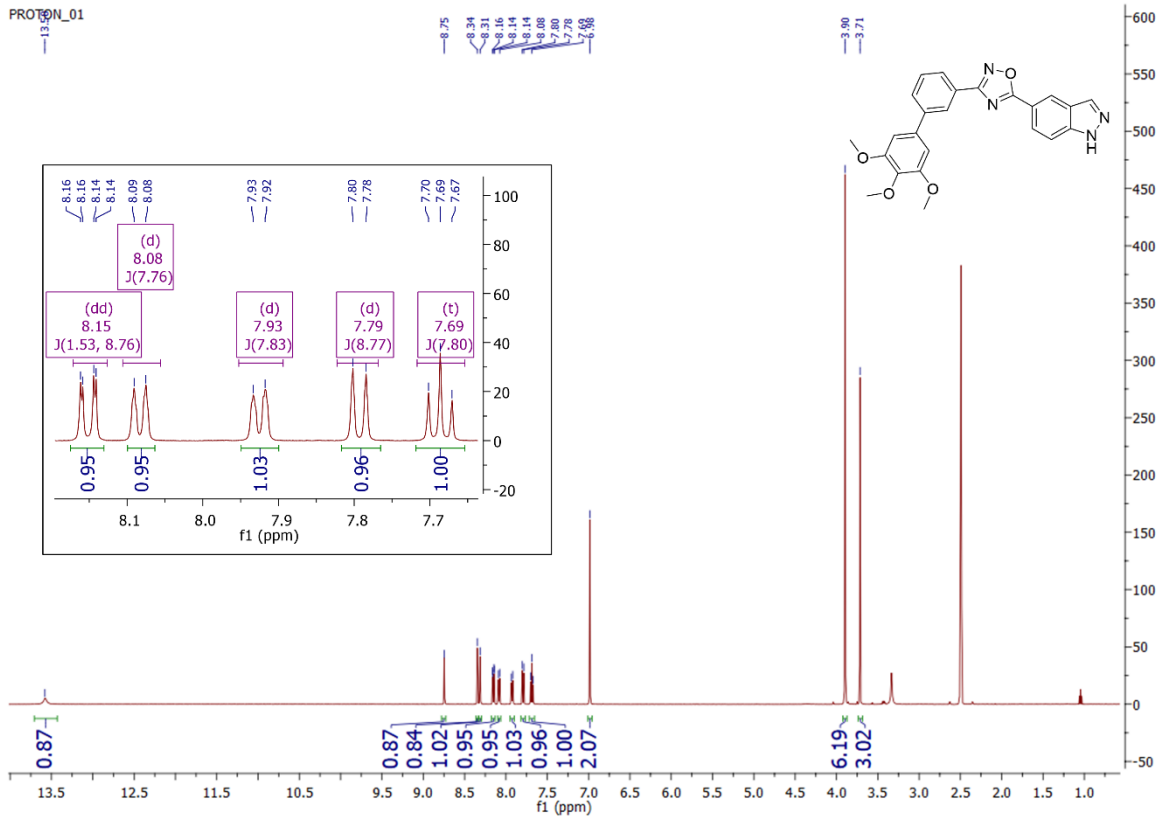

Fig. S8b. [13]C NMR spectra (126 MHz, DMSO-d_6) for compound **19**

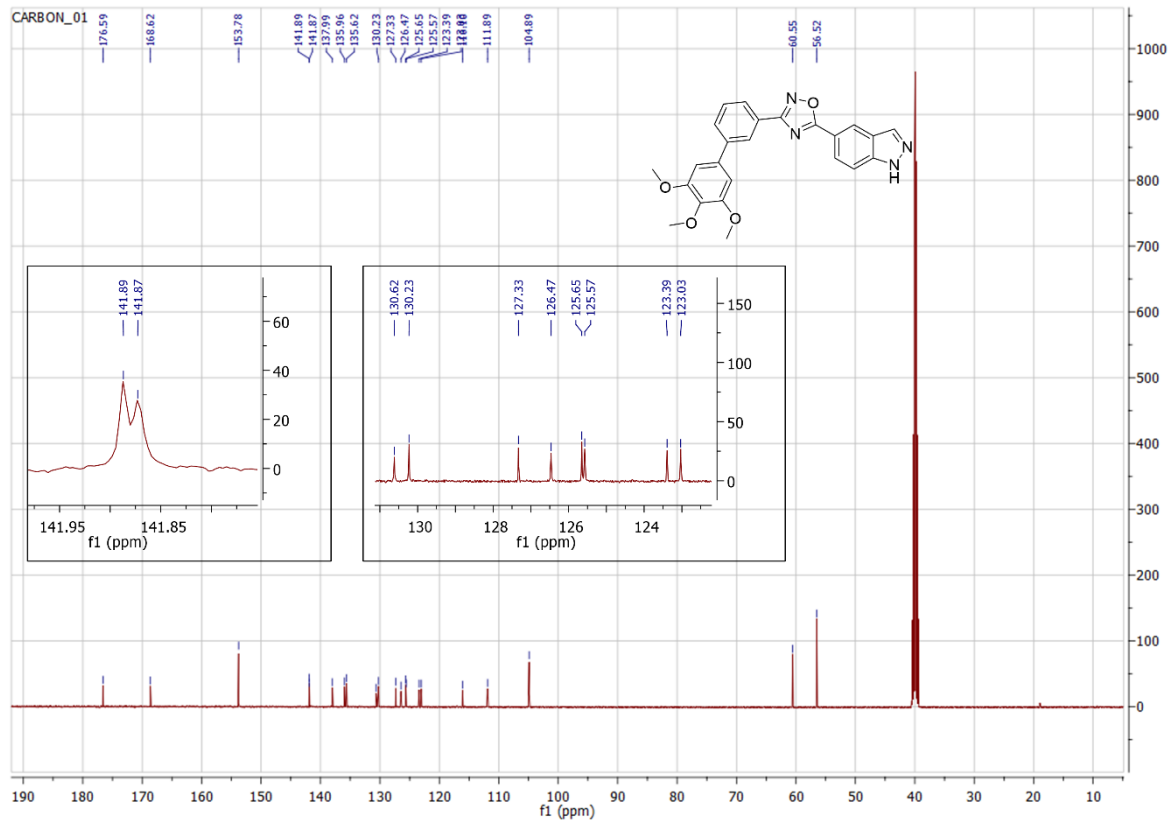

Fig. S9a. [1]H NMR spectra (300 MHz, DMSO-d_6) for compound **20**

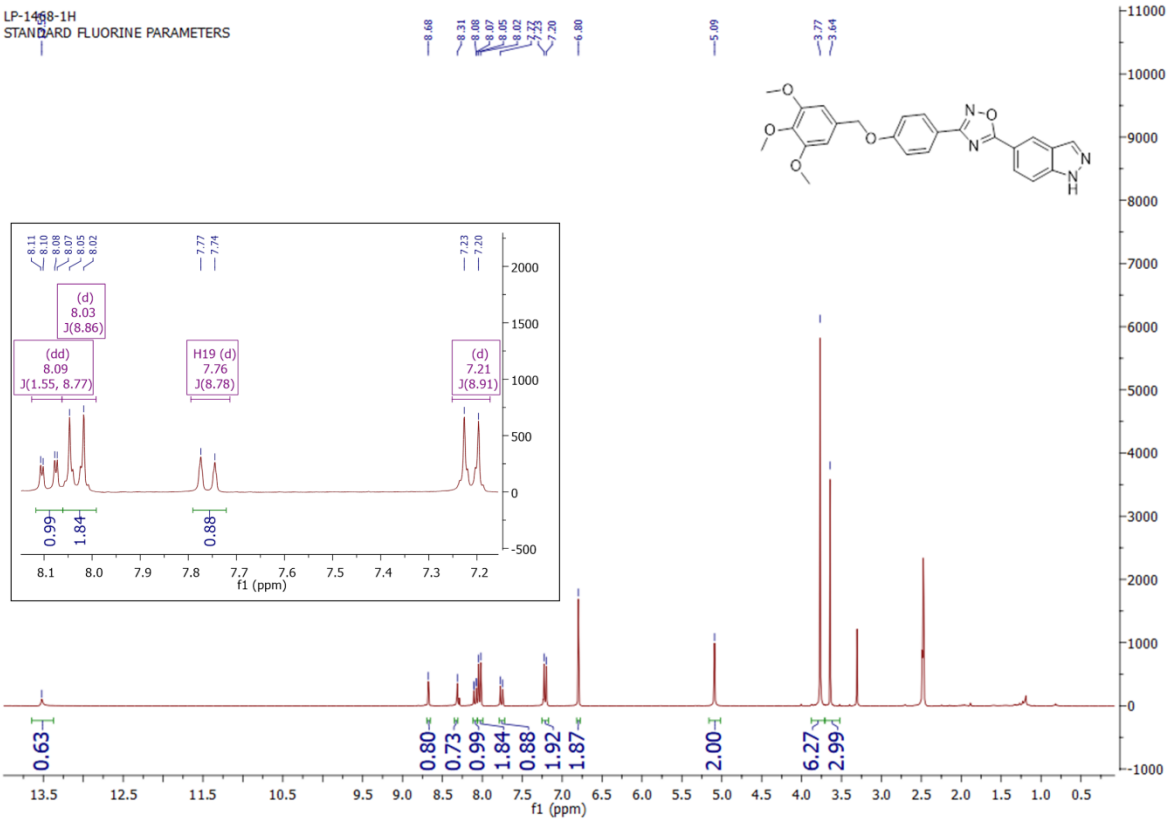

Fig. S9b. [13]C NMR spectra (126 MHz, DMSO-d_6) for compound **20**

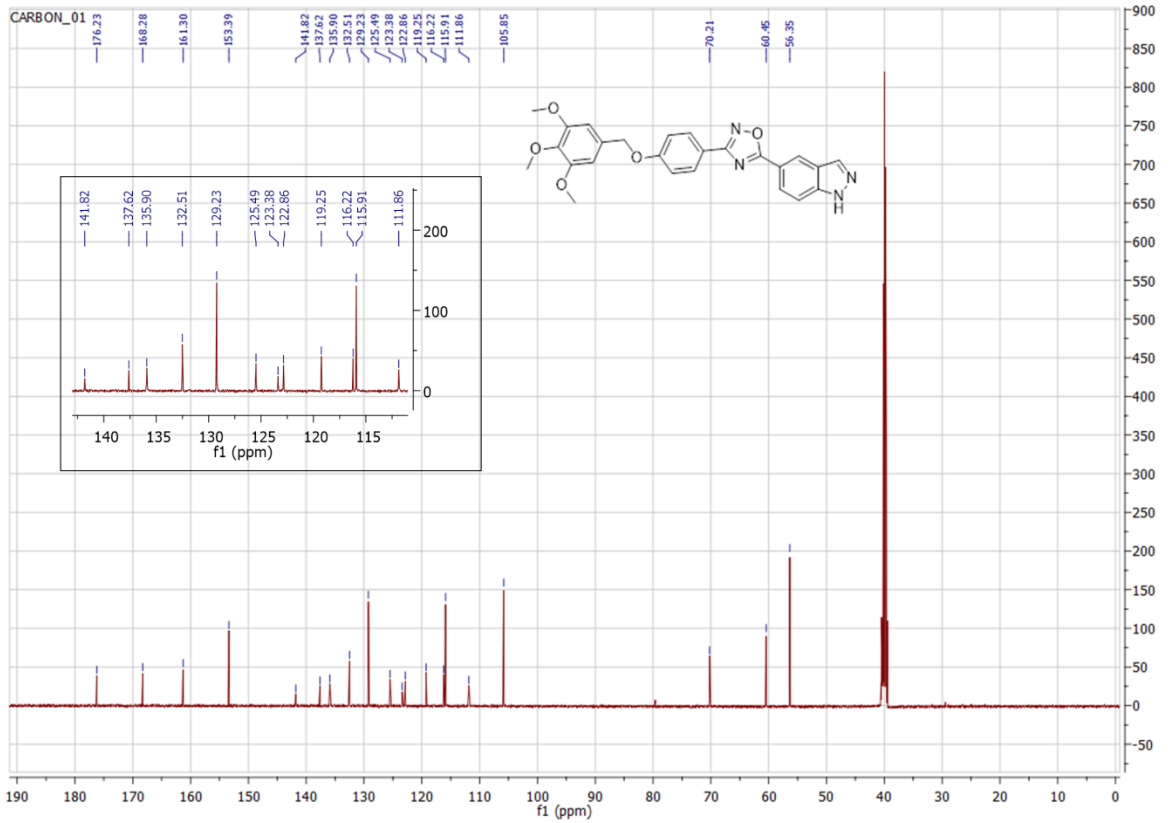

Fig. S10a. ^{1}H NMR spectra (500 MHz, DMSO-d_6) for compound **23**

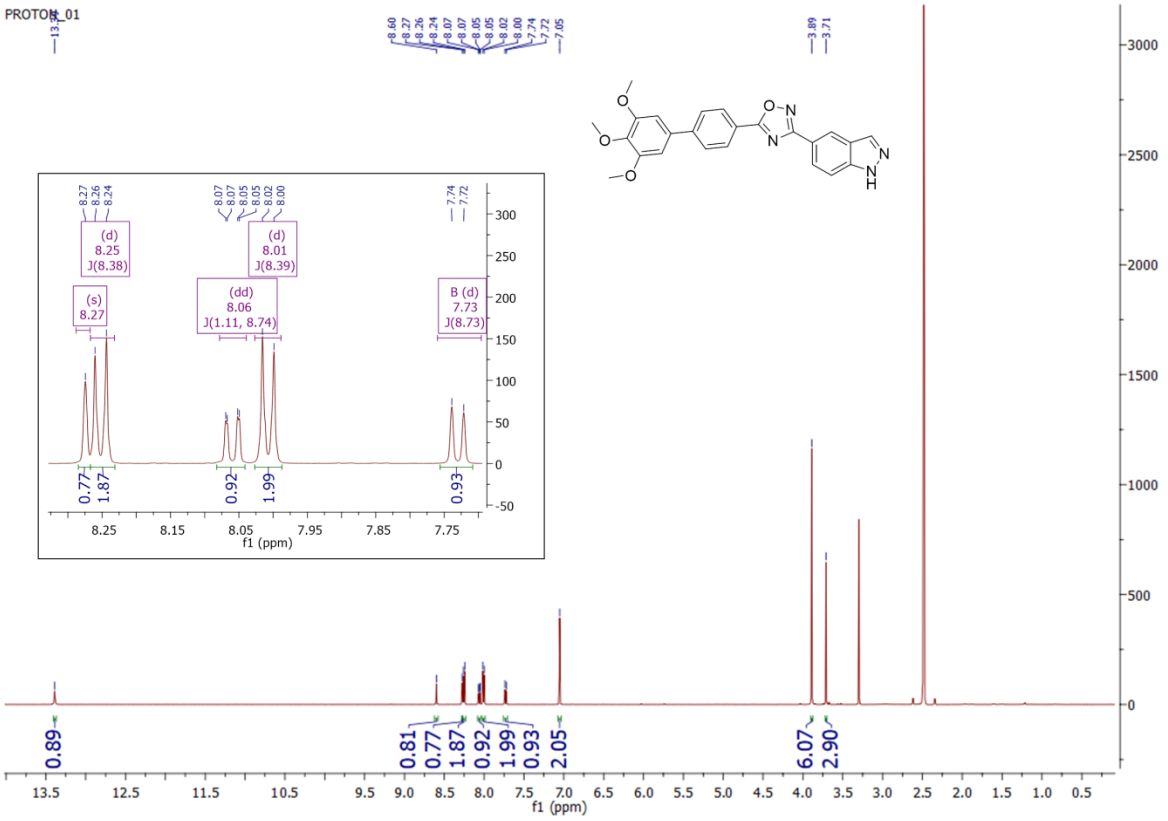

Fig. S10b. ^{13}C NMR spectra (126 MHz, DMSO-d_6) for compound **23**

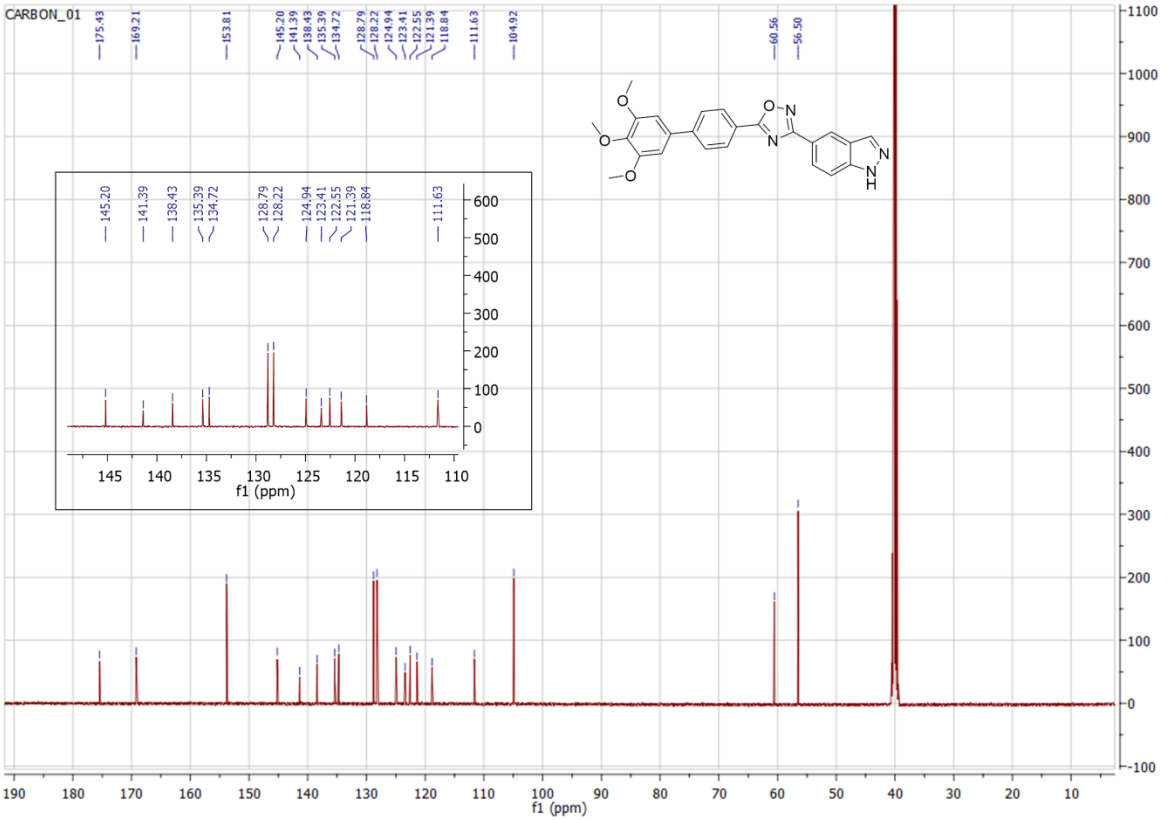

Fig. S11a. ^{1}H NMR spectra (500 MHz, DMSO-d_6) for compound **24**

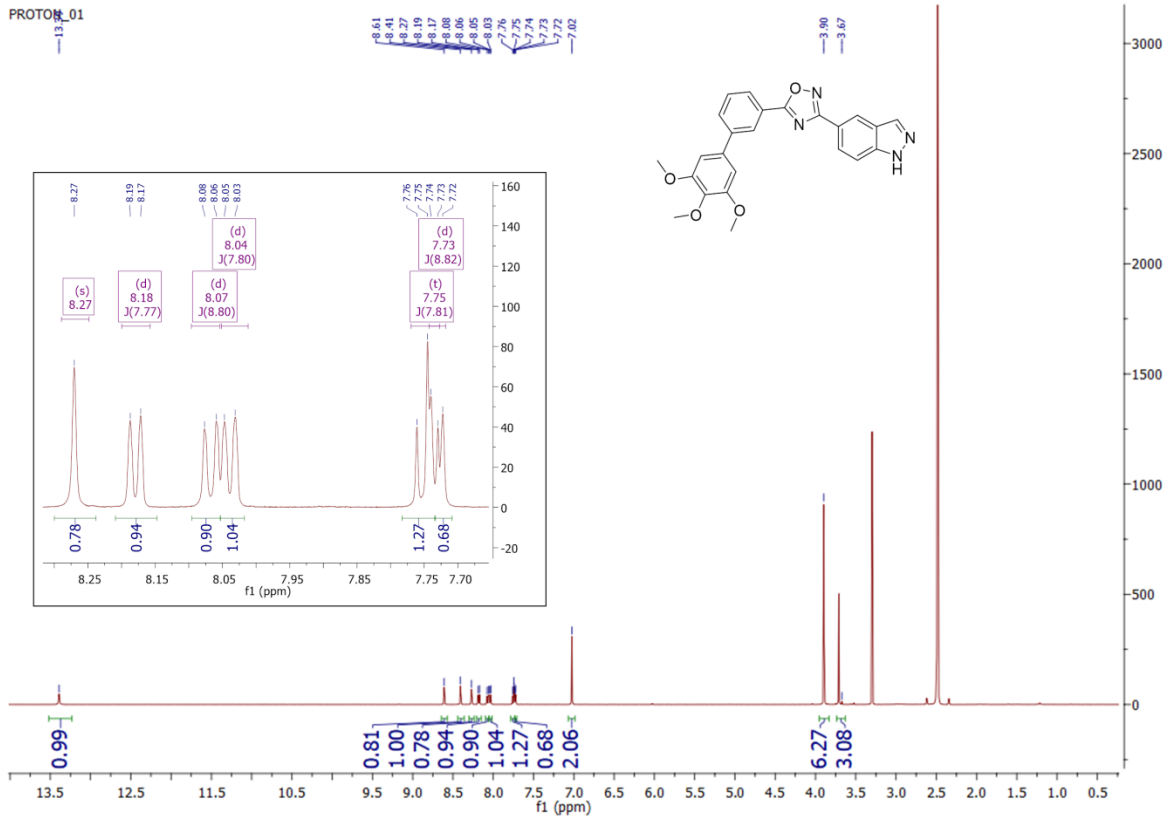

Fig. S11b. ^{13}C NMR spectra (126 MHz, DMSO-d_6) for compound **24**